12-17-2015

Biochemical and Mechanistic Studies of Nitronate Monooxygenase and Roles of Histidine Residues in Select Flavoprotein Oxidases

Crystal L. Smitherman

BIOCHEMICAL AND MECHANISTIC STUDIES OF NITRONATE MONOOXYGENASE AND ROLES OF HISTIDINE RESIDUES IN SELECT FLAVOPROTEIN OXIDASES

by

CRYSTAL SMITHERMAN

Under the Direction of Dr. Giovanni Gadda, PhD

ABSTRACT

Nitronate monooxygenase (NMO) catalyzes the flavin-dependent oxidation of propionate 3-nitronate (P3N) via the formation of an anionic flavosemiquinone. The oxidation of substrate includes the formation of a peroxy-nitro acid intermediate. P3N is activated to its radical form via a single electron transfer onto the FMN cofactor forming the anionic flavosemiquinone. Reoxidation of FMN cofactor from the anionic semiquinone has been proposed to go through two routes dependent upon which radical species oxygen reacts with first, radical P3N or the semiquinone. The recent crystallographic determination of NMO from *Cyberlindnera saturnus* and steady-state kinetics revealed an allosteric activation effect on the enzyme by PEG 3350 with respect to P3N.

Choline oxidase (CHO) catalyzes the two-step oxidation of choline to glycine betaine via an enzyme-bound FAD cofactor. In the first redox reaction, choline is activated to it alkoxide form by means of an enzyme-derived catalytic base, H466. This histidine residue has been shown to not only act as a general base but an electrostatic catalyst stabilizing the negative charge accumulated on the reduced flavin species as shown by replacing the residue with alanine, aspartate, and glutamine using site-directed mutagenesis. CHO was also observed to catalyze excited state reactions as facilitated by H466. Evidence for the ESR comes from the observation of a pL-dependence on the fluorescence emission of CHO in H_2O and D_2O. Using fluorescence spectroscopy and pH effects, a hydroxy-C4a flavin intermediate was detected in the wild-type and S101A variant with and without oxygen indicating the adduct formation was with an active site hydroxide ion. The mechanism of formation has been elucidated.

INDEX WORDS: Nitronate monooxygenase, choline oxidase, fluorescence spectroscopy, propionate 3-nitronate, electron transfer, circular dichroism

BIOCHEMICAL AND MECHANISTIC STUDIES OF NITRONATE MONOOXYGENASE AND ROLES OF HISTIDINE RESIDUES IN SELECT FLAVOPROTEIN OXIDASES

by

CRYSTAL SMITHERMAN

A Dissertation Submitted in Partial Fulfillment of the Requirements for the Degree of

Doctor of Philosophy

in the College of Arts and Sciences

Georgia State University

2015

BIOCHEMICAL AND MECHANISTIC STUDIES OF NITRONATE MONOOXYGENASE AND ROLES OF HISTIDINE RESIDUES IN SELECT FLAVOPROTEIN OXIDASES

by

CRYSTAL SMITHERMAN

Committee Chair: Giovanni Gadda

Committee: Dabney White Dixon

Markus Germann

Electronic Version Approved:

Office of Graduate Studies

College of Arts and Sciences

Georgia State University

December 2015

DEDICATION

This dissertation is dedicated to my loving fiancé, Adam Scott Rosenberg, for his unending support and unconditional love.

ACKNOWLEDGEMENTS

I would like to thank my parents, for their continued support and encouragement. I would like to thank my mother, especially. I was raised by a single mother most of my childhood who dedicated everyday of her life to make mine better. She is the reason I love science for more than just a hobby but now a career. She taught me to never give less than my utmost best in everything I went after.

I would like to thank my advisor, Dr. Giovanni Gadda, for his continued support throughout my PhD career. It was his "tough love" strategy that drove me to be the best scientist I could be. I am grateful for my committee members, Dr. Dabney Dixon and Dr. Markus Germann, for their advice and encouragement for which my PhD work would not have been improved.

I would like to thank all of the past and current lab members. You made being in lab on a beautiful, sunny day worth it. The friends that I have made in the PhD program will be those I will cherish forever.

TABLE OF CONTENTS

LIST OF SCHEMES

LIST OF TABLES

LIST OF FIGURES

1 Introduction

1.1 Riboflavin

Bacteria and plants produce riboflavin, or vitamin B2, which is enzymatically converted to flavin mononucleotide (FMN) or flavin adenine dinucleotide (FAD) (Figure 1.1).[1-5] FMN and FAD are the two most common active flavins used as cofactors in enzymatic catalysis.[6] The versatility of the flavin in chemical reactions is due to the redox active isoalloxazine ring which allows the molecule to accept one and two electrons, protons, or form a covalent bond via flavin adduct (Scheme 1.1). Reduction by one or two electrons or formation of a covalent adduct at the N(5) or C4a atoms of the flavin (Figure 1.1, Scheme 1.1) can be observed spectrophotometrically due to the conjugation of the bonds of the isoalloxazine. Three redox states (oxidized, one-electron reduced, and two-electron reduced) cause distinct absorbance changes in the UV and visible spectral region and have been observed in several flavin-dependent enzymes as observed in glucose oxidase for example (Figure 1.2). Spectral changes of the flavin cofactor provide evidence for the detection of the flavin redox states allowing for the spectral detection of chemical reactions in flavin-dependent proteins.

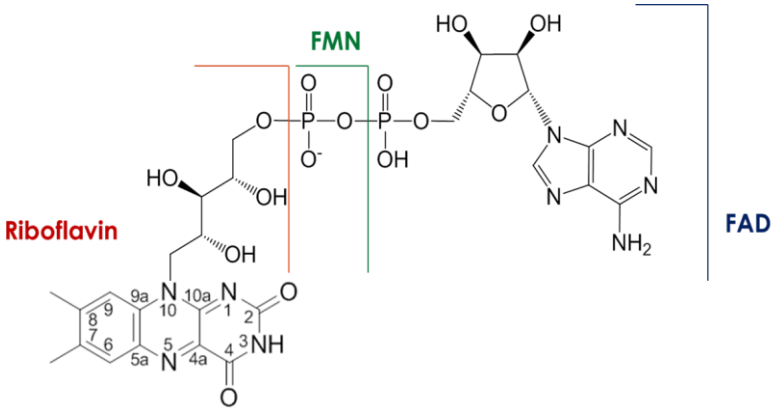

Figure 1.1 Flavin Structure modified from (2).
Chemical structure of the isoalloxazine moiety drawn as using IUPAC numbering.

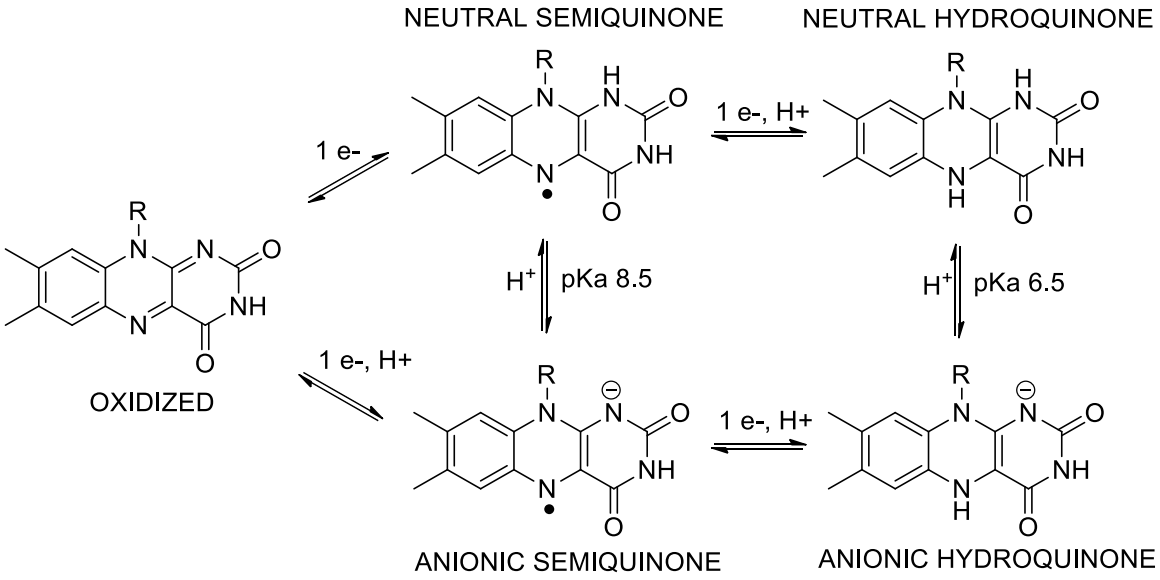

Scheme 1.1 Various redox states of the flavin. Modified from Gibson *et al.*[7]

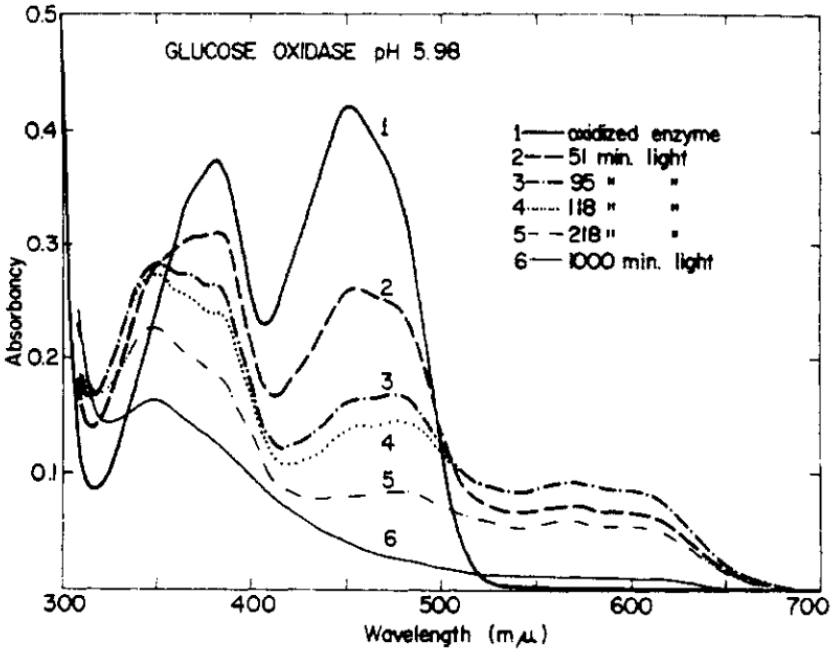

Figure 1.2 UV-visible absorption changes due to the change in redox state of glucose oxidase. Taken from Wohlfart *et al.*[8]

1.2 Modulating Flavin Chemistry

The environment surrounding the flavin can cause a shift in the UV-visible absorption, fluorescence and circlular dichroism spectra from, but not limited to, hydrophobicity, hydrogen bonding or electrostatics.[9-11] The influence from the environment, i.e. amino acid residues, solvent components, and substrates or products from the enzymatic reaction can directly affect the UV-visible absorption spectra of flavin cofactors. The redox of the flavin and enzymatic catalysis, in turn, are modulated dependent upon the surrounding environment. For example, choline oxidase from *Arthrobacter globiformis* (CHO) contains an active site comprised of hydrophilic amino acids, such as H466, E312, and H351, which accommodate the hydrophilic substrate, choline and observed to modulate flavin redox.[12] In contrast, nitronate monooxygenase from *Cyberlindnera saturnus* (CsNMO) contains an active site of mostly hydrophobic residues, such as A24, F79, and Y321, and two histidine amino acids (H147 and H197) suitable for alkyl nitronate compounds with a charged nitro group and aliphatic chain. Enzymes have evolved to contain conserved active sites in order to hone flavin reactivity designed for a specific chemical reaction. Monitoring spectral changes of enzyme-bound flavin cofactors using techniques such as UV-visible absorbance, circular dichroic, and fluorescence spectroscopy can yield additional knowledge regarding the flavin environment and reactivity.

1.2.1 Histidine Residues and Select Flavin-dependent Enzymes

Only a select few amino acid residues within 4 Å, typically, of the isoalloxazine ring have been shown to modulate the redox potentials of the enzymes (i.e. flavin cofactor and protein), flavinylation, and facilitating catalysis between organic compounds and enzyme.[13-17] The presence of a histidine residue in the active site of choline oxidase was shown to be directly involved the flavinylation of the cofactor forming a covalent bond between the protein construct

and the flavin at the C8 position of the isoalloxazine.[16] Tyrosine residues have been shown to modulate redox potentials of flavin cofactors in flavodoxins and enzymes catalyzing excited state reactions.[18] While examples for all ionizable amino acid side chains catalytically involved in the active sites of enzymes are known, this dissertation will focus solely on the roles of histidine residues in enzymatic catalysis. Histidine residues have been observed in a wide-array of physiological functions including, but not limited to, coordinating heme in hemopexin[19], general base catalyst in chymotrypsin,[20] and flavinylation of human liver glycolate oxidase.[17]

The versatility of histidine residues observed in a wide array of enzymatic reactions derives from the biophysical properties of imidazole side chain to ionize at physiological pH and have polar and hydrophilic properties. The nitrogen atoms of the imidazole ring have the ability to hydrogen bond with the OH and NH groups found on the protein, substrate and products. The versatility of this amino acid leads to the residue being utilized as an electrostatic catalyst, general acid, or a general base. A number of flavoproteins catalyze reactions using histidine residues, such as glucose oxidase, pyranose-2-oxidase and choline oxidase.[8, 21-24] All three of these enzymes contain a conserved histidine residue that initiates catalysis through the use of an active site base that abstracts a hydroxyl proton from the substrate followed by a hydride transfer onto the N(5) atom of the flavin. In glucose oxidase, Klinman and colleagues proposed that the placement of charged amino acids provide an optimum cavity for oxygen reactivity.[25] The positive charge on H516 was shown to increase the k_{cat}/K_{O2} at low pH. Further studies of the alanine variant show that H516 is responsible for reducing the activation energy barrier for catalysis by enhancing the driving force of the reaction.[25] Monomeric sarcosine oxidase contains a histidine in the active site that does not behave as a catalytic base but rather is involved in substrate orientation. The alanine, asparagine, and glutamine variants exhibited a loss of more

than two orders of magnitude of activity and were structurally the same.[26, 27] Therefore, H269 is shown to be important in orienting the substrate and facilitating the reduction of the flavin cofactor during catalysis.

1.3 Mechanistic and Structural Studies on Choline Oxidase from *Arthrobacter globiformis*

The majority of residues in the active site choline oxidase from *A. globiformis* (CHO) have been mutated and biochemically characterized making CHO a good model system for the Glucose-Methanol-Choline oxidoreductase superfamily in identifying the catalytic base.[13-16, 21, 28, 29] CHO catalyzes the oxidation of choline to glycine betaine through a two-step hydride transfer (Scheme 1.2). The steady-state kinetic parameters for choline oxidation, k_{cat}/K_m and k_{cat}, increase with increasing pH, both parameters reach limiting values at high pH. This was consistent with the requirement of an unprotonated group with a pK_a value of ~7.5 for catalysis and substrate binding.[28] Ionizable groups in the active site that could behave as a catalytic bases are H99, E312, H351, and H466. H99 is important for flavinylation and covalently-linked through an 8α-N(3)-histidyl linkage.[16] An asparagine variant of H99 revealed the importance for optimal positioning of the flavin cofactor for hydride tunneling and steady-state kinetics similar to the wild-type enzyme.[16] E312 is located too far from the hydroxyl group on the choline substrate on the opposite side of the catalytic cavity, better positioned for interacting with the positive head group of the substrate.[12, 15] Evidence for this conclusion comes from the distances measured between the side chain of E312 and the glycine betaine product observed in the crystal structure from Salvi *et al* (Figure 1.3).[30] E312 was shown to be important in binding and positioning of the choline substrate utilizing mutations with glutamine and aspartate residues.[15, 31] Hydride transfer in the active site of the E312D variant of CHO was decreased by 260-fold but still active consistent with the glutamate residue not being the catalytic base.[32] Two ionizable

side chains exist in the active site that are plausible as a catalytic base, H351 and H466 (Figure 1.3). H351 was shown to be involved in substrate binding and as a hydrogen bond donor to stabilize and position the hydroxyl head group of choline.[14] Steady-state kinetics, anaerobic substrate reduction, and competitive inhibition studies with H351A variant are consistent with H351 not being the catalytic base.[14, 21] H351 was important but not essential in enzyme catalysis by providing hydrogen bonding interactions with the histidine side chain and the substrate for optimum positioning for catalysis.[14] Initial studies of H466 with alanine and aspartic acid variants revealed the importance of this residue in stabilizing the transition state due to the protonation state of the histidine.[13, 14, 16]

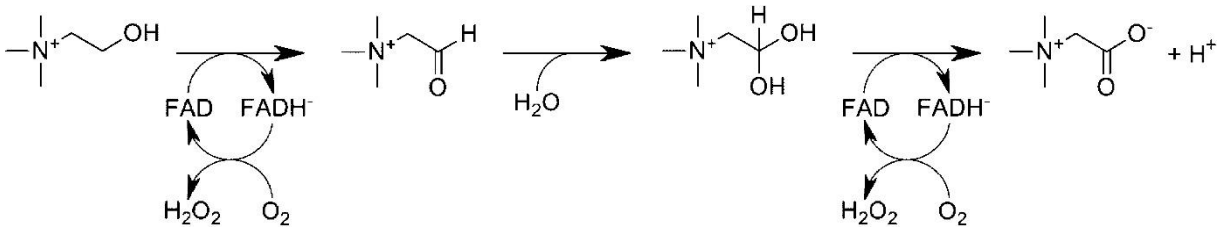

Scheme 1.2 Oxidation of choline as catalyzed by choline oxidase. Taken from (53).

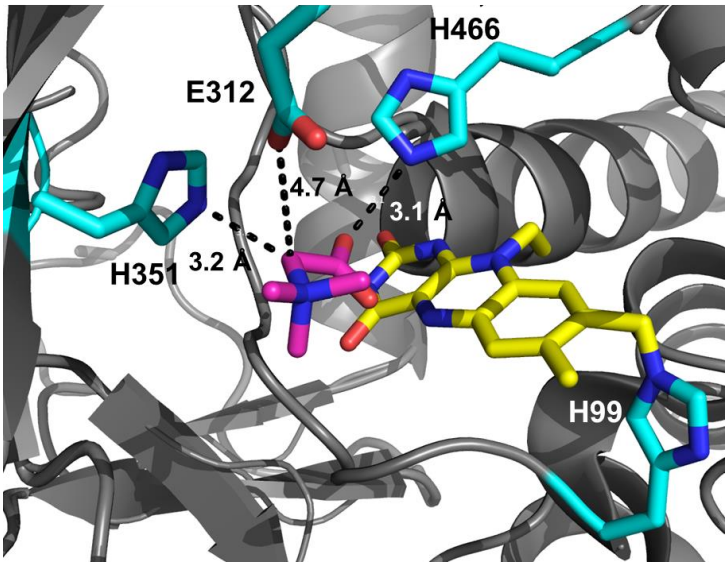

Figure 1.3 Interactions of E312, H466 and H351 with FAD and glycine betaine. Modified from (53).

1.4 CHO as the Model Flavin-dependent Enzyme to Investigate the Multiple Roles of Histidine Residues

H466 residue in CHO is has been previously mutated to alanine and aspartate to understand the roles of the residue in catalysis and substrate binding.[13, 33] Steady-state and rapid kinetics, UV-Visible absorbance and fluorescence spectroscopy, pH and kinetic isotope effects, and redox potentials were measured and compared between H466 variants and the wild-type enzyme. With the alanine mutation, the enzymatic turnover of the variant with choline substrate was more than 60-fold lower than turnover with the wild-type.[13] The effect on activity was attributed to a loss in electrophilic contributions due to the imidazole ring on the protein-bound flavin cofactor. The aspartate mutation was used to probe the role of a negative charge near the N(1)-C(2) locus of the flavin and the influence of the charge on enzyme catalysis. With the presence of the negative charge, an inactive enzyme was produced incapable of turning over with substrate and contained 75% non-covalently bound flavin whereas the wild-type contained covalently-bound flavin.[33] The variant also altered the redox potential from +73 mV to -89 mV in the variant.[33]

H466 has been previously postulated as the catalytic base in choline activation by site-directed mutagenesis, biochemical and kinetic studies.[13, 33] The imidazole ring of H466 was replaced with an alanine residue and apparent steady-state kinetics of the variant enzyme with choline as substrate was measured from pH 7 to 11 with and without the addition of imidazole.[13] The imidazole recovery assay revealed an increase in k_{cat} with decreasing pH consistent with the requirement of a protonated imidazole moiety important for catalysis.[13] In the wild-type enzyme, OH bond cleavage occurs faster than the rate-limiting CH bond cleavage as observed using solvent, substrate, and multiple kinetic isotope effects.[28] Solvent kinetic isotope effects

measured on the H466A variant were shown to have increased from 1 to 2 revealing a hindered OH bond cleavage.[13] A cavity is likely formed by the removal of the imidazole ring in the H466A variant that may have allowed a water molecule to be positioned in its place. This active site water molecule could serve as a surrogate base activating the choline substrate. The mechanistic studies published in this dissertation have shown that H466 is indeed the catalytic base in choline oxidase.

1.5 Excited State Reactions in Choline Oxidase from *Arthrobacter globiformis*

Fluorescence studies have shown that flavin-dependent enzymes and flavin analogs in solution can catalyze chemical reactions from their singlet and triplet states.[34-40] Reactions occurring in the ground state (i.e. electron/proton transfers, adduct formation) have also been observed to occur once the flavin has been excited to either the singlet or triplet states. Proton transfers have been observed to occur from the N(1) to N(10) atoms of lumichrome and onto the N(5) atoms in flavin analogs once excited to the singlet state.[36, 40] Song *et al.* described an intramolecular phototautomerization occurring in the alloxazine form of lumichrome as facilitated by a pyridine and acetic acid molecule (Scheme 1.3).[40] This was observed by following spectral changes of the flavin fluorescence emissions with increasing percentages of pyridine in the system (Figure 1.4), in which the decrease in fluorescence emission at 440 nm was accompanied by a simultaneous increase at 540 nm.[40] Excited state proton transfers (ESPT) have also been observed from the N(1) to the N(5) atoms of flavin analogs when the N10 is bound to a methyl group (see numbering in Figure 1.1).[36] The biophysical properties, i.e. dipole moments and ionization constants at the N1, N3 and N5 atoms of the isoalloxazine ring (Figure 1.1) have been calculated to change in the singlet and triplet states which lead to the excited state reactions occurring.[34, 36, 40] Although ESPT are the most common, adduct formation has also

been observed at the C4a position in flavin-dependent light receptors via a thiolate group of an active site cysteine.[38, 41]

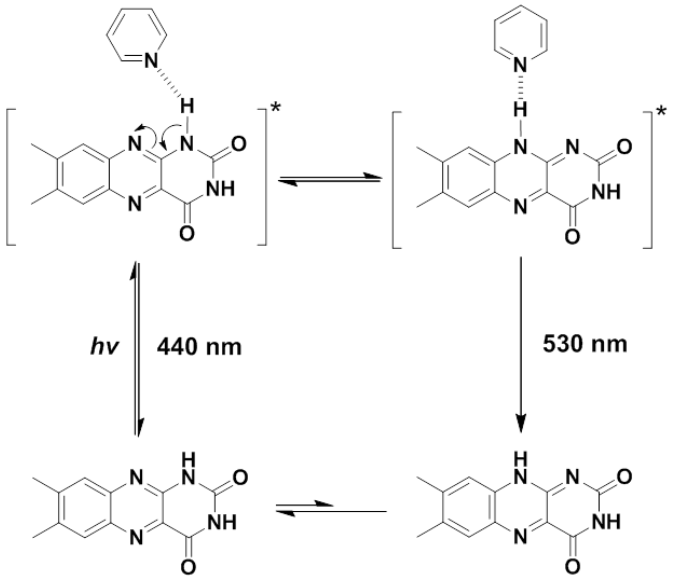

Scheme 1.3 Mechanism of action of intramolecular excited state proton transfer of alloxazine as facilitated by pyridine. Adapted from Song *et al.*[42]

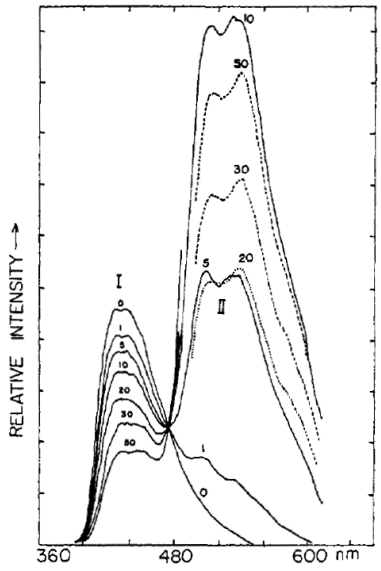

Figure 1.4 Mechanism of action of intramolecular excited state proton transfer of alloxazine as facilitated by pyridine. Adapted from Song *et al.*[42]

Larger flavin-containing biological systems that have been observed to carry out excited state reactions as their physiological roles are phototropins, light-oxygen-voltage (LOV) domains, cryptochromes, and blue-light sensing using FAD (BLUF) receptors. These flavin-dependent proteins and protein domains are specialized photoreceptors that utilize a flavin cofactor to detect and respond to changes in light intensity, direction and duration.[43] Flavins behave as the photoreceptor to harvest light and then utilize the absorbed energy to facilitate protein conformational changes.[38, 44] Conformational changes in the protein trigger downstream cell signaling dependent upon the chromophore, type of cell, and location of the protein.[45] Flavin-dependent proteins that catalyze excited state reactions have been shown to be involved in regulating circadian rhythms of animals and plants, cellular cross-talk, photosynthesis, and stress responses.[44, 46] A brief review over the published literature will be discussed here.

Phototropins are serine-threonine kinases activated by light to undergo autophosphorylation.[43, 47] These proteins contain two LOV domains, one of which non-covalently binds an FMN as the chromophore.[41] These intra-cellular membrane proteins assist in relocating chloroplasts based on light exposure.[48] Depending on the intensity of light, these proteins are responsible for accumulating or removing the chloroplasts to avoid too much light.[38] LOV domains of photoreceptors carry out reactions through the formation of a covalent bond at the C4a position of FMN and a protein-derived sulfur atom of a conserved cysteine residue.[49, 50] This FMN adduct species produces a distinct spectral signature (Figure 1.5) and is the active state of the photoreceptor.[50]

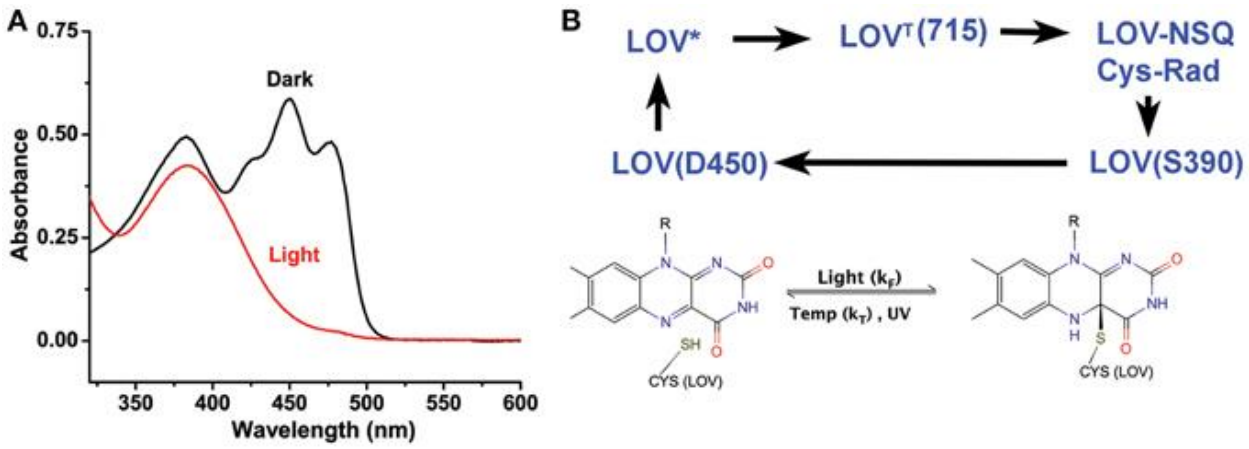

Figure 1.5 Mechanistic characteristics of LOV proteins.
A) Characteristic UV-visible absorption spectra of LOV proteins. B) Mechanism of photocycle carried out by LOV and formation of C4a adduct. Taken from [51] who adapted it from [50].

Cryptochromes were the first blue-light receptors characterized and found to contain (LOV) domains.[52] The first gene encoding a cryptochrome was isolated in 1993 from *Arabidopsis* but the physiological role was not identified until 2001.[52, 53] Cryptochromes have been shown to carry out the same mechanism of a thiolate-flavin adduct using FAD, FMN or 8-hydroxy-5-deazaflavin cofactor.[54] The flavin cofactor is non-covalently bound and buried within the protein. A second cofactor, 5,10-methenyltetrahydrofolate, harvests and transfers the light to the flavin which behaves as a light sensor triggering the enzymatic reaction.[55] The enzymatic reaction has been proposed to trigger protein conformational changes that activate downstream signaling pathways in cell and is completely reversible in the dark.[43] Another LOV domain-containing protein is a BLUF receptor and is primarily involved in regulating circadian rhythms.[46] Structurally, LOV and BLUF receptors contain very similar αβ-like folds and retain small and compact domains due to the peptide sequences typically containing less than 150 amino acids.[38] Cryptochromes are much larger because they are constructed of two chromophore proteins, each containing a flavin molecule. A comprehensive review summarizing the mechanisms of action, structural differences, and biophysical relevance of these proteins can be

found in [38] (Figure 1.6). These flavin-dependent proteins that utilize light to activate an enzymatic reaction have been shown to initiate stomatal opening and leaf expansions.[38, 56] Cryptochromes in animals have even been shown to facilitate changes in neurons and firing rates.[56]

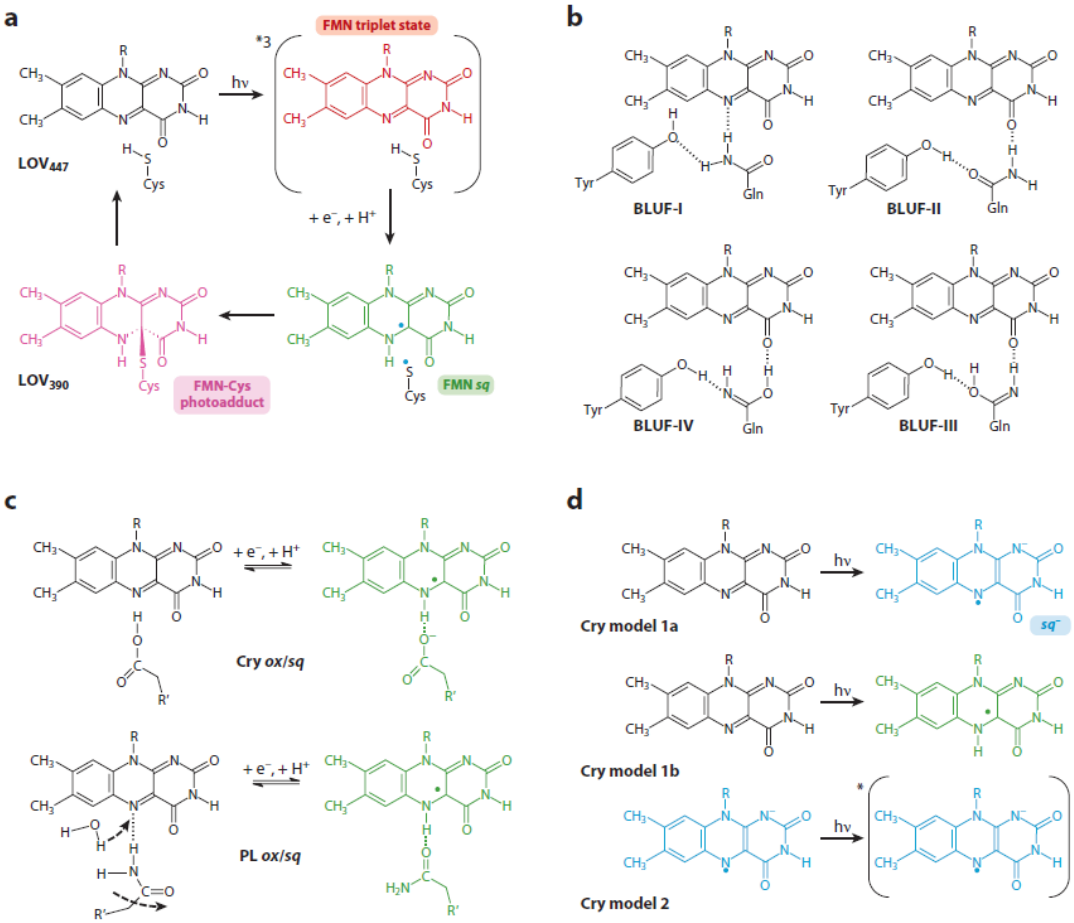

Figure 1.6 Proposed mechanisms of action of A) LOV, B) BLUF, C) plant cryptochromes and photolyases, and D) cryptochrome proteins insects. Taken from Losi *et al*.[38]

This biophysical process of excited state proton transfers has been observed in model systems and small proteins, such as malonaldehyde, green fluorescent protein, and flavin-dependent photoreceptors by using NMR, isotopic replacement, or fluorescence. The consistent

synopsis for this phenomenon to occur was the presence of an ionizable fluorophore and a proton donor/acceptor. Although not classified as a flavin-dependent photoreceptor, CHO was used to investigate excited state reactions of the flavin cofactor in the absence of active site ligands or substrates.

1.6 Mechanistic and Structural Studies of Nitronate Monooxygenase

Nitronate monooxygenase from *Cyberlindnera saturnus* (CsNMO) has been biochemically characterized using various alkyl nitronate compounds as substrates to better understand the mechanism for enzymatic catalysis.[57, 58] The enzyme from *C. saturnus* (previously *Hansenula mrakii* and then *Williopsis saturnus*) was observed to catalyze the oxidation of nitronates as evidence of oxygen consumption and anaerobic reduction with alkyl nitronates from 2-6 carbon chain lengths.[57] The physiological substrate of NMO enzymes was recently shown to be propionate 3-nitronate (P3N) in the study conducted by Francis *et al*.[59] P3N is a highly toxic nitro aliphatic compound that has been shown to poison livestock and humans and in extreme cases even cause death.[59, 60] The conjugate base of 3-nitropropionate, P3N, is formed through a slow deprotonation at the alpha carbon position which has a pK_a of ~9.1 (Scheme 1.4).[61] NMOs have been observed to oxidize P3N to product using a single electron transfer mechanism with k_{cat} and k_{cat}/K_m values of >1000 s^{-1} and $\geq 10^6$ $M^{-1}s^{-1}$, respectively, at atmospheric oxygen.[58, 59, 62] Evidence of a single electron transfer mechanism comes from the formation of the red anionic semiquinone when the enzyme is mixed with P3N in the absence of oxygen (Figure 1.7).[58, 62] Research published in this dissertation has advanced the working knowledge of NMOs as a family of enzymes, the understanding of enzymatic catalysis using single-electron transfers, and the oxidation of the toxin, P3N.

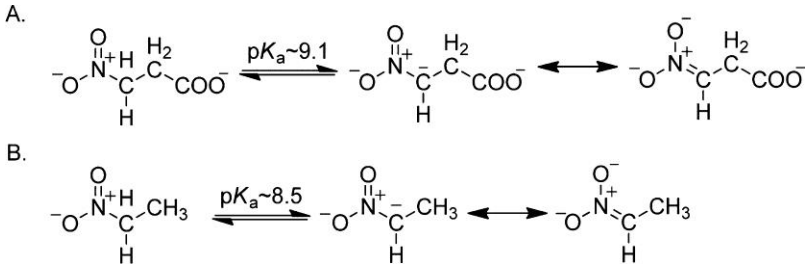

Scheme 1.1 A) Ionization of 3-NPA (left) to yield P3N (right); B) Ionization of nitroethane (left) to yield EN (right). Taken from Francis *et al.*[60]

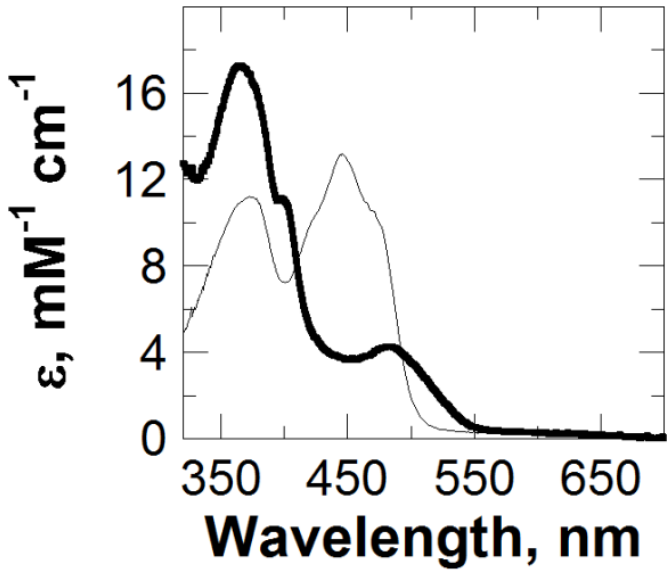

Figure 1.7 Comparison of the UV-vis absorbance spectra of the oxidized enzyme (thin curve) and the semiquinone state (thick curve) of CsNMO after complete depletion of oxygen due to enzyme turnover. Taken from Smitherman and Gadda.[58]

Over 4000 genes are currently annotated as NMOs using amino acid sequence alignments while less than 1% are annotated as NMOs based on biochemical experimental evidence.[62, 63] The rate of genome sequencing being exponentially faster than biochemical characterizations has led to a large discrepancy between the amount of sequences analyzed and the corresponding biochemical studies for each gene product. Computational techniques (Clustal Omega, BlastP) have advanced the processing of sequence analyses turning the process into a high through-put screening process. Developing high through-put assays for the biochemical characterizations of

gene products have not evolved at the same rate. However, identifying conserved consensus motifs in proteins of known structure and biochemical function would expedite the classification of annotating gene products. A study in 2014 has been published using a combined technique of identifying a minimal number of amino acid sequence similarities alongside biochemical characterization and identified 4 consensus sequences (Motifs I-IV) that categorized a new class of NMO enzymes (Figure 1.8).[62] The structural-functional approach of using the recently crystallized enzyme of known biological function, NMO from *Pseudomonas aeruginosa* (PaNMO), has created a better prediction of function based on the conserved sequences.[62] From the study published by Salvi *et al*, 475 of the more than 4000 originally annotated NMO gene products have been identified as containing these conserved sequences and have been grouped into the new Class I NMO family.[62] NMO enzymes that have been biochemically characterized in Class I oxidize P3N through the formation of the anionic flavin semiquinone.[62] The majority of the amino acid sequences annotated as Class I are from bacterial and fungal sources, which may suggest a conserved physiological role in detoxification of P3N or another conserved, yet unknown, function.

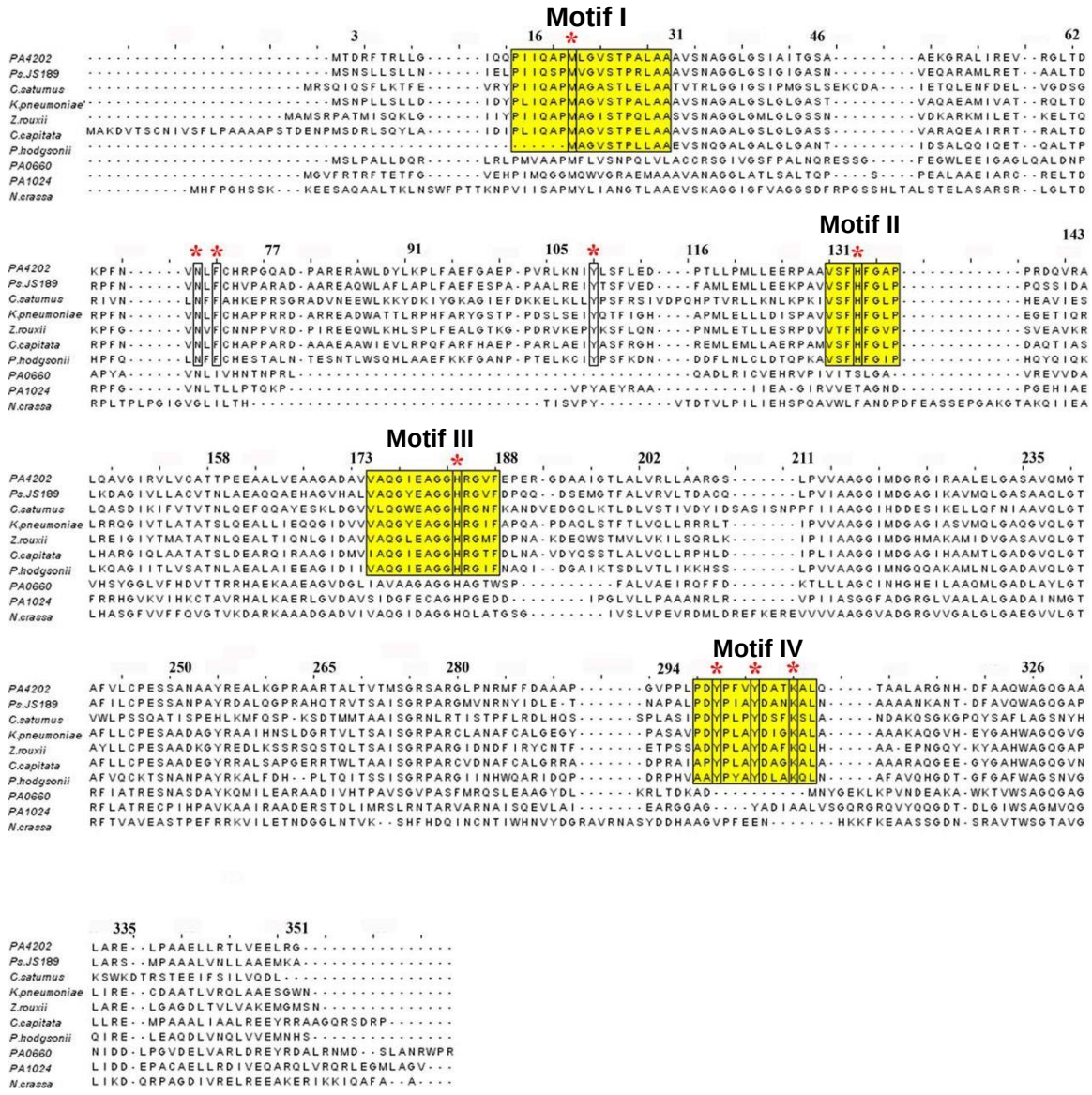

Figure 1.8 Multiple sequence alignment of protein sequences annotated as NMO enzymes including the enzyme of focus in this dissertation, CsNMO. Taken from Salvi *et al*.[62]

A second class of NMO enzymes (i.e. Class II) was determined from the study in 2014 by Salvi *et al.* consisting of NMO from *Neurospora crassa* (NcNMO) and nine other fungal genes annotated as NMOs.[62] These gene products contained only two of the four conserved sequences (Motifs I and III). Only one NMO enzyme has been biochemically characterized in Class II, NcNMO, which can oxidize both nitroalkanes and alkyl nitronate compounds.[64, 65] NcNMO has a catalytic base in the active site capable of deprotonating the α-carbon of nitroalkane

substrates.[66] Catalysis continues with a single electron transfer from the enzymatically formed alkyl nitronate.[65, 67] NcNMO has also been shown to carry out single-electron transfers with alkyl nitronate compounds as suggested by of steady-state kinetics and anaerobic substrate reduction.[66] Site-directed mutagenesis has been carried out on NcNMO in which H196 has been mutated to asparagine; it was concluded that the histidine residue was likely the catalytic base involved in proton abstraction of the nitroalkane substrates.[66] This histidine residue is shown to be fully conserved among all genes annotated as NMOs, Class I and Class II inclusive.[62] However, the histidine residue has been eliminated as a catalytic base in the CsNMO and PaNMO enzymes because of the lack of activity of either enzyme with nitroalkanes.[57, 58, 62] Nonetheless, the histidine residue is proposed to be involved in other aspects of catalysis in Class I enzymes (i.e. electrostatic catalysis).[58]

1.7 Specific Goals

The dissertation aims to investigate the roles of histidine residues in select flavoprotein oxidases and the kinetic mechanism of NMOs in the detoxification of P3N to gain insight into single-electron transfers of monooxygenases. Two flavin-dependent enzymes are chosen as model systems to investigate the two-fold study, nitronate monooxygenase from *Cyberlindnera saturnus* (CsNMO) and choline oxidase from *Arthobacter globiformis* (CHO). CHO contains an active site with two histidine residues that exhibit multiple roles throughout catalysis and substrate binding.[13, 14, 21, 33] The oxidation of choline to glycine betaine is catalyzed by CHO through two redox reactions in which an active site base has been shown to be required for both reactions.[28] Most of the active site residues of CHO have been identified and thoroughly characterized except for the identification of a catalytic base resolved later in the dissertation. The active site base is responsible for activating the substrate through proton removal at the

hydroxyl group which triggers a hydride transfer from the alpha carbon to the N(5) atom of the flavin. Betaine aldehyde, product of the first redox reaction with choline and CHO, is further oxidized to glycine betaine through general base catalysis too.[68] The enzymatic production of glycine betaine by CHO is of great interest to agricultural and biotechnology fields due to the effects of glycine betaine on controlling the osmotic pressure in the cell.

The second specific aim charges to understand the radical mechanism that nitronate monooxygenase (NMO) employs on detoxifying the cells in protection against propionate 3-nitronate (P3N). P3N has been observed to irreversibly inhibit succinate dehydrogenase, an enzyme of the Krebs cycle and oxidative phosphorylation, through the formation of an irreversible covalent adduct.[73-74] Toxicity of P3N has affected livestock and humans across the United States, Australia, and China.[74] At low levels of P3N poisoning side effects have been shown to include, but not limited to, the same or similar effects of Parkinson's disease and degradation of the organisms' neurological system.[74] Identifying the products of P3N oxidation by NMO enzymes and the mechanism by which the enzyme employs would provide useful insight into single-electron transfer mechanisms of monooxygenases and by alleviating the toxic effects of this compound in poisoned animals and humans. The single-electron transfer mechanism of a flavin-dependent monooxygenase will provide insight into the flavin chemistry field that has otherwise observed covalent adduct formation as a means of catalysis in monooxygenase enzymes.

1.8 References

1. Bacher, A., Eberhardt, S., Fischer, M., Kis, K., and Richter, G. (2000) Biosynthesis of vitamin b2 (riboflavin), *Annu. Rev. Nutr. 20*, 153-167.

2. Fischer, M., and Bacher, A. (2008) Biosynthesis of vitamin B2: Structure and mechanism of riboflavin synthase, *Arch. Biochem. Biophys.474*, 252-265.

3. Efimov, I., Kuusk, V., Zhang, X., and McIntire, W. S. (1998) Proposed steady-state kinetic mechanism for *Corynebacterium ammoniagenes* FAD synthetase produced by *Escherichia coli*, *Biochemistry 37*, 9716-9723.

4. Manstein, D. J., and Pai, E. F. (1986) Purification and characterization of FAD synthetase from *Brevibacterium ammoniagenes*, *J. Biol. Chem. 261*, 16169-16173.

5. Wu, M., Repetto, B., Glerum, D. M., and Tzagoloff, A. (1995) Cloning and characterization of FAD1, the structural gene for flavin adenine dinucleotide synthetase of *Saccharomyces cerevisiae, Mol. Cell. Biol. 15*, 264-271.

6. Medina, M. (2013) Enzymes of FMN and FAD Metabolism, In *Handbook of Flavoproteins: Volume 1 Oxidases, Dehydrogenases, and Related Systems* (Hille, R., Miller, S., and Palfey, B., Eds.), Walter de Gruyter.

7. Gibson, Q. H., Swoboda, B. E., and Massey, V. (1964) Kinetics and mechanism of action of glucose oxidase, *J. Biol. Chem. 239*, 3927-3934.

8. Wohlfahrt, G., Trivic, S., Zeremski, J., Pericin, D., and Leskovac, V. (2004) The chemical mechanism of action of glucose oxidase from *Aspergillus niger*, *Mol. Cell Biochem. 260*, 69-83.

9. Yagi, K., Ohishi, N., Nishimoto, K., Choi, J. D., and Song, P. S. (1980) Effect of hydrogen bonding on electronic spectra and reactivity of flavins, *Biochemistry 19*, 1553-1557.

10. Weber, G., and Farris, F. J. (1979) Synthesis and spectral properties of a hydrophobic fluorescent probe: 6-propionyl-2-(dimethylamino)naphthalene, *Biochemistry 18*, 3075-3078.

11. Kotaki, A., and Yagi, K. (1970) Fluorescence properties of flavins in various solvents, *J. Biochem. (Tokyo) 68*, 509-516.

12. Orville, A. M., Lountos, G. T., Finnegan, S., Gadda, G., and Prabhakar, R. (2009) Crystallographic, spectroscopic, and computational analysis of a flavin C4a-oxygen adduct in choline oxidase, *Biochemistry 48*, 720-728.

13. Ghanem, M., and Gadda, G. (2005) On the catalytic role of the conserved active site residue His466 of choline oxidase, *Biochemistry 44*, 893-904.

14. Rungsrisuriyachai, K., and Gadda, G. (2008) On the role of histidine 351 in the reaction of alcohol oxidation catalyzed by choline oxidase, *Biochemistry 47*, 6762-6769.

15. Quaye, O., Lountos, G. T., Fan, F., Orville, A. M., and Gadda, G. (2008) Role of Glu312 in binding and positioning of the substrate for the hydride transfer reaction in choline oxidase, *Biochemistry 47*, 243-256.

16. Quaye, O., Cowins, S., and Gadda, G. (2009) Contribution of flavin covalent linkage with histidine 99 to the reaction catalyzed by choline oxidase, *J. Biol. Chem. 284*, 16990-16997.

17. Pennati, A., and Gadda, G. (2009) Involvement of ionizable groups in catalysis of human liver glycolate oxidase, *J. Biol. Chem. 284*, 31214-31222.

18. Stockman, B. J., Richardson, T. E., and Swenson, R. P. (1994) Structural changes caused by site-directed mutagenesis of tyrosine-98 in *Desulfovibrio vulgaris* flavodoxin

delineated by 1H and 15N NMR spectroscopy: implications for redox potential modulation, *Biochemistry 33*, 15298-15308.

19. Satoh, T., Satoh, H., Iwahara, S., Hrkal, Z., Peyton, D. H., and Muller-Eberhard, U. (1994) Roles of heme iron-coordinating histidine residues of human hemopexin expressed in baculovirus-infected insect cells, *Proc. Natl. Acad. Sci. USA 91*, 8423-8427.
20. Genest, M., and Ptak, M. (1982) Interactions between Asp, His, Ser residues within models of the active site of serine proteases. A theoretical empirical study, *Int. J. Pept. Protein Res. 19*, 420-431.
21. Smitherman, C., Rungsrisuriyachai, K., Germann, M. W., and Gadda, G. (2015) Identification of the catalytic base for alcohol activation in choline oxidase, *Biochemistry 54*, 413-421.
22. Romero, E., and Gadda, G. (2014) Alcohol oxidation by flavoenzymes, *Biomol. Concepts 5*, 299-318.
23. Leskovac, V., Trivic, S., Wohlfahrt, G., Kandrac, J., and Pericin, D. (2005) Glucose oxidase from *Aspergillus niger*: the mechanism of action with molecular oxygen, quinones, and one-electron acceptors, *Int. J. Biochem. Cell Biol. 37*, 731-750.
24. Wongnate, T., and Chaiyen, P. (2013) The substrate oxidation mechanism of pyranose 2-oxidase and other related enzymes in the glucose-methanol-choline superfamily, *FEBS J. 280*, 3009-3027.
25. Roth, J. P., and Klinman, J. P. (2003) Catalysis of electron transfer during activation of O2 by the flavoprotein glucose oxidase, *Proc. Natl. Acad. Sci. USA 100*, 62-67.

26. Jorns, M. S., Chen, Z. W., and Mathews, F. S. (2010) Structural characterization of mutations at the oxygen activation site in monomeric sarcosine oxidase, *Biochemistry 49*, 3631-3639.

27. Zhao, G., Song, H., Chen, Z. W., Mathews, F. S., and Jorns, M. S. (2002) Monomeric sarcosine oxidase: role of histidine 269 in catalysis, *Biochemistry 41*, 9751-9764.

28. Fan, F., and Gadda, G. (2005) On the catalytic mechanism of choline oxidase, *J. Amer. Chem. Soc. 127*, 2067-2074.

29. Yuan, H., and Gadda, G. (2011) Importance of a serine proximal to the C(4a) and N(5) flavin atoms for hydride transfer in choline oxidase, *Biochemistry 50*, 770-779.

30. Salvi, F., Wang, Y. F., Weber, I. T., and Gadda, G. (2014) Structure of choline oxidase in complex with the reaction product glycine betaine, *Acta Crystallogr. Sect. D: Biol. Crystallogr. 70*, 405-413.

31. Quaye, O., and Gadda, G. (2009) Effect of a conservative mutation of an active site residue involved in substrate binding on the hydride tunneling reaction catalyzed by choline oxidase, *Arch. Biochem. Biophys. 489*, 10-14.

32. Quaye, O., Nguyen, T., Gannavaram, S., Pennati, A., and Gadda, G. (2010) Rescuing of the hydride transfer reaction in the Glu312Asp variant of choline oxidase by a substrate analogue, *Arch. Biochem. Biophys. 499*, 1-5.

33. Ghanem, M., and Gadda, G. (2006) Effects of reversing the protein positive charge in the proximity of the flavin N(1) locus of choline oxidase, *Biochemistry 45*, 3437-3447.

34. Sun, M., Moore, T. A., and Song, P.-S. (1971) Molecular luminescence studies of flavins. I. The excited states of flavins., *J. Amer. Chem. Soc. 94*, 1730-1740.

35. Song, P. S., and Kurtin, W. E. (1969) The charge distribution in the excited states of some indoles, *Photochem. Photobiol. 9*, 175-177.

36. Salzmann, S., and Marian, C. M. (2008) Effects of protonation and deprotonation on the excitation energies of lumiflavin, *Chem. Physics Lett. 463*, 400-404.

37. Schulman, S. G. (1971) pH dependence of fluorescence of riboflavin and related isoalloxazine derivatives, *J. Pharm. Sci. 60*, 628-631.

38. Losi, A., and Gartner, W. (2012) The evolution of flavin-binding photoreceptors: an ancient chromophore serving trendy blue-light sensors, *Annu. Rev. Plant Biol. 63*, 49-72.

39. Song, P. S., and Kurtin, W. E. (1969) The nature of the triplet states of flavins: a further study, *Photochem. Photobiol. 10*, 211-214.

40. Song, P.-S., Sun, M., Koziolowa, A., and Koziol, J. (1973) Phototautomerism of lumichromes and alloxazines, *J. Am. Chem. Soc. 96*, 4319-4323.

41. Christie, J. M., Salomon, M., Nozue, K., Wada, M., and Briggs, W. R. (1999) LOV (light, oxygen, or voltage) domains of the blue-light photoreceptor phototropin (nph1): binding sites for the chromophore flavin mononucleotide, *Proc. Natl. Acad. Sci. USA 96*, 8779-8783.

42. Song, P. S., Sun, M., Koziolow, A., and Koziol, J. (1973) Phototautomerism of lumichromes and alloxazines, *J. Amer. Chem. Soc. 96*, 4319-4323.

43. Christie, J. M., Blackwood, L., Petersen, J., and Sullivan, S. (2015) Plant flavoprotein photoreceptors, *Plant Cell Physiol. 56*, 401-413.

44. Zoltowski, B. D., and Gardner, K. H. (2011) Tripping the light fantastic: blue-light photoreceptors as examples of environmentally modulated protein-protein interactions, *Biochemistry 50*, 4-16.

45. Zoltowski, M. (2011) Insight into DNA periodicity by a single-channel sequence data approach, *Conference proceedings : ... Annual International Conference of the IEEE Engineering in Medicine and Biology Society. IEEE Engineering in Medicine and Biology Society. Annual Conference 2011*, 2438-2441.

46. Somers, D. E., Schultz, T. F., Milnamow, M., and Kay, S. A. (2000) ZEITLUPE encodes a novel clock-associated PAS protein from *Arabidopsis*, *Cell 101*, 319-329.

47. Takemiya, A., Inoue, S., Doi, M., Kinoshita, T., and Shimazaki, K. (2005) Phototropins promote plant growth in response to blue light in low light environments, *Plant Cell 17*, 1120-1127.

48. Kong, S. G., Suetsugu, N., Kikuchi, S., Nakai, M., Nagatani, A., and Wada, M. (2013) Both phototropin 1 and 2 localize on the chloroplast outer membrane with distinct localization activity, *Plant Cell Physiol. 54*, 80-92.

49. Salomon, M., Christie, J. M., Knieb, E., Lempert, U., and Briggs, W. R. (2000) Photochemical and mutational analysis of the FMN-binding domains of the plant blue light receptor, phototropin, *Biochemistry 39*, 9401-9410.

50. Swartz, T. E., Corchnoy, S. B., Christie, J. M., Lewis, J. W., Szundi, I., Briggs, W. R., and Bogomolni, R. A. (2001) The photocycle of a flavin-binding domain of the blue light photoreceptor phototropin, *J. Biol. Chem. 276*, 36493-36500.

51. Pudasaini, A., El-Arab, K. K., and Zoltowski, B. D. (2015) LOV-based optogenetic devices: light-driven modules to impart photoregulated control of cellular signaling, *Front. Mol. Biosci. 2*, 18.

52. Ahmad, M., and Cashmore, A. R. (1993) HY4 gene of *A. thaliana* encodes a protein with characteristics of a blue-light photoreceptor, *Nature 366*, 162-166.

53. Young, M. W., and Kay, S. A. (2001) Time zones: a comparative genetics of circadian clocks., *Nat. Rev. Genet. 2*, 702-715.

54. Chaves, I., Pokorny, R., Byrdin, M., Hoang, N., Ritz, T., Brettel, K., Essen, L. O., van der Horst, G. T., Batschauer, A., and Ahmad, M. (2011) The cryptochromes: blue light photoreceptors in plants and animals, *Annu. Rev. Plant Biol. 62*, 335-364.

55. Hoang, N., Bouly, J. P., and Ahmad, M. (2008) Evidence of a light-sensing role for folate in Arabidopsis cryptochrome blue-light receptors, *Mol. Plant 1*, 68-74.

56. Fogle, K. J., Parson, K. G., Dahm, N. A., and Holmes, T. C. (2011) CRYPTOCHROME is a blue-light sensor that regulates neuronal firing rate, *Science 331*, 1409-1413.

57. Mijatovic, S., and Gadda, G. (2008) Oxidation of alkyl nitronates catalyzed by 2-nitropropane dioxygenase from *Hansenula mrakii*, *Arch. Biochem. Biophys. 473*, 61-68.

58. Smitherman, C., and Gadda, G. (2013) Evidence for a transient peroxynitro acid in the reaction catalyzed by nitronate monooxygenase with propionate 3-nitronate, *Biochemistry 52*, 2694-2704.

59. Francis, K., Nishino, S. F., Spain, J. C., and Gadda, G. (2012) A novel activity for fungal nitronate monooxygenase: detoxification of the metabolic inhibitor propionate-3-nitronate, *Arch. Biochem. Biophys. 521*, 84-89.

60. Francis, K., Smitherman, C., Nishino, S. F., Spain, J. C., and Gadda, G. (2013) The biochemistry of the metabolic poison propionate 3-nitronate and its conjugate acid, 3-nitropropionate, *IUBMB Life 65*, 759-768.

61. Bush, M. T., Touster, O., and Brockman, J. E. (1951) The production of beta-nitropropionic acid by a strain of *Aspergillus flavus*, *J. Biol. Chem. 188*, 685-693.

62. Salvi, F., Agniswamy, J., Yuan, H., Vercammen, K., Pelicaen, R., Cornelis, P., Spain, J. C., Weber, I. T., and Gadda, G. (2014) The combined structural and kinetic characterization of a bacterial nitronate monooxygenase from *Pseudomonas aeruginosa* PAO1 establishes NMO class I and II, *J. Biol. Chem. 289*, 23764-23775.

63. Anton, B. P., Chang, Y. C., Brown, P., Choi, H. P., Faller, L. L., Guleria, J., Hu, Z., Klitgord, N., Levy-Moonshine, A., Maksad, A., Mazumdar, V., McGettrick, M., Osmani, L., Pokrzywa, R., Rachlin, J., Swaminathan, R., Allen, B., Housman, G., Monahan, C., Rochussen, K., Tao, K., Bhagwat, A. S., Brenner, S. E., Columbus, L., de Crecy-Lagard, V., Ferguson, D., Fomenkov, A., Gadda, G., Morgan, R. D., Osterman, A. L., Rodionov, D. A., Rodionova, I. A., Rudd, K. E., Soll, D., Spain, J., Xu, S. Y., Bateman, A., Blumenthal, R. M., Bollinger, J. M., Chang, W. S., Ferrer, M., Friedberg, I., Galperin, M. Y., Gobeill, J., Haft, D., Hunt, J., Karp, P., Klimke, W., Krebs, C., Macelis, D., Madupu, R., Martin, M. J., Miller, J. H., O'Donovan, C., Palsson, B., Ruch, P., Setterdahl, A., Sutton, G., Tate, J., Yakunin, A., Tchigvintsev, D., Plata, G., Hu, J., Greiner, R., Horn, D., Sjolander, K., Salzberg, S. L., Vitkup, D., Letovsky, S., Segre, D., DeLisi, C., Roberts, R. J., Steffen, M., and Kasif, S. (2013) The COMBREX project: design, methodology, and initial results, *PLoS biology 11*, e1001638.

64. Francis, K., Russell, B., and Gadda, G. (2005) Involvement of a flavosemiquinone in the enzymatic oxidation of nitroalkanes catalyzed by 2-nitropropane dioxygenase, *J. Biol. Chem. 280*, 5195-5204.

65. Rungsrisuriyachai, K., and Gadda, G. (2010) Role of asparagine 510 in the relative timing of substrate bond cleavages in the reaction catalyzed by choline oxidase, *Biochemistry 49*, 2483-2490.

66. Francis, K., and Gadda, G. (2008) The nonoxidative conversion of nitroethane to ethylnitronate in *Neurospora crassa* 2-nitropropane dioxygenase is catalyzed by histidine 196, *Biochemistry 47*, 9136-9144.

67. Francis, K., and Gadda, G. (2006) Probing the chemical steps of nitroalkane oxidation catalyzed by 2-nitropropane dioxygenase with solvent viscosity, pH, and substrate kinetic isotope effects, *Biochemistry 45*, 13889-13898.

68. Fan, F., Germann, M. W., and Gadda, G. (2006) Mechanistic studies of choline oxidase with betaine aldehyde and its isosteric analogue 3,3-dimethylbutyraldehyde, *Biochemistry 45*, 1979-1986.

2 Evidence for a Transient Peroxynitro Acid in the Reaction Catalyzed by Nitronate Monooxygenase with Propionate 3-Nitronate

(This chapter has been published verbatim in Smitherman, C. and Gadda, G. (2013), *Biochemistry* 52(15): 2694-704.)

2.1 Abstract

Nitronate monooxygenase is a flavin-dependent enzyme that catalyzes the denitrification of propionate 3-nitronate (P3N) and other alkyl nitronates. The enzyme was previously known as 2-nitropropane dioxygenase, until its reclassification in 2010 by the IUBMB. Physiologically, the monooxygenase from fungi protects the organism from the environmental occurrence of P3N, which shuts down the Krebs cycle by inactivating succinate dehydrogenase and fumarase. The inhibition of these enzymes yields severe neurological disorders or death. Here, we have used for the first time steady-state and rapid kinetics, viscosity and pH effects, and time-resolved absorbance spectroscopy of the enzyme in turnover with P3N and the substrate analogue ethyl nitronate (EN) to elucidate the mechanism of the reaction. A transient increase in absorbance at ~300 nm, never reported before, was seen during steady-state turnover of the enzyme with P3N and oxygen, with no concomitant changes between 400 and 600 nm. The transient species was not detected when oxygen was absent. Anaerobic reduction of the enzyme with P3N yielded anionic flavosemiquinone and was fast (e.g., ≥1900 s^{-1}). Steady-state kinetics demonstrated that oxygen reacts before the release of the product of P3N oxidation from the enzyme. No pH effects were seen with P3N on k_{cat}/K_m, k_{cat}/K_{oxygen}, and k_{cat}; in contrast, with EN, the k_{cat}/K_m and k_{cat} decreased with increasing pH defining two plateaus and a pK_a ~ 8.0. Solvent viscosity at the pH optima suggested product release as being partially controlling the overall

rate of turnover with the physiological substrate and its analogue. A mechanism that satisfies the kinetic results is proposed.

2.2 Introduction

Nitronate monooxygenase (NMO, E.C. 1.13.12.16) is an FMN-dependent enzyme that catalyzes the oxidative denitrification of alkyl nitronates and the nitro acid propionate 3-nitronate (P3N) through the formation of an anionic flavosemiquinone.[1, 2] The enzyme was known as 2-nitropropane dioxygenase until 2010 when the IUBMB reclassified it. NMO has been characterized biochemically and kinetically in fungi, mostly *Neurospora crassa* and, to a lesser extent, *Williopsis saturnus var. Mrakii*.[1-7] The three-dimensional structure of the enzyme from *Pseudomonas aeruginosa* is available to a resolution of 2.3 Å.[8] However, the bacterial and fungal enzymes share less than 5% sequence identity,[1] precluding structural–functional studies beyond the identification of a fully conserved histidine residue in the active site of the enzyme. In the enzyme from *N. crassa*, replacement of the conserved histidine with asparagine abolishes the ability in catalysis to utilize nitroalkanes, i.e., the conjugated acid forms of nitronates.[5] The role of the conserved histidine in the active site of the *W. saturnus* NMO is not obvious, since the enzyme can only utilize nitronates as substrates, but not nitroalkanes.[2]

The physiological role of NMO had remained elusive for decades until recent *in vivo* studies with a knockout mutant of *N. crassa* and a recombinant strain of *Escherichia coli* containing the gene encoding NMO demonstrated that the enzyme exerts a protective action from the environmental occurrence of the metabolic toxin P3N.[7] The toxicity of P3N, which is the conjugate base of 3-nitropropionic acid, arises from its ability to form an irreversible covalent adduct with succinate dehydrogenase, rendering the enzyme and the Krebs cycle completely inactive.[9-11] P3N is also a transition state analogue of fumarase.[12] The inhibition of

these essential metabolic enzymes by P3N results in severe neurological disorders[13-15] and even death,[16, 17] with several cases of P3N poisoning reported in livestock and hundreds of deaths in humans.[18-20] In small quantities (e.g., 20 mg/kg), P3N is routinely used to induce symptoms that mimic Huntington's disease in animal models to develop and test treatments for the disease.[21-23]

The oxidation of alkyl nitronates by NMO has been previously studied using the recombinant enzyme from *N. crassa* expressed in *E. coli* and ethyl nitronate (EN) as substrate.[3, 5, 6, 24] Enzymatic turnover begins with the transfer of a single electron from the nitronate to the enzyme-bound FMN, yielding an anionic flavosemiquinone, as indicated by anaerobic rapid reaction data in a stopped-flow spectrophotometer.[4] The subsequent oxidation of the flavosemiquinone restores the oxidized flavin and generates a highly reactive superoxide anion, with a second-order rate constant k_{cat}/K_{oxygen} of 6 × 106 M–1 s–1 (pH 6.0 and 30 °C).[4] The EN radical and superoxide anion have been proposed to collapse in the active site of the enzyme to form α-peroxynitroethane.[3, 4] This would then decay through the effect of a nucleophile to form nitrite and acetaldehyde either on the enzyme or in solution. Evidence for the proposed radical recombination comes from the observation of an inverse α-secondary kinetic isotope effect of 0.76 on the k_{cat}/K_m with [1-2H]-EN at atmospheric oxygen, which is consistent with a change in hybridization of the α-carbon atom of the EN radical from sp2 to sp3.[3] However, direct experimental evidence for the transient formation of α-peroxynitroethane has yet to become available. With nitroethane as substrate, enzymatic catalysis requires an extra deprotonation step catalyzed by His196 (*N. crassa* numbering), which activates the organic molecule for the subsequent one electron reaction with the flavin.[3-5] In the *N. crassa* NMO, steady-state kinetics is complicated by the partition of the EN–enzyme complex between oxidative and non-oxidative turnover due to the partial release of the EN from the enzyme active site as indicated by kinetic

isotope effects, mutagenesis, and colorimetric studies.[6] Presumably the oxidation of alkyl nitronates by the *W. saturnus* NMO occurs through a similar one electron chemistry involving the organic substrate and the flavin, since the anionic flavosemiquinone is stabilized upon mixing anaerobically the enzyme with various alkyl nitronates.[2] However, no detailed mechanistic studies have been performed on the latter enzyme. With both enzymes, hydrogen peroxide is not detected during turnover with various nitronates, consistent with NMO being a monooxygenase rather than an oxidase.[1] Neither of the fungal enzymes has been characterized with the physiological substrate P3N yet. In this regard, the *W. saturnus* NMO offers itself as the best candidate for such a study because it does not catalyze the reversible conversion of the nitronate to and from the nitroalkane, being active solely with the former but not the latter.[2]

In this study, we have used steady-state kinetics, solvent viscosity, pH effects, rapid-reaction kinetics, and time-resolved absorbance spectroscopy to investigate the mechanism of NMO from *W. saturnus* with its physiological substrate P3N. The substrate analogue EN, which lacks a carboxylate group, has also been used in this study.

2.3 Materials and methods

Materials. 3-Nitropropionic acid and nitroethane were from Sigma-Aldrich (St. Louis, MO). Recombinant NMO from *W. saturnus* was obtained through expression and purification methods previously described.[2] Similar to primary and secondary nitroalkanes the α-carbon of 3-nitropropionic acid has a pK_a of ~9.1, allowing for a slow deprotonation with a strong base (Scheme 1).[25] P3N, the conjugate base of 3-nitropropionic acid, was therefore prepared in water by incubating the nitro compound with a 2.2 molar excess of KOH for 24 h at 4 °C. Addition of KOH was slow to avoid sample boiling and possible decomposition of P3N,[26] which was stable up to a week. EN was prepared in 100% ethanol as previously described[2] by incubating

nitroethane with a 1.2 molar excess of KOH for 24 h at room temperature. The final concentration of ethanol in each assay mixture was kept constant at 1% to minimize possible effects on enzymatic activity. All other reagents were of the highest purity commercially available.

Methods. Enzymatic activity of NMO was measured by monitoring the initial rate of oxygen consumption with a computer-interfaced Oxy-32 oxygen-monitoring system (Hansatech Instruments, Inc., Norfolk, England) at 30 or 7 °C. Initial rates of reaction were calculated based on the flavin bound to the enzyme, as established spectrophotometrically. The steady-state kinetic parameters were determined by varying the concentration of oxygen and P3N (or EN), with the enzyme being gel-filtered into 10% glycerol and 50 mM potassium phosphate, pH 7.4, using a PD-10 column immediately prior to the experiment. Assay reaction mixtures were equilibrated at the desired oxygen concentrations by bubbling with an O_2/N_2 gas mixture for at least 5 min before the reaction was started with the addition of the enzyme and the substrate. When atmospheric oxygen was used with EN, the assay reaction mixtures were equilibrated with air before the reaction was started. Since the second-order rate constants for protonation of the nitronates are in the range 15–75 M^{-1} s^{-1},[27] enzymatic activity assays were initiated with the addition of the nitronate to the reaction mixture to ensure that a negligible amount of the neutral species of the nitronate was present during the time required to acquire initial rates of reaction (typically ∼30 s).

The pH dependences of the steady-state kinetic parameters of the enzyme were determined as described above in the pH range between 5.5 and 11.0 in 50 mM sodium pyrophosphate at 30 °C, with the exception of pH 7.4 and 8.0 where 50 mM potassium phosphate was used. The effect of solvent viscosity on the steady-state kinetic parameters of the

enzyme was determined with glycerol as viscosigen and ≥91% oxygen saturation by bubbling with an O_2/N_2 gas mixture for at least 5 min (when necessary) at pH 6.5 with P3N as substrate and pH 5.5 or pH 11.0 with EN. The relative viscosities at 30 °C were calculated from the values at 20 °C reported by Lide.[28]

Time-resolved absorbance spectroscopy of NMO in turnover was determined with a Hi-Tech SF-61 stopped-flow spectrophotometer (TgK Scientific, United Kingdom) at 30 °C, using either a xenon lamp and a photodiode array detector or a deuterium lamp and a photomultiplier detector. NMO (10 μM final) was mixed with 1 mM P3N and 0.23 mM oxygen in 50 mM potassium phosphate, pH 7.4, and allowed to turn over while acquiring 300 absorbance spectra over 1.48 s in the range from 320 to 700 nm. To identify the λ_{max} and the time course for formation and decay of the transient species observed during turnover, the experiment was repeated using the same conditions. A deuterium lamp source was used to monitor absorbance changes in the UV region and a photomultiplier detector, which allowed for acquisition of several data points in the first few milliseconds of the reaction. Single wavelength traces were acquired at 5 nm intervals from 260 to 380 nm with 8192 data points over 5 s. Using the Kinetic Studio software package of the stopped-flow instrument, the time-resolved absorbance spectra were compiled from the data points. The control experiment in the absence of oxygen was carried out in the same fashion, except the tonometer containing the enzyme was subjected to several cycles of flushing with oxygen-free argon and gas removal through applied vacuum. The syringe containing the substrate was flushed with oxygen-free argon for 20 min. Both the enzyme and substrate solutions contained a mixture of glucose (5 mM) and glucose oxidase (1 μM) as oxygen scavenger to ensure removal of trace amounts of lingering oxygen.

The reductive half-reaction of NMO with P3N was monitored using a Hi-Tech SF-61 stopped-flow spectrophotometer thermostated at 7 °C. Using a xenon lamp and photomultiplier mode, flavin reduction was established in the presence of 10% glycerol and 50 mM sodium pyrophosphate, pH 6.0, by monitoring the decrease in absorbance at 445 nm that results from the anaerobic mixing of the enzyme and substrate. An NMO solution was loaded into a tonometer and made anaerobic by a 20-cycle treatment of flushing with oxygen-free argon and gas removal by applying vacuum. The tonometer containing the anaerobic enzyme solution was mounted onto the stopped-flow instrument, which had been pretreated with an oxygen-scrubbing system composed of 5 mM glucose and 1 μM of glucose oxidase, which was also present in the tonometer. P3N was prepared in water and made anaerobic by flushing with oxygen-free argon for at least 20 min before mounting onto the stopped-flow spectrophotometer. Glucose/glucose oxidase was present in the substrate solution. After mixing in the stopped-flow spectrophotometer, the enzyme was ∼10 μM and the substrate was 100 μM, ensuring pseudo-first-order kinetics. The reductive half-reaction of NMO was also examined with EN as substrate at pH 6.0 and 7 °C. The substrate was prepared in water, with a 1:1 mol equivalents of KOH to avoid lingering of excess base in the solution. After mixing, the enzyme was 10 μM and the substrate between 0.8 and 42 mM. For each concentration of substrate, traces were recorded in triplicate, and the average value is reported (typically with variations ≤5%).

Data Analysis. Steady-state kinetic data were fit with KaleidaGraph (Synergy Software, Reading, PA) or Enzfitter (Biosoft, Cambridge, U.K.) software. Kinetic parameters determined with EN at atmospheric oxygen were obtained by fitting the data to the Michaelis–Menten equation for one substrate. In all cases, substrate concentrations were between 0.2 and 5 times K_m, ensuring accurate determinations of k_{cat} and k_{cat}/K_m values. When initial rates of

reaction were determined at varying concentrations of P3N and oxygen, the kinetic data were fit to eq 1, which describes a steady-state kinetic mechanism in which the second substrate (oxygen) reacts before the release of the organic product of the reaction from the enzyme. k_{cat} is the first-order rate constant for the reaction in the presence of saturating concentrations of P3N and oxygen, K_a and K_b are the Michaelis constants for P3N (A) and oxygen (B), K_{ia} is a kinetic constant that accounts for the intersecting line pattern in the double reciprocal plot, and *e* is the concentration of enzyme.

$$\frac{v_0}{e} = \frac{k_{cat}[A][B]}{K_a[B] + K_b[A] + [A][B] + K_{ia}K_b} \quad (1)$$

The values of eq 2 determined the corresponding pH dependencies with EN. Here, Y_H and $Y_L$are the limiting values at high and low pH of the parameter of interest, and K_a is the dissociation constant for relevant ionizable group(s).

$$\log Y = \log\left(\frac{Y_L + Y_H\left(\frac{10^{-pK_a}}{10^{-pH}}\right)}{1 + 10^{\frac{-pK_a}{-pH}}}\right) \quad (2)$$

The viscosity effects on the steady-state kinetic parameters of the enzyme with P3N or EN at pH 5.5 and 6.5 were fit with eq 3 and those with EN at pH 11.0 with eq 4. The kinetic parameters measured in the absence and presence of viscosigen are k_0 and k_η, respectively, *S* is the degree of viscosity dependence, η_{rel} is the relative viscosity of the buffered solution, and *A* and *B*are parameters required to describe the hyperbolic behavior of the observed effect.

$$\frac{k_o}{k_\eta} = S(\eta_{rel} - 1) + 1 \quad (3)$$

$$\frac{k_o}{k_\eta} = \frac{1}{1 + A\left(\frac{\eta_{rel-1}}{(\eta_{rel}-1)+B}\right)} \quad (4)$$

Stopped-flow traces for the reductive half-reaction were fit with eq 5, which describes a double-exponential process. The observed first-order rate constants associated with absorbance changes of the flavin are denoted by λ_1 and λ_2, the absorbance at 445 nm at any given time is represented by *A*, the amplitudes of the absorbance changes associated with the two phases are denoted *B* and *C*, the absorbance at infinite time is defined as *D*, and time is *t*. The phase exhibiting the most prominent amplitude values (≥85%) is indicated as λ_1 and was plotted as a function of substrate concentration using eq 6, where k_{red} is the limiting first-order rate constant for flavin reduction at saturating substrate concentrations, K_d is the apparent dissociation constant for substrate binding, and *S* is the concentration of the substrate.

$$A = Be^{(-\lambda_1 t)} + Ce^{(-\lambda_2 t)} + D \quad (5)$$

$$\lambda_1 = \frac{k_{red} S}{K_d + S} \quad (6)$$

2.4 Results

Time-Resolved Absorbance Spectroscopy of NMO in Turnover. As a first step toward the characterization of the W. saturnus NMO reaction with its physiological substrate P3N, time-resolved UV–vis absorbance spectra of the enzyme in turnover were monitored between 320 and 700 nm. The enzyme (10 μM) was allowed to turn over with 1 mM P3N and 0.23 mM oxygen. Data were acquired in a stopped-flow spectrophotometer equipped with a photodiode array detector at pH 7.4 and 30 °C. After an immediate decrease in absorbance at 445 nm from 0.137 to 0.040, occurring in the mixing time of the instrument (i.e., 2.2 ms), the enzyme was primarily present as an anionic flavosemiquinone during the first 8 ms in which the steady-state persisted (Figure 1A, B). A progressive decrease of absorbance at 445 nm occurred over longer times (Figure 1A–C), yielding a final absorbance spectrum with maxima at 365 and 483 nm (Figure 1D). Thus, the enzyme-bound flavin was reduced to the anionic flavosemiquinone upon complete depletion of oxygen from the reaction mixture. Based on the molar absorption of the oxidized flavin in the resting state,[(2)] the extinction coefficient of the anionic flavosemiquinone was calculated to be 17 300 M^{-1} cm^{-1} at 365 nm (Figure 1D). Interestingly, a transient increase in absorbance at 321 nm occurred within the first few milliseconds of reaction, while the enzyme was turning over with the flavin in steady state, before decreasing at longer times (Figure 1A). This suggested the formation and decay of a reaction intermediate not involving the flavin cofactor.

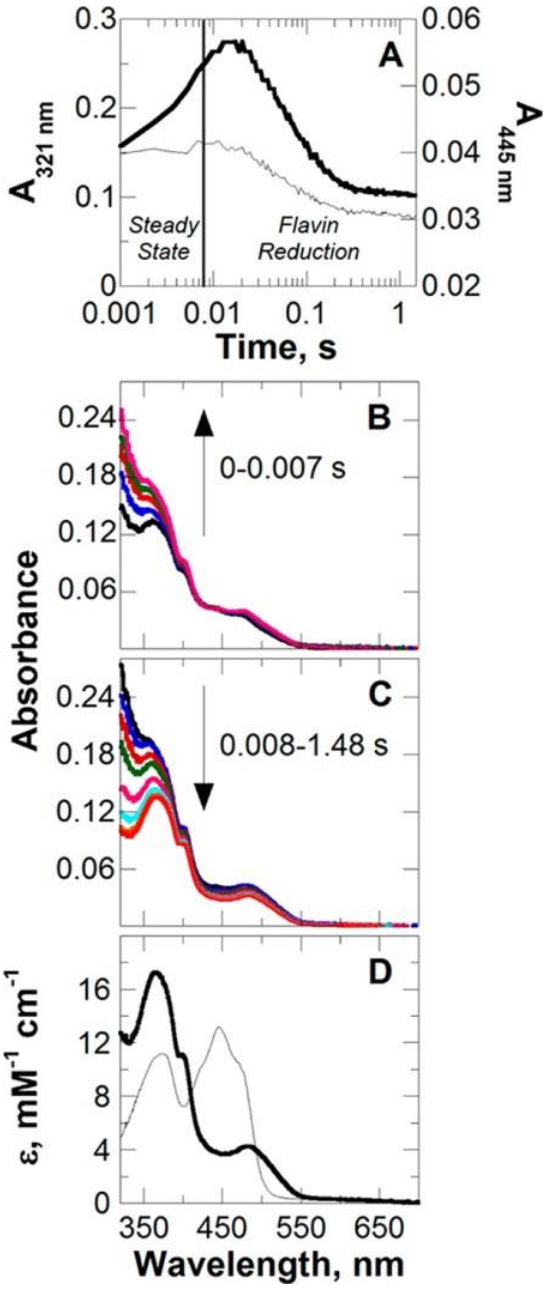

Figure 2.1 Time-resolved absorbance spectra of NMO (10 µM) in turnover with 1 mM P3N and 0.23 mM oxygen, in 50 mM potassium phosphate, pH 7.4 and 30 °C.

The enzyme was mixed aerobically with the substrate in a stopped-flow spectrophotometer equipped with with photomultiplier detector and a xenon lamp, and 300 absorbance spectra were acquired over a time of 1.48 s. All times indicated are after the end of flow, i.e., ~2.2 ms after mixing. Panel A: time course of the spectral changes at 321 nm (thick curve) and 445 nm (thin curve) associated with the absorbance spectra in panels B and C; note the log time for the *x*-axis; prior to mixing with substrates, the flavin absorbance at 445 nm was 0.137, as determined by mixing the resting oxidized enzyme with the reaction buffer in a 1:1 ratio. Time-resolved absorbance spectra are shown in panels B and C, where the arrows illustrate the direction of the spectral changes observed in the UV region. Panel D: comparison of the UV–vis absorbance spectra of the resting enzyme in the oxidized state (thin curve) and the semiquinone state (thick curve) obtained at 1.48 s, after complete depletion of oxygen due to enzyme turnover; note the *y*-axis in units of extinction coefficient rather than absorbance.

To determine the absorbance maximum of the transient species observed during turnover of NMO with P3N, the experiment was repeated using a monochromator and a photomultiplier detector. Single wavelength traces were acquired every 5 nm intervals from 260 to 380 nm. The time-resolved absorbance spectra were then compiled from these data points. The analysis of the absorbance spectra acquired within the first 8 ms of reaction was conducted after subtraction of the first UV–vis absorbance spectrum acquired in the stopped-flow spectrophotometer, i.e., before any transient increase in absorbance was observed. Spectral evidence showed that the reaction intermediate had maximal absorbance at ∼300 nm (Figure 2A). The time course at 300 nm confirmed the preliminary data obtained at 321 nm, with transient accumulation of the reaction intermediate within the first ∼8 ms of reaction and its disappearance within 0.1 s (Figure 2B). A control experiment in which the enzyme was allowed to react with P3N under the same conditions, but in the absence of oxygen, showed lack of transient changes in the trace at 300 nm (Figure 2B), and other wavelength between 260 and 360 nm (data not shown), consistent with oxygen being required for the transient accumulation of the reaction intermediate.

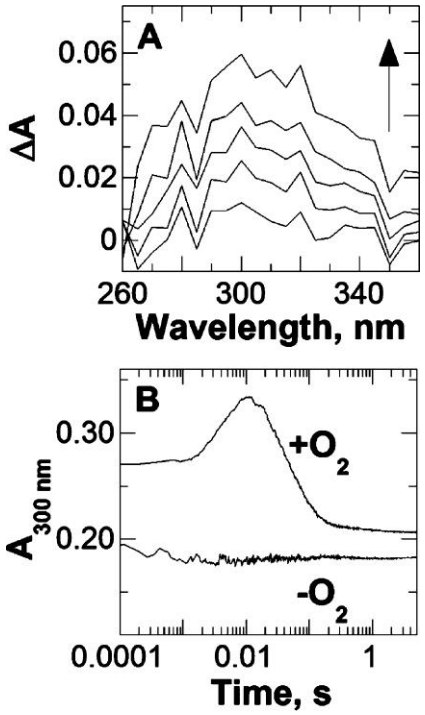

Figure 2.2 Time-resolved absorbance spectroscopy of NMO (10 μM) reacting with 1 mM P3N and presence and absence of 0.23 mM oxygen, in 50 mM potassium phosphate, pH 7.4 and 30 °C.
The enzyme was mixed aerobically with the substrate in a stopped-flow spectrophotometer equipped with the photomultiplier detector and deuterium lamp. Traces were recorded at 5 nm intervals from 260 to 360 nm and used to compile the time-resolved absorbance spectra. All times indicated are after the end of a flow, i.e., ~2.2 ms after mixing. Panel A: spectra compiled at 2, 3, 4, 6, and 8 ms from 260 to 365 nm are shown after subtraction of the initial absorbance spectrum at 0.02 ms, yielding the difference in absorbance spectra after the initial scan is observed. Panel B: time courses of the spectral changes at 300 nm in presence and absence of oxygen; note the log time scale.

Reductive Half-Reaction. The reductive half-reaction of NMO was investigated in a stopped-flow spectrophotometer at pH 6.0 and 7 °C by monitoring the loss of absorbance of the oxidized flavin at 445 nm upon mixing anaerobically the enzyme with P3N. Reactions with 100 μM P3N were completed within the mixing time of the instrument (i.e., 2.2 ms). The absorbance spectrum of the anionic flavosemiquinone was obtained at the end of the reduction (data not shown). With EN as reducing substrate, the traces at 445 nm displayed a biphasic pattern (Figure 3A), with the fast phase (λ_1) accounting for the majority of the $\Delta A_{445\ nm}$ (85%). The absorbance spectrum of the anionic flavosemiquinone was obtained at the end of the reduction (Figure 3A). A plot of λ_1 as a function of EN concentration yielded a hyperbola with zero *y*-

intercept, consistent with a negligible reverse reaction of flavin reduction (Figure 3B). The first-order rate constant for flavin reduction at saturating EN (k_{red}) was calculated to be 300 ± 20 s^{-1}, whereas the apparent K_d was 8 ± 2 mM. λ_2 had an average value of 27 ± 7 s^{-1}, which was independent of EN concentration (data not shown). This was possibly due to not fully functional enzyme resulting from the preparation of the anaerobic sample or release of the organic radical product of the reaction from the enzyme active site. Since the average value of λ_2 was lower than k_{cat} (see below), the slow phase seen in the stopped-flow spectrophotometer was not associated with a kinetic step that occurred in the normal catalytic pathway of the enzyme was not investigated further.

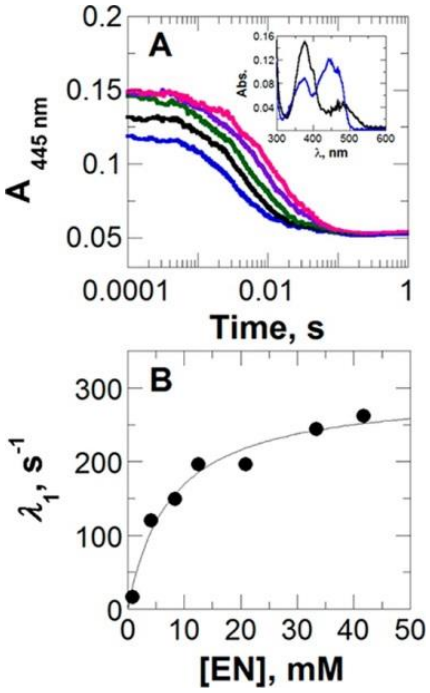

Figure 2.3 Anaerobic reduction of NMO with EN as substrate in 50 mM sodium pyrophosphate, pH 6.0, 7 °C, in the presence of 10% glycerol.
Panel A: selected traces of flavin reduction with 50 mM (blue), 25 mM (black), 15 mM (green), 10 mM (purple), and 5 mM (pink) EN. All traces were fit with eq 5. Time indicated is after the end of flow, i.e., ~2.2 ms after mixing. Note the log time scale. Inset: absorbances of the enzyme prior to (blue) and after reacting for 1 s with 15 mM EN. Panel B: observed rate constants for flavin reduction as a function of substrate concentration. Data fit with eq 6.

Steady-State Kinetic Mechanism. The steady-state kinetic mechanism of NMO was determined by measuring initial rates of oxygen consumption at varying concentrations of P3N and oxygen at pH 5.5 and 30 °C. As shown in Figure 4A, intersecting lines were obtained in a double reciprocal plot of the initial rate of reaction and the substrate concentration, consistent with the second substrate reacting before release of the first product of the reaction from the enzyme active site.[29] Accordingly, the data were fit best with eq 1, yielding the steady-state kinetic parameters listed in Table 1.

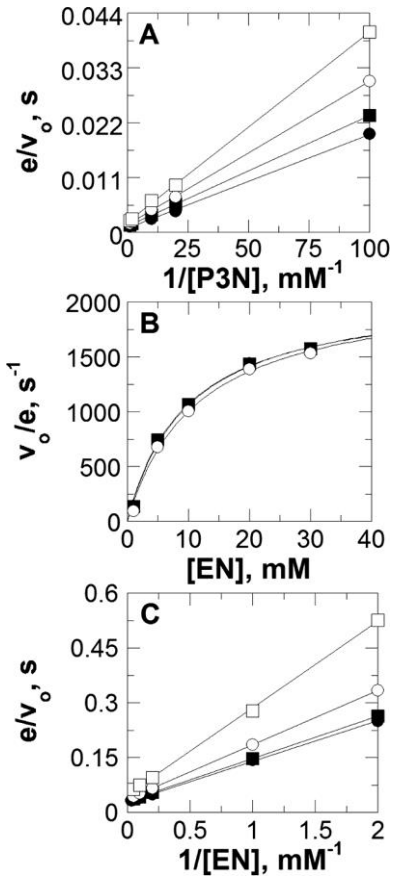

Figure 2.4 Steady-state kinetics of NMO with P3N or EN.
Panel A: double reciprocal plot of the initial rates of reaction versus [P3N] at pH 5.5 and 30 °C with fixed oxygen concentrations of 44 μM (□), 73 μM (○), 115 μM (■), and 145 μM (●). Panel B: plot of the initial rates of reaction versus [EN] at pH 5.5 and 30 °C with fixed oxygen concentrations of 11 μM (○), 40 μM (■), and 90 μM (●). Panel C: double reciprocal plot of the initial rates of reaction versus [EN] at pH 6.0 and 7 °C with fixed oxygen concentrations of 9 μM (□), 28 μM (○), 56 μM (■), and 230 μM (●), in the presence of 50 units of SOD. The lines in panels A and C represent the fit of the data with eq 1; the overlapping curves in panel B represent the fits of the data at each concentration of oxygen with the Michaelis–Menten equation for one substrate.

Table 2.1 Steady-state kinetic parameters of NMO from *W. saturnus*.

substrate	pH	T (°C)	k_{cat} (s^{-1})	K_m (mM)	k_{cat}/K_m (M^{-1} s^{-1})	K_{O_2} (μM)	k_{cat}/K_{O_2} (M^{-1} s^{-1})	K_{ia} (mM)
P3N[a,d]	5.5	30	860 ± 8	0.06 ± 0.01	(1.5 ± 0.3) × 10^7	80 ± 1	(1.1 ± 0.02) × 10^7	0.31 ± 0.01
EN[a,e]	5.5	30	4100 ± 200	20 ± 2	(3.0 ± 0.3) × 10^5			
EN[b,e]	8.0	30	840 ± 10	4.0 ± 0.1	(2.0 ± 0.1) × 10^5			
EN[c,e]	11.0	30	40 ± 2	10 ± 1	(4.1 ± 0.4) × 10^3			
EN[a,d,f]	6.0	7	40 ± 1	4.0 ± 0.2	(9.6 ± 0.5) × 10^3	9 ± 1	(4.4 ± 0.3) × 10^6	4.8 ± 0.7

[a]50 mM sodium pyrophosphate. [b]50 mM potassium phosphate. [c]50 mM sodium phosphate. [d]Data were acquired at varying concentrations of substrate and oxygen and fit with eq 1 ($R^2 \geq 0.998$). [e]Data were acquired at varying concentrations of substrate and fixed oxygen concentrations of 11, 45, and 90 μM yielding overlapping saturation curves (Figure 1); kinetic parameters represent the average of the three independent measurements. [f]In the presence of 50 units of SOD.

When EN was used as substrate for the enzyme at pH 5.5 and 30 °C, no differences in the apparent steady-state kinetic parameters were observed when oxygen was kept fixed between 11 and 90 μM (Figure 4B). This is consistent with the enzyme being fully saturated at concentrations of oxygen significantly lower than atmospheric conditions (i.e., 0.23 mM at 30 °C). Similar results were obtained with EN at pH 8.0 and 11.0 (data not shown). The overlapping saturation curves seen at different concentrations of oxygen are consistent with K_{oxygen} values not larger than 1 μM, i.e., at least 10 times smaller than the lowest concentration of oxygen used, irrespective of the pH between 5.5 and 11.0. When the steady-state kinetics with EN was determined at 7 °C, a kinetic pattern in the double reciprocal plot similar to that seen with P3N at 30 °C was obtained (Figure 4C). Unusually fast initial rates were observed at the lower temperature (data not shown). To minimize any potential radical side reaction occurring nonenzymatically[30] that might originate from EN reacting with superoxide if the latter was produced and released during turnover of the enzyme, 50 units of superoxide dismutase (SOD) were added to the reaction mixture.[30] With SOD present the initial rates were significantly lower, establishing that at low temperature superoxide was produced and released by NMO in turnover with EN. In this regard, previous studies demonstrated that SOD was not required at 30 °C with both P3N and EN.[2, 7] The kinetic parameters determined with EN at low temperature are summarized in Table 1.

pH Profiles. With P3N, the effects of pH on the steady-state kinetic parameters were determined by measuring initial rates of reaction at varying concentrations of organic substrate and oxygen at 30 °C. As shown in Figure 5, there were no pH effects on the steady-state kinetic parameters between pH 5.5 and 10.5, with average values of 800 ± 100 s^{-1} for k_{cat}, (10 ± 1) × 10^6 M^{-1} $s^{-1}$for k_{cat}/K_m, and (15 ± 5) × 10^6 M^{-1} s^{-1} for k_{cat}/K_{oxygen}.

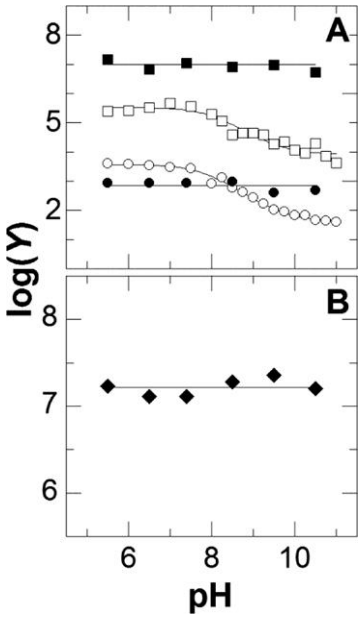

Figure 2.5 Effect of pH on the steady-state kinetic parameters of NMO with P3N or EN as substrate.
With P3N, initial rates of reaction were determined at varying concentrations of substrate and oxygen. Kinetic parameters were determined by using eq 1. With EN, initial rates of reaction were determined at atmospheric oxygen, yielding apparent $k_{cat}$and k_{cat}/K_m values that approximate well the true values due to low K_{oxygen} values (see text). All determinations were carried out at 30 °C. Panel A: k_{cat} (●) and k_{cat}/K_m (■) with P3N; k_{cat} (○) and k_{cat}/K_m (□) with EN. Data for k_{cat} and k_{cat}/K_m with EN were fit with eq 2. Panel B: pH profile of k_{cat}/K_{oxygen} with P3N.

Because of the K_{oxygen} value being less than 1 μM (see above), pH effects with EN could only be determined at atmospheric oxygen for the k_{cat} and k_{cat}/K_m values. The k_{cat} decreased with increasing pH from an upper limiting value of 4000 ± 400 s^{-1} to a lower limiting value of 44 ± 5 s^{-1} (Figure 5). Similarly, the k_{cat}/K_m value decreased from (3.4 ± 0.7) × 10^5 M^{-1} s^{-1} at low pH to (9 ± 2) × 10^3 M^{-1} s^{-1} at high pH (Figure 5). The pH profiles with EN defined apparent pK_a values of 7.8 ± 0.1 for k_{cat} and 7.9 ± 0.2 for k_{cat}/K_m.

Solvent Viscosity Effects. The effects of solvent viscosity on k_{cat} and k_{cat}/K_m with either P3N or EN were studied using glycerol as viscosigen to establish whether diffusion-controlled events of substrate binding and product release contributed to catalysis. These determinations were carried out at pH 6.5 with P3N and at pH 5.5 and 11.0 with EN, which correspond to the pH-independent regions identified in the pH studies (Figure 5). With P3N, the normalized k_{cat} and k_{cat}/K_m values determined at increasing relative viscosity of the solvent yielded lines with slopes of 0.34 ± 0.01 and 0.38 ± 0.03 (Figure 6). Lines with slopes of 0.48 ± 0.02 and 0.42 ± 0.04 were obtained for the k_{cat} andk_{cat}/K_m values with EN at low pH (Figure 6). Thus, similar effects were seen in k_{cat} and k_{cat}/K_m at those pH values where these kinetic parameters have maximal values. In contrast, with EN at high pH an inverse hyperbolic pattern of the normalized kinetic parameters as a function of increasing viscosity was observed (Figure 6).

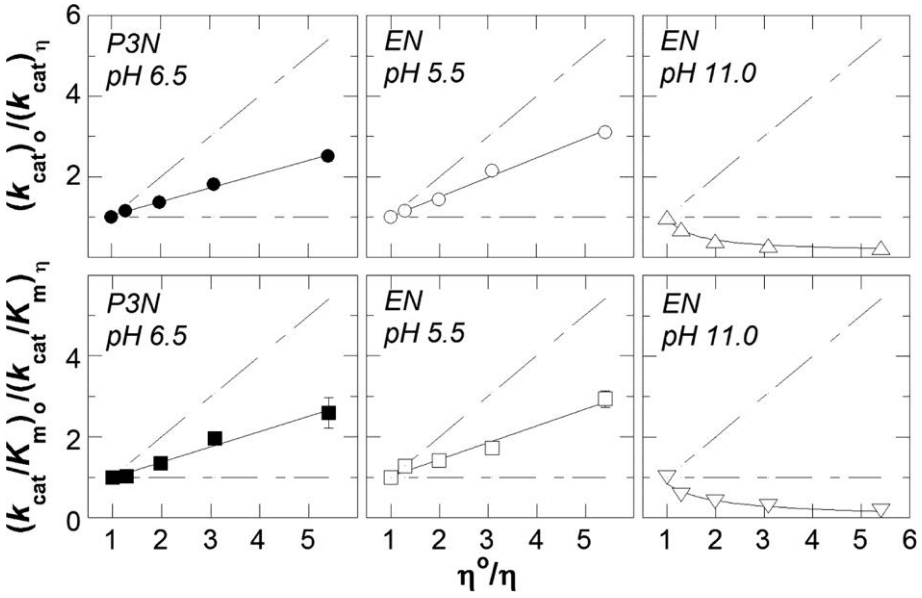

Figure 2.6 Effect of solvent viscosity on the steady-state kinetic parameters with P3N or EN.
Initial rates were measured at 30 °C in either 50 mM sodium pyrophosphate (pH 6.5, 5.5) or sodium phosphate (pH 11.0) at varying relative viscosity of the reaction mixture. Normalized k_{cat} and k_{cat}/K_m values are shown as a function of the relative solvent viscosity. The dashed lines with a slope of +1 indicate the results expected for a fully diffusion-limited reaction. The dashed lines with a slope of 0 indicate results expected for lack of solvent viscosity effects. The values of the relative viscosities of the solvent were taken

from Lide[28] and adjusted for 30 °C. Solvent viscosity data at pH 5.5 and 6.5 were fit with eq 3, and data at pH 11.0 were fit with eq 4.

2.5 Discussion

The mechanistic study presented here provides evidence that a highly reactive peroxynitro acid is formed enzymatically during turnover of NMO with its physiological substrate, P3N. Through a single-electron transfer, P3N and NMO react to form a P3N radical species and an anionic flavosemiquinone (step B in Scheme 2). A subsequent electron transfer from the flavosemiquinone to molecular oxygen results in the oxidation of the flavin and formation of superoxide anion (step C). The two highly reactive radical species, P3N radical and superoxide, then react in the active site of the enzyme to yield 3-peroxy-3-nitro-propanoate (step D), which subsequently decays to products. Alternatively,[1] the P3N radical could react with oxygen to give a 3-peroxy-3-nitropropanoate radical (step E), which would subsequently receive an electron from the flavosemiquinone forming 3-peroxy-3-nitropropanoate (step F). Irrespective of the path, a transient 3-peroxy-3-nitropropanoate intermediate is formed in the chemical mechanism of Scheme 2, for which evidence is presented below.

[1] The production and release of superoxide by the enzyme in turnover with P3N at 15 ^{o}C is consistent with superoxide being a reaction intermediate that is formed in catalysis (steps C and D in Scheme2). However, and as pointed out by one of the reviewers, the fact that superoxide leaks out of the enzyme active site during turnover under some conditions does not necessarily demonstrate that superoxide is an obligatory reaction intermediate. Thus, an alternative reaction path that leads to the formation of 3-peroxy-3-nitropropanoate through reaction of the organic radical and oxygen, followed by electron transfer from the flavosemiquinone to form the 3-peroxy-3-nitropropanoate intermediate (steps E and F in Scheme 2), cannot be ruled out. Both catalytic paths allow formation of the two species for which evidence is available in this study, i.e. the flavosemiquinone and 3-peroxy-3-nitropropanoate.

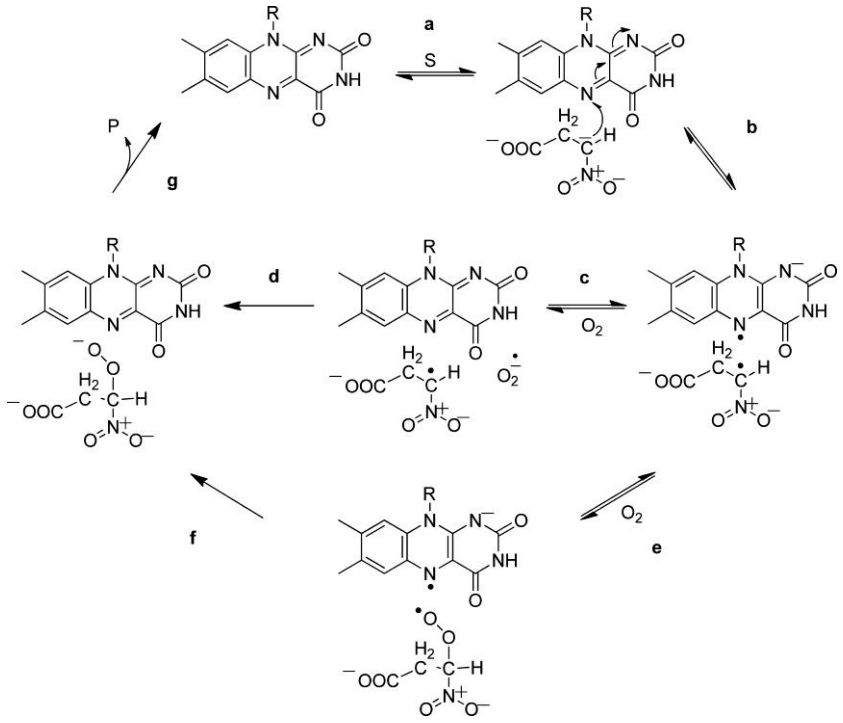

Figure 2.7 Minimal Chemical Mechanism of NMO with P3N and Oxygen as Substrates.
(a) Michaelis Complex Formation; (b) One-Electron Flavin Reduction; (c) Oxygen Activation; (d) Formation of 3-Peroxy-3-nitropropanoate; (e) Formation of Radical 3-Peroxy-3-nitropropanoate; (f) One-Electron Transfer from the Flavosemiquinone; (g) Release of Products.

After formation of a Michaelis complex in the active site of the enzyme, NMO and P3N react through a single-electron transfer to form a P3N radical species and an anionic flavosemiquinone (step B in Scheme 2). Evidence supporting this conclusion comes from the anaerobic mixing of oxidized NMO and P3N, or its analogue EN, in a stopped-flow spectrophotometer. This experiment showed the rapid formation of a flavin species with λ_{max} at 365 nm, a shoulder at around 400 nm, and a less intense peak at 483 nm, which are typical of anionic flavosemiquinones.[31] The ε value of 17 300 $M^{-1}\,cm^{-1}$ at 365 nm for the flavosemiquinone in NMO is comparable to those of other flavin-dependent enzymes, including D-amino acid oxidase,[31] NMO from *N. crassa*,[3] choline oxidase,[32] glycine oxidase,[33] and cholesterol oxidase,[34] to name a few. With the physiological substrate P3N, the single-electron transfer reaction in NMO is too fast to be measured with a stopped-flow spectrophotometer, even

when the temperature is lowered to 7 °C. On the basis of the mixing time of the instrument (i.e., 2.2 ms), one can estimate a rate constant for flavin reduction ≥1900 s^{-1} with P3N at 7 °C and pH 6.0. With EN, instead, the reduction of the flavin could be measured at low temperature, showing a limiting rate constant of 300 s^{-1} at pH 6.0 and 7 °C. This value is 7 times larger than the turnover number of the enzyme at saturating concentrations of EN and oxygen (e.g., 40 s^{-1}), indicating that the transfer of the single-electron from the substrate to the flavin contributes minimally to the overall turnover of the enzyme at the pH optimum. Upon lowering the temperature from 30 to 7 °C, there is 100-fold decrease in the k_{cat} value with EN from 4100 s^{-1} (pH 5.5) to 40 s^{-1} (pH 6.0). It is conceivable that with P3N the k_{cat} similarly decreases from its value of 860 s^{-1} at 30 °C to ∼10 s^{-1} at 7 °C. Thus, the single-electron transfer with P3N at 7 °C, with an estimated value of ≥1900 s^{-1}, does not contribute to the overall turnover of the enzyme with the physiological substrate.

Molecular oxygen is activated to superoxide through the transfer of an electron from the anionic flavosemiquinone, yielding oxidized FMN (step C in Scheme 2). The intersecting lines observed in double reciprocal plots of the initial rates of reaction as a function of P3N (or EN) concentration are consistent with oxygen reacting with the enzyme in complex with the organic product of the first electron transfer reaction, i.e., before the P3N radical is released from the enzyme active site. Further evidence in support of oxygen reacting with the flavosemiquinone comes from time-resolved absorbance spectroscopy of the enzyme turning over with P3N and oxygen and steady-state kinetics. The former experiment showed that the enzyme in turnover is primarily present as anionic flavosemiquinone, which then fully accumulates when oxygen is completely depleted from the enzyme reaction mixture. This establishes the flavosemiquinone as the species that reacts with oxygen in turnover and therefore the species that accumulates once

oxygen is depleted. The effect of SOD on the steady-state kinetics with EN at low temperature showed that superoxide is produced and released from the enzyme active site during turnover. While a similar effect of SOD was not observed at 30 °C with EN or P3N irrespective of the temperature,[2, 7] these results establish superoxide as a reaction intermediate that can escape from the active site at low temperature when the enzyme turns over with the substrate analogue, EN. We can speculate that the escape of superoxide from the enzyme active site may be due to an increased rigidity of the enzyme at 7 °C as compared to 30 °C.[35-37] Alternatively, if superoxide is not an obligatory intermediate, one can envision oxygen reacting directly with the P3N radical (step E in Scheme 2), followed by an electron transfer from the flavosemiquinone to form a 3-peroxy-3-nitropropanoate (step F). In this alternate mechanism the flavin would act as an electron sink that activates P3N for reaction with oxygen, instead of activating oxygen for reaction with P3N radical.

Irrespective of the flavin activating oxygen or reacting with the 3-peroxy-3-nitropropanoate radical, a 3-peroxy-3-nitropropanoate species is formed in catalysis. Evidence for the formation of 3-peroxy-3-nitropropanoate comes from the transient increase in absorbance at ∼300 nm observed when the enzyme is turning over with P3N and oxygen. Lack of changes in the absorbance at 445 nm, while that at ∼300 nm increases, establishes that the flavin is in steady state and is not involved in the reaction. The requirement of oxygen for the formation of 3-peroxy-3-nitropropanoate is established by the lack of spectral changes in the 260–360 nm region of the absorbance spectrum when the oxidized enzyme is mixed anaerobically with P3N. The UV absorbance spectrum of P3N in aqueous solution exhibits two maxima at 225 and 300 nm (data not shown). The increase in absorbance at ∼300 nm observed in this study is consistent with previous results in other systems demonstrating that superoxide acts as an auxochrome after

reacting with other radicals, causing increases in absorbance intensity.[38-41] Alternatively, the auxochromic effect may be explained if the pK_a for the peroxy/hydroperoxy equilibrium in 3-(hydro)peroxy-3-nitropropanoate is lower than that defining the ionization of the α-carbon of P3N, yielding a reaction intermediate that is more highly ionized than the substrate.

The capture of P3N in the active site of NMO to yield a Michaelis complex competent to catalysis is very effective, as suggested by the k_{cat}/K_m value of 10^7 M^{-1} s^{-1}. High values of k_{cat}/K_m are typically seen in detoxifying enzymes involved in the elimination of reactive oxygen species, such as carbonic anhydrase, catalase, and SOD.[42-44] Besides these, only a limited number of enzymes active on organic molecules have been described to date with k_{cat}/K_m values comparable to that of NMO with P3N, namely acetyl cholinesterase, crotonase, fumarase, triose phosphate isomerase, β-lactamase, and chymotrypsin.[45-50] All of these enzymes catalyze reactions relevant to the organism as either source of energy, neurotransmitter signaling, or detoxification. In this context, the k_{cat}/K_m of 10^7 M^{-1} s^{-1} agrees well with the physiological role of NMO as an enzyme that protects fungi from the environmental occurrence of P3N, as recently established with *in vivo* studies using *N. crassa* and *E. coli*.[7]

As oftentimes observed for enzymes with k_{cat}/K_m values of 10^7–10^8 M^{-1} s^{-1},[42-51] the second-order rate constant for capture of P3N by NMO is partially controlled by the diffusion of the substrate into the active site of the enzyme. Evidence for this conclusion comes from the linear dependence of the normalized k_{cat}/K_m values on the relative viscosity of the solvent exhibiting a positive slope of 0.4. As expected for an enzyme displaying a k_{cat} with a high value of 800 s^{-1}, turnover with P3N is controlled to a significant extent by the rate of release of the product of the reaction from the active site of the enzyme. This conclusion is supported by the

linear dependence with a positive slope of 0.4 of the normalized k_{cat} values as a function of the relative viscosity of the solvent. Substitution of the physiological substrate with EN, a substrate analogue lacking the carboxylate moiety, results in a 4-fold increase in k_{cat} and only a 1.3-fold increase in the solvent viscosity effect on the normalized k_{cat} values, e.g., from 0.4 with P3N to 0.5 with EN upon comparing data obtained at low pH. These data are consistent with the carboxylate group of P3N playing a major role in retaining the product in the active site of the enzyme. The carboxylate is also important for substrate binding, as demonstrated by the k_{cat}/K_m value observed at low pH with P3N being 3 orders of magnitude larger than with EN. An energetic contribution of ∼17 kJ/mol can be estimated for the interaction of the carboxylate moiety of P3N toward the substrate capture by NMO. This value agrees well with that of ∼15 kJ/mol previously established with the use of substrate analogues for the enzyme carboxylate in the active site of choline oxidase.[(52)] In that case, site-directed mutagenesis established the presence of an ionic bond between the substrate and the enzyme.[(53)]

The effects of pH and solvent viscosity on the k_{cat}/K_m and k_{cat} values with either P3N or EN as substrate provide the basis to explain why NMO is very proficient in capturing the organic substrate for catalysis, activating oxygen for the reaction with P3N, and a very effective catalyst in the overall turnover with P3N. The pH effects with EN demonstrate that the enzyme is 2 orders of magnitude more proficient and faster at acidic pH values than alkaline values, establishing protonation of an ionizable group as an important feature in this context. No relevant ionizations are seen in the pH profiles of k_{cat} and k_{cat}/K_m with P3N. However, the comparison of the patterns of solvent viscosity effects with EN and P3N suggests that the same enzyme species is present during turnover with the physiological substrate or EN at low pH, i.e., with a similar pattern of ionization for groups that are relevant to catalysis. Without considering the substrate

carboxylate, which is likely neutralized upon substrate binding in the active site of the enzyme and does not undergo rearrangements in catalysis, all the enzyme complexes occurring in catalysis are anionic. The charge is initially on the substrate α-carbon, then on the anionic flavosemiquinone, subsequently on the superoxide, and finally on the 3-peroxy-3-nitro acid (Scheme 2). Consequently, the kinetic steps of substrate capture and oxygen activation in the mechanism of NMO, as well as the overall turnover of the enzyme, are likely enhanced by the presence of either a positive charge or a protonated group acting as a hydrogen bond donor in the active site. Studies are ongoing to determine the three-dimensional structure of the enzyme by using X-ray crystallography, which will provide a framework for future identification of the group acting as catalyst in the reaction catalyzed by fungal NMO through site-directed mutagenesis.

In conclusion, time-resolved absorbance spectroscopy of NMO in turnover with its physiological substrate P3N has allowed for the first-time detection of a proposed reaction intermediate, 3-peroxy-3-nitropropanoate. This transient intermediate is formed in the enzyme-catalyzed reaction of P3N radical and either oxygen or superoxide produced enzymatically from the reaction of oxygen with the flavosemiquinone. The flavin is instrumental for the formation of the organic radical species participating in the reaction, which is formed through a single-electron transfer from the P3N to the flavin. The study presented herein also represents the first biochemical and mechanistic characterization of NMO, which was first isolated from fungi 6 decades ago,[(54)] with its physiological substrate. In the GenBank, there are currently over 3000 genes annotated as NMO, or as 2-nitropropane dioxygenase as the enzyme was officially classified until 2010. Most of the products of these genes, with the exception of those from the fungi *N. crassa* and *W. saturnus*, have not been characterized biochemically. A similar

physiological role in the oxidation of P3N has been established only for a single bacterial P3N monooxygenase,[55] for which limited biochemical data are available. Interestingly, bacterial and fungal NMOs appear to be only distantly related, with 20–25% amino acid similarity. This study provides therefore the groundwork for future studies that will be aimed at the characterization of other enzymes annotated as NMO with their physiological substrate, P3N.

2.6 Acknowledgements

We thank the two anonymous reviewers for their insightful suggestions.

2.7 References

1. Gadda, G., and Francis, K. (2010) Nitronate monooxygenase, a model for anionic flavin semiquinone intermediates in oxidative catalysis. *Arch. Biochem. Biophys. 493*, 53−61.

2. Mijatovic, S., and Gadda, G. (2008) Oxidation of alkyl nitronates catalyzed by 2-nitropropane dioxygenase from *Hansenula mrakii*. *Arch. Biochem. Biophys. 473*, 61−68.

3. Francis, K., Russell, B., and Gadda, G. (2005) Involvement of a flavosemiquinone in the enzymatic oxidation of nitroalkanes catalyzed by 2-nitropropane dioxygenase. *J. Biol. Chem. 280*, 5195−5204.

4. Francis, K., and Gadda, G. (2006) Probing the chemical steps of nitroalkane oxidation catalyzed by 2-nitropropane dioxygenase with solvent viscosity, pH, and substrate kinetic isotope effects. *Biochemistry 45*, 13889−13898.

5. Francis, K., and Gadda, G. (2008) The nonoxidative conversion of nitroethane to ethylnitronate in *Neurospora crassa* 2-nitropropane dioxygenase is catalyzed by histidine 196. *Biochemistry 47*, 9136−9144.

6. Francis, K., and Gadda, G. (2009) Inflated kinetic isotope effects in the branched mechanism of *Neurospora crassa* 2-nitropropane dioxygenase. *Biochemistry 48*, 2403−2410.

7. Francis, K., Nishino, S. F., Spain, J. C., and Gadda, G. (2012) A novel activity for fungal nitronate monooxygenase: detoxification of the metabolic inhibitor propionate-3-nitronate. *Arch. Biochem. Biophys. 521*, 84−89.

8. Ha, J. Y., Min, J. Y., Lee, S. K., Kim, H. S., Kim do, J., Kim, K. H., Lee, H. H., Kim, H. K., Yoon, H. J., and Suh, S. W. (2006) Crystal structure of 2-nitropropane dioxygenase complexed with FMN and substrate. Identification of the catalytic base. *J. Biol. Chem. 281*, 18660−18667.

9. Alston, T. A., Mela, L., and Bright, H. J. (1977) 3- Nitropropionate, the toxic substance of Indigofera, is a suicide inactivator of succinate dehydrogenase. *Proc. Natl. Acad. Sci. USA 74*, 3767−3771.

10. Coles, C. J., Edmondson, D. E., and Singer, T. P. (1979) Inactivation of succinate dehydrogenase by 3-nitropropionate. *J. Biol. Chem. 254*, 5161−5167.

11. Huang, L. S., Sun, G., Cobessi, D., Wang, A. C., Shen, J. T., Tung, E. Y., Anderson, V. E., and Berry, E. A. (2006) 3-nitropropionic acid is a suicide inhibitor of mitochondrial respiration that, upon oxidation by complex II, forms a covalent adduct with a catalytic base. *Biochemistry 52*, 2694−2704.

12. Porter, D. J., and Bright, H. J. (1980) 3-Carbanionic substrate analogues bind very tightly to fumarase and aspartase. *J. Biol. Chem. 255*, 4772−4780.

12. Scallet, A. C., Nony, P. L., Rountree, R. L., and Binienda, Z. K. (2001) Biomarkers of 3-nitropropionic acid (3-NPA)-induced mitochondrial dysfunction as indicators of neuroprotection. *Ann. N.Y. Acad. Sci. 939*, 381−392.

14. Ludolph, A. C., He, F., Spencer, P. S., Hammerstad, J., and Sabri, M. (1991) 3-Nitropropionic acid-exogenous animal neurotoxin and possible human striatal toxin. *Can. J. Neurol. Sci. 18*, 492−498.

15. Pang, Z., and Geddes, J. W. (1997) Mechanisms of cell death induced by the mitochondrial toxin 3-nitropropionic acid: acute excitotoxic necrosis and delayed apoptosis. *J. Neurosci. 17*, 3064−3073.

16. Burdock, G. A., Carabin, I. G., and Soni, M. G. (2001) Safety assessment of B-nitropropionic acid: a monograph in support of an acceptable daily intake in humans. *Food Chem. 75*, 1−27.

17. Ming, L. (1995) Moldy sugarcane poisoning–a case report with a brief review. *J. Toxicol. Clin. Toxicol. 33*, 363−367.

18. Hamilton, B. F., Gould, D. H., and Gustine, D. L. (2000) History of 3-nitropropionic acid, in *Mitochondrial Inhibitors and Neurodegenerative Disorders Contemporary Neuroscience*, Humana Press, Totowa, NJ.

19. Mathews, F. P. (1940) The toxicity of red-stemmed peavine (*Astragalus emoryanus*) for cattle, sheep, and goats. *J. Am. Vet. Med. Assoc. 97*, 125−134.

20. Liu, X., Luo, X., and Hu, W. (1992) Studies on the epidemiology and etiology of moldy sugarcane poisoning in China. *Biomed. Environ. Sci. 5*, 161−177.

21. Beal, M. F., Brouillet, E., Jenkins, B. G., Ferrante, R. J., Kowall, N. W., Miller, J. M., Storey, E., Srivastava, R., Rosen, B. R., and Hyman, B. T. (1993) Neurochemical and histologic characterization of striatal excitotoxic lesions produced by the mitochondrial toxin 3-nitropropionic acid. *J. Neurosci. 13*, 4181−4192.

22. Guyot, M. C., Hantraye, P., Dolan, R., Palfi, S., Maziere, M., and Brouillet, E. (1997) Quantifiable bradykinesia, gait abnormalities and Huntington's disease-like striatal lesions in rats chronically treated with 3-nitropropionic acid. *Neuroscience 79*, 45−56.

23. Tsang, T. M., Haselden, J. N., and Holmes, E. (2009) Metabonomic characterization of the 3-nitropropionic acid rat model of Huntington's disease. *Neurochem. Res. 34*, 1261−1271.

24. Francis, K., and Gadda, G. (2009) Kinetic evidence for an anion binding pocket in the active site of nitronate monooxygenase. *Bioorg. Chem. 37*, 167−172.

25. Bush, M. T., Touster, O., and Brockman, J. E. (1951) The production of beta-nitropropionic acid by a strain of *Aspergillus flavus*. *J. Biol. Chem. 188*, 685−693.

26. Lewis, R. J. (1996) Sax's Dangerous Properties of Industrial Materials, 9th ed., Van Nostrand Reinhold, New York.

27. Nielsen, A. T. (1969) Nitronic acids and esters, in The Chemistry of the Nitro and Nitroso Groups (Feuer, H., Ed.), pp 349−486, Interscience Publishers, New York.

28. Lide, D. R. (2000) Handbook of Chemistry and Physics, 6th ed., CRC Press, Boca Raton, FL.

29. Segel, I. H. (1975) Enzyme Kinetics, Wiley, New York.

30. Kuo, C. F., and Fridovich, I. (1986) Free-radical chain oxidation of 2-nitropropane initiated and propagated by superoxide. *Biochem. J. 237*, 505−510.

31. Massey, V., and Palmer, G. (1966) On the existence of spectrally distinct classes of flavoprotein semiquinones. A new method for the quantitative production of flavoprotein semiquinones. *Biochemistry 5*, 3181−3189.

32. Ghanem, M., Fan, F., Francis, K., and Gadda, G. (2003) Spectroscopic and kinetic properties of recombinant choline oxidase from *Arthrobacter globiformis*. *Biochemistry 42*, 15179−15188.

33. Job, V., Marcone, G. L., Pilone, M. S., and Pollegioni, L. (2002) Glycine oxidase from *Bacillus subtilis*. Characterization of a new flavoprotein. *J. Biol. Chem. 277*, 6985−6993.

34. Gadda, G., Wels, G., Pollegioni, L., Zucchelli, S., Ambrosius, D., Pilone, M. S., and Ghisla, S. (1997) Characterization of cholesterol oxidase from *Streptomyces hygroscopicus* and *Brevibacterium sterolicum*. *Eur. J. Biochem. 250*, 369−376.

35. Dougherty, R. C. (1998) Temperature and pressure dependence of hydrogen bond strength: A perturbation molecular orbital approach. *J. Chem. Phys. 109*, 7372−7378.

36. Jaenicke, R. (1990) Protein structure and function at low temperatures. *Philos. Trans. R. Soc. London*, B 326, 535−551; discussion: 551−553.

37. Cordier, F., and Grzesiek, S. (2002) Temperature-dependence of protein hydrogen bond properties as studied by high-resolution NMR. *J. Mol. Biol. 317*, 739−752.

38. Takahashi, K., Numata, N., Kinoshita, N., Utoguchi, N., Mayumi, T., and Mizuno, N. (2004) Characterization of the influence of nitric oxide donors on intestinal absorption of macromolecules. *Int. J. Pharm. 286*, 89−97.

39. Kelm, M., Dahmann, R., Wink, D., and Feelisch, M. (1997) The nitric oxide/superoxide assay. Insights into the biological chemistry of the NO/O-2 interaction. *J. Biol. Chem. 272*, 9922−9932.

40. Bamdad, F., Wu, J., and Chen, L. (2011) Effects of enzymatic hydrolysis on molecular structure and antioxidant activity of barley hordein. *J. Cereal Sci. 54*, 20−28.

41. Evans, J. P., Niemevz, F., Buldain, G., and de Montellano, P. O. (2008) Isoporphyrin intermediate in heme oxygenase catalysis. Oxidation of alpha-meso-phenylheme. *J. Biol. Chem. 283*, 19530− 19539.

42. Fielden, E. M., Roberts, P. B., Bray, R. C., Lowe, D. J., Mautner, G. N., Rotilio, G., and Calabrese, L. (1974) Mechanism of action of superoxide dismutase from pulse radiolysis and electron paramagnetic resonance. Evidence that only half the active sites function in catalysis. *Biochem. J. 139*, 49−60.

43. Maehly, A. C., and Chance, B. (1954) The assay of catalases and peroxidases. *Methods Biochem. Anal. 1*, 357−424.

44. Hasinoff, B. B. (1984) Kinetics of carbonic anhydrase catalysis in solvents of increased viscosity: a partially diffusion-controlled reaction. *Arch. Biochem. Biophys. 233*, 676−681.

45. Quinn, D. M. (1987) Acetylcholinesterase: Enzyme structure, reaction dynamics, and virtual transition states. *Chem. Rev. 87*, 955− 979.

46. Waterson, R. M., and Hill, R. L. (1972) Enoyl coenzyme A hydratase (crotonase). Catalytic properties of crotonase and its possible regulatory role in fatty acid oxidation. *J. Biol. Chem. 247*, 5258−5265.

47. Sweet, W. L., and Blanchard, J. S. (1990) Fumarase: viscosity dependence of the kinetic parameters. *Arch. Biochem. Biophys. 277*, 196−202.

48. Blacklow, S. C., Raines, R. T., Lim, W. A., Zamore, P. D., and Knowles, J. R. (1988) Triosephosphate isomerase catalysis is diffusion controlled. Appendix: Analysis of triose phosphate equilibria in aqueous solution by 31P NMR. *Biochemistry 27*, 1158−1167.

49. Christensen, H., Martin, M. T., and Waley, S. G. (1990) Beta-lactamases as fully efficient enzymes. Determination of all the rate constants in the acyl-enzyme mechanism. *Biochem. J. 266*, 853−861.

50. Brouwer, A. C., and Kirsch, J. F. (1982) Investigation of diffusion-limited rates of chymotrypsin reactions by viscosity variation. *Biochemistry 21*, 1302−1307.

51. Wilcox, P. E. (1970) Chymotrypsinogens-chymotrypsins. *Methods Enzymol. 19*, 64−108.

52. Gadda, G., Powell, N. L., and Menon, P. (2004) The trimethylammonium headgroup of choline is a major determinant for substrate binding and specificity in choline oxidase. *Arch. Biochem. Biophys. 430*, 264−273.

53. Quaye, O., Lountos, G. T., Fan, F., Orville, A. M., and Gadda, G. (2008) Role of Glu312 in binding and positioning of the substrate for the hydride transfer reaction in choline oxidase. *Biochemistry 47*, 243− 256.

54. Little, H. N. (1951) Oxidation of nitroethane by extracts from *Neurospora. J. Biol. Chem. 193*, 347−358.

55. Nishino, S. F., Shin, K. A., Payne, R. B., and Spain, J. C. (2010) Growth of bacteria on 3-nitropropionic acid as a sole source of carbon, nitrogen, and energy. *Appl. Environ. Microbiol. 76*, 3590−3598.

3 PEG Binding Site in Nitronate Monooxygenase from *Cyberlindnera saturnus*

3.1 Abstract

Nitronate monooxygenases are flavin-dependent enzymes that oxidize the toxin, propionate 3-nitronate (P3N), using molecular oxygen as the final electron acceptor. NMO from *C. saturnus* was crystallized in this study to 1.65 Å resolution, showing a single FMN cofactor bound to the protein. An unusual binding of a polyethylene glycol (PEG) molecule was found on the surface of the enzyme. In the presence of PEG 3350, the k_{cat} and K_m values for CsNMO with P3N as substrate were 7 times higher and 125 times lower, respectively. Conversely, kinetic parameters of NMO from *P. aeruginosa* were not significantly altered in the presence of PEG, indicative of an activation effect specific for the fungal enzyme. The overall structure of CsNMO was highly conserved in comparison to the bacterial NMO enzyme previously reported. The results presented provide new insights for non-essential activation providing new scopes on the structural-functional investigations on NMOs.

3.2 Introduction

Nitronate monooxygenases (NMO, E.C. 1.13.12.16) catalyze the oxidation of propionate 3-nitronate (P3N) and alkyl nitronates of 2-6 carbon atoms in length.[1-4] P3N is a highly toxic nitro acid compound that is prevalent in legumes and fungi and is an irreversible inhibitor of mitochondrial succinate dehydrogenase.[5-9] Poisoning by P3N leads to a variety of neurological disorders and even death at sufficiently high concentrations.[5] NMO from *Cyberlindnera saturnus* (CsNMO) utilizes a single-electron transfer mechanism of catalysis, in which the protein-bound FMN cofactor oxidizes P3N forming an anionic flavosemiquinone in the enzyme-substrate complex.[4] The radical P3N molecule further reacts with molecular oxygen (or

superoxide) to form a spectrophotometrically-detectable peroxynitro acid intermediate concomitantly reoxidizing the flavin.[4] The peroxynitro acid collapses to the final products, likely malonic semialdehyde, nitrate, and nitrate as determined in NMO from *P. aeruginosa* JS189.[10] Mechanistic characterizations with the physiological substrate, P3N, have been carried out solely with CsNMO using pH effects, UV-visible and time-resolved absorbance spectroscopy, and steady-state kinetics.[4] On the other hand, the only crystal structure available thus far of NMO was from *Pseudomonas aeruginosa* (PaNMO) and was recently resolved to a 1.44 Å resolution.[5]

A recent bioinformatics, biochemical, and structural study on PaNMO has established two new classes within the NMO family of enzymes. CsNMO is a member of the Class I NMO enzyme family[3], along with PaNMO and more than 450 NMO gene products, including mostly fungi and bacteria and two animals.[3] This family of enzymes has been shown to rapidly oxidize P3N at atmospheric oxygen with $^{app}(k_{cat}/K_m)$ values $\geq 10^6\ M^{-1}s^{-1}$. The flavin becomes reduced to a flavin anionic semiquinone, and the final electron accepter is oxygen. Within the four motifs identified in Class I NMOs, a number of amino acid residues are conserved in the active site of the enzyme including (PaNMO numbering): M20, N69, F71, Y109, H133, H183, Y299, Y303, and K329. H133 is located ~4 Å from the N1 atom of the isoalloxazine and is proposed to stabilize the negative charge on the anionic flavosemiquinone.[3] T109, Y299, Y303 and F71 have been proposed to form a substrate binding pocket and K307 may function to attract the negatively-charged substrate into the active site. Aside from CsNMO and PaNMO, only one other known enzyme is currently characterized as an NMO from *Neurospora crassa*.[2, 3] This enzyme does not contain all four conserved motifs of Class I and is active on both nitronates and

nitroalkanes[11], rather than on nitronates. Therefore it was separated into a much smaller Class II NMO enzymes, which includes only ten other hypothetical NMOs enzymes from fungi.[3]

In this study, structural and kinetics approaches were used to investigate a eukaryotic NMO enzyme in the Class I NMO family. The crystal structure of CsNMO was solved to a 1.65 Å resolution revealing a binding site for a PEG molecule. Steady-state kinetics experiments on both the fungal and bacterial enzymes revealed the effects of PEG on the kinetic parameters. Differences occurring between amino acid sequences of the fungal and bacterial enzymes were used to identify distinct structural inconsistencies in these catalytically similar enzymes.

3.3 Materials and Methods

3.3.1 Materials

3-Nitropropionic acid (3-NPA) and PEG 3350 were from Sigma-Aldrich (St. Louis, MO). Recombinant NMO from *C. saturnus* and *P. aeruginosa* were obtained through expression and purification methods previously described.[3, 32] Propionate 3-nitronate (P3N) was prepared as previously described using excess KOH for 24 h.[4] Similar to primary and secondary nitroalkanes, the α-carbon of 3-NPA has a pK_a of ~9.1 at allowing for a slow deprotonation with a strong base producing the conjugate base, P3N.[33] All crystallography trays, cover slips, and supplies were purchased from Hampton Research (Aliso Viejo, CA). All other reagents were of the highest purity commercially available.

3.3.2 Crystallization and Data Collection

Crystals of CsNMO were grown in hanging drops at room temperature with 21% PEG 3350, 70 mM sodium citrate, pH 4.0, and 100 mM ammonium acetate. The crystals were cryo-cooled in the mother liquor and the diffraction data at 100 K were collected on beamline X4A of

the National Synchrotron Light Source at Brookhaven National Laboratory. The X-ray data were integrated and scaled with HKL2000.[34]

3.3.3 Structure Determination

The structure of CsNMO was solved by molecular replacement employing PHASER.[35, 36] With 34% sequence identity of CsNMO, PaNMO (PDB code 4Q4K) was used as the initial model of the main chain atoms by pruning the N-terminal six residues and the C-terminal five residues of PaNMO and using serine instead of the dissimilar amino acids in the PaNMO sequence.[3] The CsNMO structure model was constructed from the molecular replacement phases using the Arp/wArp[37, 38] program, which docked 90% of the sequence into the electron density. The model was subjected to several rounds of refinement in REFMAC[39] and the remaining protein structure was manually built with COOT.[40] Solvent molecules were inserted at stereochemically reasonable positions using 2Fo-Fc and Fo-Fc maps at 1 and 3 sigma (σ) levels, respectively.

3.3.4 Steady-state Kinetics of CsNMO and PaNMO with P3N

Enzymatic assays were carried out using a computer-interfaced Oxy-32 oxygen-monitoring system (Hansatech Instruments, Inc., Norfolk, England) by monitoring the initial rate of oxygen consumption. Steady-state kinetic parameters of CsNMO or PaNMO with P3N as substrate were measured at varying concentrations of PEG 3350 (12.5-50 mM for CsNMO, 2-25 mM for PaNMO) in 50 mM NaPPi, pH 6.0, 30 ºC, at atmospheric oxygen. Solutions of PEG 3350 were prepared in water. Initial rates of the reactions were calculated based on enzyme-bound flavin using experimentally determined extinction coefficients ε_{442nm} = 11,400 $M^{-1}s^{-1}$ for CsNMO and ε_{443nm} = 12,500 $M^{-1}s^{-1}$ for PaNMO as measured spectrophotometrically using an Agilent Technologies diode-array model HP 8453 spectrophotometer.[3, 32] The enzyme was

allowed to incubate in the reaction vessel with PEG 3350 for 30 s prior to addition of the P3N substrate to initiate the reaction. Enzymatic assays were initiated by the addition of P3N to the reaction mixture to ensure that negligible amounts of 3-NPA were present during the time required to acquire initial rates of the reaction since the second order rate constants for protonation of nitronates are in the range of 15-75 $M^{-1}s^{-1}$.[4, 41]

3.3.5 Data Analysis

Steady-state kinetic data were fit with KaleidaGraph (Synergy Software, Reading, PA) or Enzfitter (Biosoft, Campbridge, UK) software. Kinetic parameters determined with P3N at atmospheric oxygen were obtained by fitting the data to the Michaelis-Menten equation for one substrate. In all cases, substrate concentrations were between 0.3 and 10 times K_m, ensuring accurate determinations of the k_{cat}/K_m and k_{cat}, and K_m values. When initial rates of reaction were determined at varying concentrations of P3N and PEG 3350, the kinetic data were fit with eq 1, which describes a mechanism for non-essential activation in which a reaction can occur in the absence of the activator.[42] $^{app}k_{cat}$ is the first-order rate constant for the reaction in the presence of saturating P3N at atmospheric oxygen, K_{P3N} is the Michaelis constant for P3N, K_A is the dissociation constant for the equilibrium between PEG 3350 and the enzyme, α is a factor by which K_{P3N} changes when the activator, A, occupies the enzyme, αK_A is the dissociation constant for the activator when P3N occupies the enzyme, β is a factor by which $^{app}k_{cat}$ changes when the activator, A, occupies the enzyme.

$$\frac{v_0}{e} = \frac{{}^{app}k_{cat}\left(\frac{[S]}{K_{PsN}}\right) + \beta\,{}^{app}k_{cat}\left(\frac{[A][S]}{\alpha K_A K_{PsN}}\right)}{1 + \frac{[S]}{K_{PsN}} + \frac{[A]}{K_A} + \frac{[A][S]}{\alpha K_A K_{PsN}}} \qquad (1)$$

3.4 Results

3.4.1 Overall Structure of CsNMO

CsNMO was crystallized in the monoclinic space group $P2_1$ with one molecule per asymmetric unit by using PaNMO (PDB code 4Q4K) as a template.[3] The structure was refined to 1.65 Å with an R-factor of 15.3% and R_{free} of 20.4%. The data collection and refinement statistics are reported in Table 1. The overall structure of CsNMO contained an FMN binding domain (residues 1-79, 122-271 and 356-374) and substrate binding domain (residues 80-121 and 272-355) as shown in Figure 1. The FMN binding domain adopted a TIM barrel-fold, while the substrate binding domain had 3 helices connected by loops (Figure 1). One FMN molecule was observed to be bound at the FMN binding domain of CsNMO (Figure 1). The active site of CsNMO was located at the cleft formed by the FMN binding domain and the substrate binding domain. Residues A24, N77, F79, Y119, H147, H197, Y321, Y325, and L348 lined the active site surrounding the isoalloxazine ring of FMN, corresponding to residues L21, N69, F71, Y109, H133, H183, Y299, Y303, and W325 in PaNMO.[3]

Table 3.1 Crystallographic data collection and refinement statistics.

Data Collection	
Space group	$P2_1$
Cell Dimensions (Å, deg)	a = 44.82, b = 68.43, c = 58.37, β = 106.3
Molecules/asymmetric unit	1
Resolution range	50.0 – 1.65
Total observations	198467
Unique reflections	39464
Completeness	96.0 (72.6)[a]
$\langle I/\sigma(I) \rangle$	18.3 (2.6)
Refinement	
R_{merge} (%)	7.8 (47.8)
Refinement resolution range	50 – 1.65
R_{cryst} (%)	15.3
R_{free} (%)	20.4
Number of solvent	273
Mean B-factor (Å²)	
Protein	16.7
FMN	9.8
Solvents	25
RMS deviations from ideality	
Bond length (Å)	0.03
Angles (°)	2.3

[a]Values in parentheses are given for the highest resolution shell (1.71-1.65 Å).

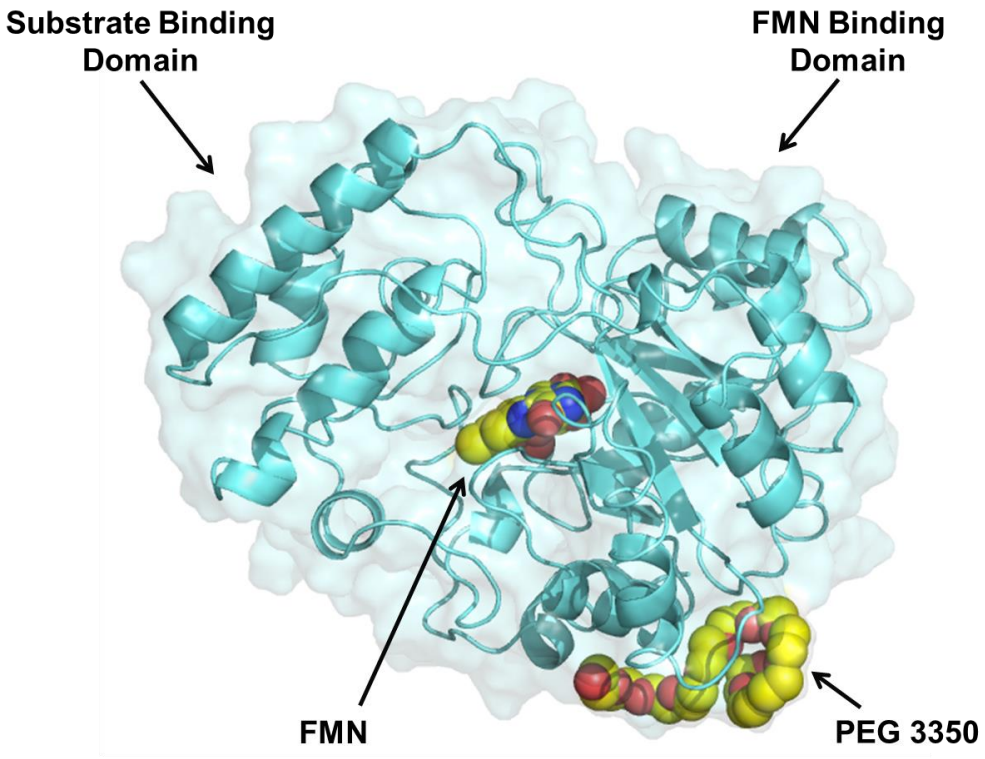

Figure 3.1 Crystal structure of CsNMO (cyan) is shown in cartoon with a surface transparency of 60%. FMN (yellow, center) and PEG (yellow, surface) are shown as spheres.

3.4.2 FMN Binding Interactions

The phosphate group of FMN was buried deep within the FMN binding domain and formed hydrogen-bonding interactions with the main chain amide groups of G240, G261 and T262. The ribityl group was held in place by hydrogen bonds between the Nε2 atom of Q190 and O3 atom of FMN and Nε2 atom of Q259 and O2 atom of FMN. The *si* face of the isoalloxazine ring was exposed to the substrate binding site, whereas the *re* face formed a van der Waals contact with the Cα atom of M23 (Figure 2). The isoalloxazine ring exhibited a butterfly bend of 169^{o} along the C7-N5-C4 atoms, compared to 185^{o} for the corresponding angle in PaNMO. The N5 and O4 atoms of FMN in CsNMO had van der Waals interactions with the main chain amide group of A24 (Figure 2). H147 was located 4 Å from the N1 atom of the cofactor (Figure

2). The O2 and N3 atoms of FMN formed hydrogen-bonding interactions with the side chain of N77. The O4 atom was likely hydrogen-bonded to the main chain amide of A24 (Figure 2). L265 (4.3 Å) and H276 (5.6 Å) made the closest contacts with the C7 and C8 atoms of the isoalloxazine ring (Figure 2). Most of the interactions between the cofactor and CsNMO were also present in PaNMO, except Y254 and W325 were H276 and L348, respectively, in CsNMO (Figure 2).

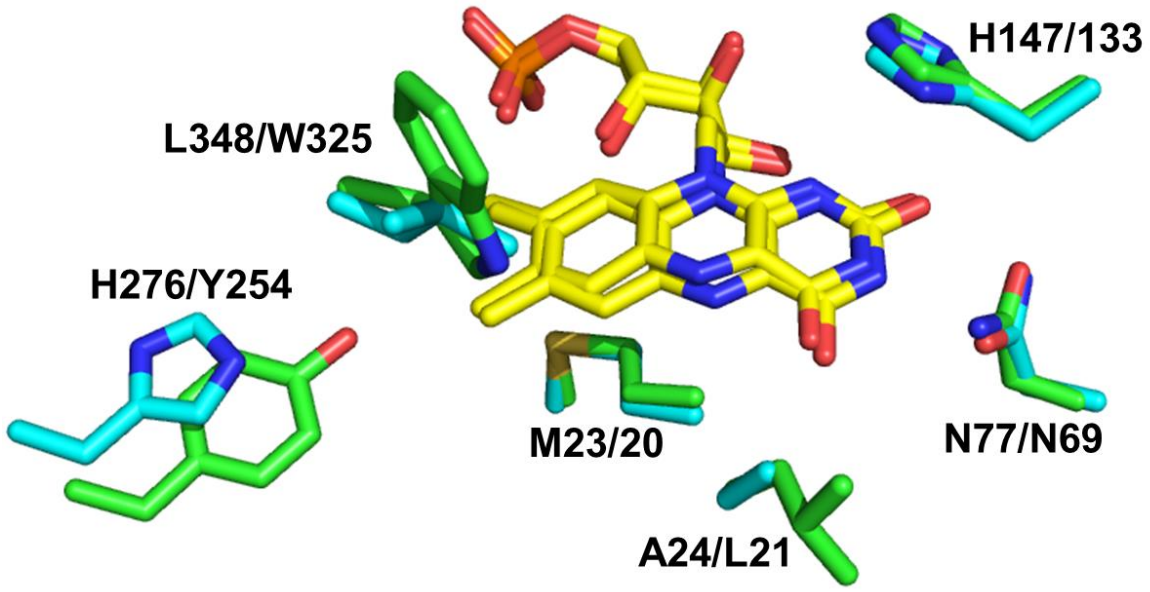

Figure 3.2 Active site residues of CsNMO (cyan, listed first) and PaNMO (green, listed second). FMN cofactors both shown in yellow.

3.4.3 PEG-binding Site

A PEG molecule from the crystallization solution was bound to one loop (residues 67-73) in the FMN binding domain. The closest distance between PEG and FMN was at the O1 atom of PEG and N5 atom of the flavin measuring a distance of 21.4 Å (Figure 3A-B). The conformation of the loop was anchored by an ion pair of R72 and D64, hydrogen bonds between the guanidinium group of R72 and the carbonyl O atom of L139 (Figure 3A-B). A polymer

composed of 12 ethylene units was clearly discernible in the crystal structure. Six monomers of the PEG molecule formed a helical turn around a central water molecule that was hydrogen-bonded with D69. The PEG molecule also formed five additional water-mediated interactions with the main chain atoms of T34, R37, and D69. In addition, the PEG molecule had a number of van der Waals contacts with E13, T34, R37, L38, V67, and D69. The extensive interactions of PEG with the protein suggested that PEG-binding was unlikely to arise from crystal lattice contacts and suggested the presence of a putative binding site for an unknown molecule.

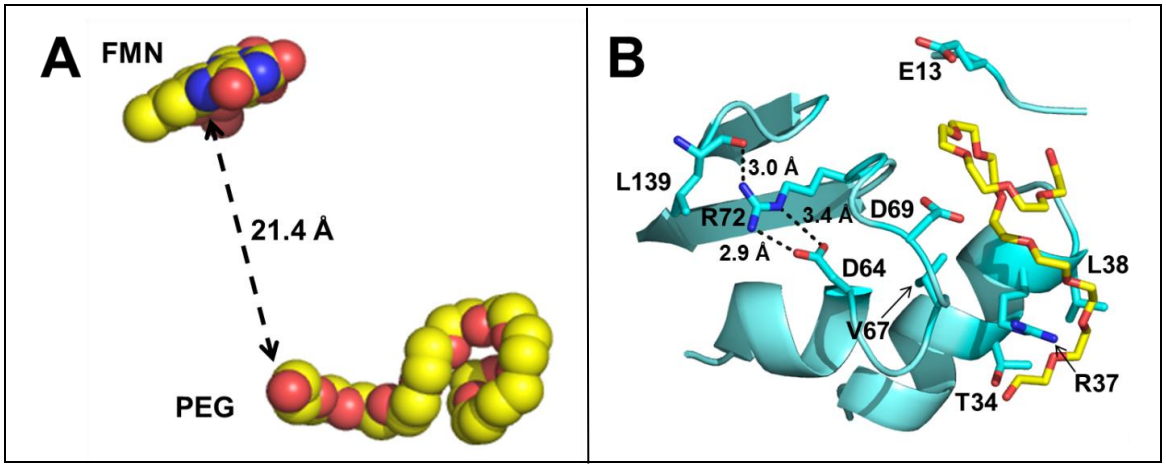

Figure 3.3 Unusual binding of PEG 3350.
Panel A: FMN and PEG are located 21.4 Å apart when measured at the closest contacts, N5 of the flavin to the O1 atom of PEG; Panel B: PEG binds directly to a loop formed by residues 67-74. R72 forms a salt bridge with D64 and the backbone O atom L139. Residues E13, D69, V67, R37, T34, and L38 form van der Waals interactions with PEG.

3.4.4 Effect of PEG 3350 on Steady-state Kinetics

In order to ascertain if PEG had an effect on the function of the enzyme, the steady-state kinetic parameters of CsNMO with P3N were determined in the presence and absence of PEG 3350 in 50 mM NaPPi, pH 6.0, 30 ^{o}C (Figure 4A-B). As shown in Figure 4B, intersecting lines were obtained in a double reciprocal plot of the initial rates of reactions and substrate

concentration. As PEG concentration increased, the slopes in the Figure 4B decreased and the intercept was in quadrant IV consistent with the activator affecting k_{cat}, K_m, and k_{cat}/K_m values. A global fitting of the kinetic data ± PEG to Eq 1 returned the parameters shown in Table 2, with a significantly large effect on K_m ($\alpha << 1$) and k_{cat} ($\beta >> 1$). These results are consistent with PEG behaving as a non-essential "V-" and "K-type" activator of CsNMO with respect to P3N (Scheme 1)[a].[(12)] A kinetic model for non-essential activation was proposed for CsNMO and PEG as the activator with respect to P3N at atmospheric oxygen (Scheme 1).

When the effect of PEG 3350 was assessed on PaNMO, for which no PEG was identified in the 3D structure resolved to 1.44 Å[3], the initial rates of reaction did not change significantly. Consistent with these results, a global fit of the data yielded α and β values not significantly different than one (Table 2), indicating that the bacterial enzyme is not regulated by PEG 3350.

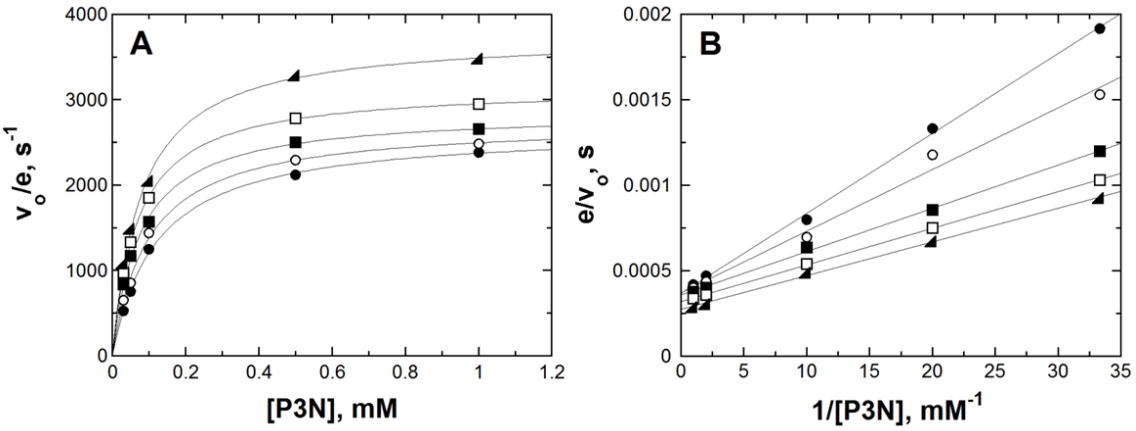

Figure 3.4 Steady-state kinetics of CsNMO with P3N as substrate in the presence of increasing concentrations of PEG 3350.
Initial rates of reaction were determined at atmospheric oxygen in 50 mM NaPPi, pH. 6.0. Kinetic data in Panel A was fit using the Michaelis-M enten equation for an enzyme with one substrate. Panel A: plot of initial rates of reaction versus [P3N] with fixed concentrations of 0 mM (●), 12.5 mM (○), 25 mM (■), 37.5 mM (□), and 50 mM (▲) PEG 3350; Panel B: double reciprocal plot of the initial rates of reaction versus [P3N] with fixed concentrations of 0 mM (●), 12.5 mM (○), 25 mM (■), 37.5 mM (□), and 50 mM (▲) PEG 3350.

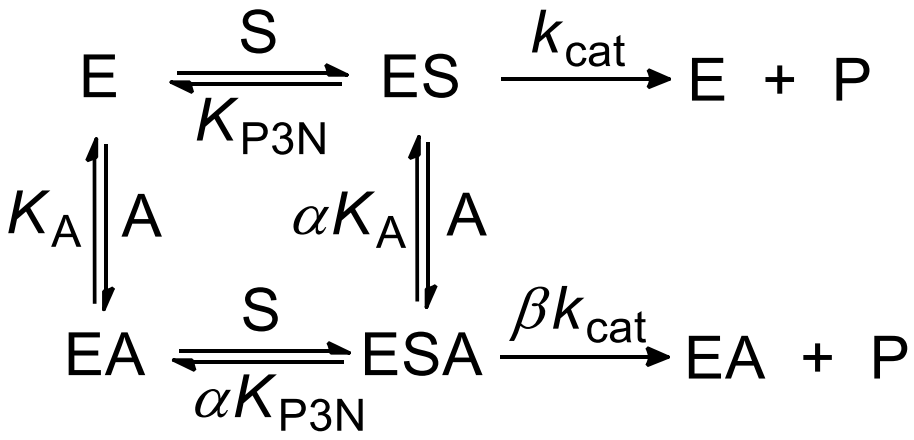

Scheme 3.1 Minimal kinetic mechanism of non-essential activation of CsNMO (E) with PEG 3350 as activator (A) with respect to P3N (S) as substrate, as originally proposed by Irwin H. Segel.[42]
ES, EA, and ESA are the enzyme complexes with the substrate, activator and both; P is the product of the reaction. The definition of k_{cat} and βk_{cat} used here is an oversimplification. However, the approach used to establish Scheme 1 does not allow the authors to dissect the kinetic steps that may contribute to k_{cat}.

Table 3.2 Effect of PEG 3350 on the steady-state kinetic parameters of CsNMO and PaNMO.[a]

Enzyme	k_{cat}, s^{-1}	K_{P3N}, µM	k_{cat}/K_{P3N}, $M^{-1}s^{-1}$	α	β	R^2
CsNMO	2000 ± 60	90 ± 20	(2.3 ± 0.1) x 10^7	0.008 ± 0.002	≥ 7[b]	0.993
PaNMO	1000 ± 50	200 ± 20	(5.0 ± 0.6) x 10^6	1.2 ± 0.3	1.2 ± 0.1	0.990

[a]Conditions: 50 mM NaPPi, pH 6.0 and 30 °C, at varying concentrations of PEG 3350 and fixed oxygen concentration at 230 µM.
[b]Saturation with PEG could not be achieved due to limited solubility, and the lower limiting value is reported.

3.5 Discussion

The crystallographic and biochemical study presented here provides evidence for an allosteric binding site for a non-essential activator of CsNMO with respect to P3N. The overall structures of CsNMO and PaNMO were highly conserved except for two loops (Figure 5) and two active site residues (Figure 2). The structure of CsNMO was resolved with a PEG molecule binding to a surface loop wrapping around a single water molecule forming hydrophobic and hydrogen-bonding interactions with multiple surface residues. This same loop in PaNMO contains a proline and lysine residue and is truncated not allowing for a PEG molecule to bind to the enzyme (Figure 6). PEG-binding in CsNMO indicated an allosteric binding site that was

catalytically relevant only in the fungal enzyme. Kinetic and structural evidences for the non-essential activation of CsNMO in the presence of PEG 3350 are presented below.

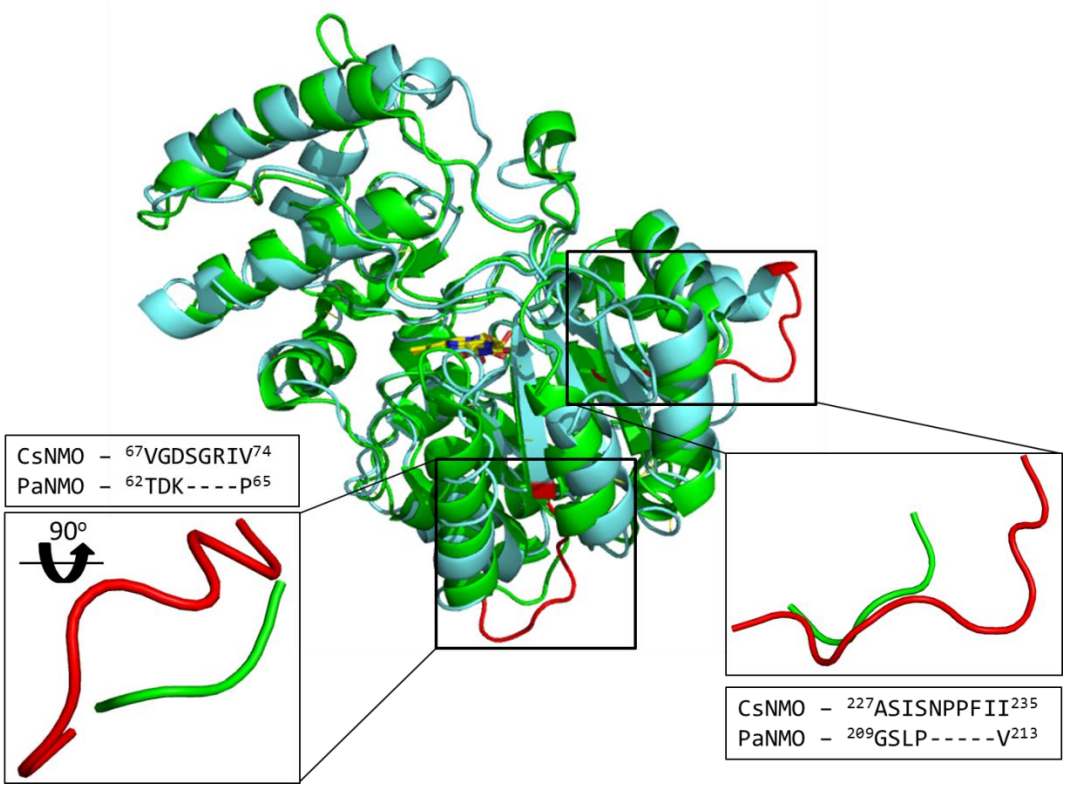

Figure 3.5 Crystal structures of CsNMO (cyan) and PaNMO (green) enzymes aligned on equivalent Cα atoms.
Two loops in CsNMO (red) have been identified as being 4 and 5 residues longer at each position. Inset: Amino acid sequences shown with loops of different conformations highlighted.

PEG is a non-essential allosteric activator of CsNMO, as indicated by the steady-state kinetic parameters with and without PEG 3350. The results with PEG revealed an increase in the steady-state kinetic parameters k_{cat} and k_{cat}/K_m and a decrease in K_m. Other enzymes, mechanistically unrelated, such as 1-deoxy-D-xylulose-5-phosphate reductoisomerase, triosephosphate isomerase and glycerol-3-phosphate dehydrogenase, have also shown non-essential allosteric activation by smaller molecules with dianion phosphate behaving as the activator with respect to the substrate.[13-15] Non-essential activation by dianion phosphate altered

the conformational changes on the enzyme-substrate or enzyme-product complexes.[13, 16] The effects on the kinetic parameters observed in CsNMO may indicate significant repercussions similar to these enzymes. The binding cleft observed in the fungal enzyme could be indicative of a protein-interacting site responsible for modulating increased reactivity with P3N. Alternatively, the binding site could act as a regulator of CsNMO in the cell turning the enzyme on or off as the needs of the cell change or toxicity levels of P3N due to its production.[5]

Irrespective of natural occurrence, catalytic effects and structural binding of PEG molecules have been reported in other enzymes. PEG molecules can be located in more than 1500 crystal structures found in the protein database (PDB), of which, more than a dozen have been shown to bind PEG molecules on the surface or in the active site cavity. Most enzymes were inhibited in regards to the natural substrate giving indications to the physiological substrate and mechanistic implications of each enzyme.[17-19] Acetylcholinesterase from *Torpedo californica* has been shown to bind a PEG molecule in the active site as the first strong example of a neutral molecule inhibiting and binding to a cation-binding site in this family of enzymes.[17] A histone methyltransferase (SMYD2) was observed to bind PEG in a distinct ω-turn conformation indicative of a potential substrate binding cleft or protein-interacting site important for regulation.[20] As a polyol that increases viscosity of a solution, PEG behaving as a non-essential activator of CsNMO may be indicative of its activity enhancement in the cell. Found in high salt/low water potentials ecosystems[21, 22], *C. saturnus* serves as the source of the enzyme in this study and has been shown to produce polyols (i.e. glycerol, mannitol, and xylitol) to maintain hydration levels in the cell.[22] Changes in viscosity and hydration levels, consequently, would affect regulation of the enzyme by osmotic pressure or during times of oxidative stress.

A salt bridge on the surface of CsNMO provided an allosteric binding site for PEG 3350. The formation and stability of the PEG-binding site originates from a salt bridge formed by K72 with D64 and the backbone O atom of L139 (Figure 3B) as evidence of the crystal structure. Previous studies have shown that surface salt bridges composed of side chain to main chain interactions similar to CsNMO have provided increased structural stability over two side chain interactions.[23-26] This same loop in PaNMO is truncated by 4 amino acids with K64 and P64 blocking the allosteric binding site indicative of a lack of salt bridge interactions (Figure 6). The formation of the allosteric site using a salt bridge anchor may have evolutionary implications for polyol binding that have developed in *C. saturnus* to thrive in the high salt/low water potential environment.

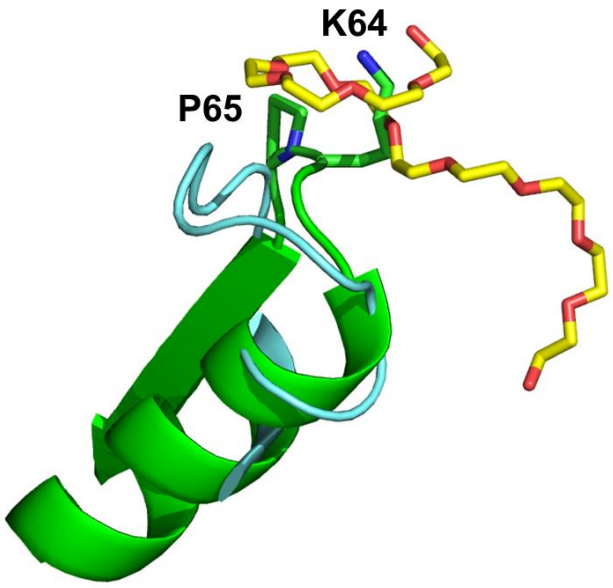

Figure 3.6 PEG-binding site in CsNMO (cyan) and the corresponding loop in PaNMO (green) illustrated as cartoon.

PEG 3350 acts as a K-type and V-type allosteric activator of CsNMO with respect to P3N. Evidence for this effect was observed in the decreasing of K_m values while simultaneously increasing k_{cat} values leading to a change in rate-limiting steps. A K-type activator affects the

binding of substrate whereas V-type affects k_{cat}, the kinetic rate constant representative of the rate-limiting step in turnover. Substrate binding and product release were previously shown to be rate limiting in P3N oxidation as evidence of linear dependences of normalized k_{cat} and k_{cat}/K_m values with respect to the relative viscosity of buffered glycerol solutions.[4] Both substrate binding and product release become less rate-limiting in the presence of PEG due to the activation (both V- and K-type) effect on the enzyme-substrate and enzyme-product complexes. The formation of the PEG-enzyme complex therefore promotes a change in rate limiting steps. Beyond conformational changes, it would be insufficient to use V- and K-type allosteric effects to explain microscopic kinetic rate constants on macroscopic mechanistic events.[27, 28] Therefore, identifying the general allosteric effects of PEG on CsNMO provides explanations on the mechanism of P3N oxidation.

In contrast, PaNMO does not exhibit any effect on its steady-state parameters or structure in the presence of PEG. The kinetic parameters of PaNMO were unaffected in the presence of PEG 3350 consistent with the lack of an allosteric binding site in the crystal structure. Evidence comes from the X-ray crystal structure and steady-state kinetic studies with and without PEG 3350. The overall structure, however, was highly conserved between the fungal and bacterial enzymes in spite of an extra surface loop occupied by PEG and two different active site residues. The two structures are superimposed with an RMSD of 1.6 Å on equivalent Cα atoms by secondary structure matching in CCP4i.[29, 30, 31] Amino acid residues near the xylene moiety of the flavin reflected the only active site differences between the two enzymes. H276 in CsNMO corresponded to Y254 in PaNMO which had no contact with the C7 atom of FMN with the closest approach of 5.6 Å (Figure 2). Leu348, the second C7-interacting residue, was W325 in PaNMO (Figure 2).

In conclusion, the first crystal structure of a eukaryotic NMO enzyme has been resolved to a resolution of 1.65 Å. An allosteric binding site was identified on the surface of the structure occupied with a PEG molecule from the crystallization solution. With respect to P3N, the polyol, PEG 3350, was a non-essential allosteric activator of CsNMO. Although highly conserved, the minute differences in surface loops and active sites residues may lead to larger biological and physiological implications between the fungal and bacterial enzymes in Class I NMOs. Future studies are needed to crystallize more Class I NMO enzymes to determine if the allosteric binding site was specific to CsNMO. If the allosteric binding site was unique to CsNMO, an *in vivo* approach to understanding the events in the cell that cause a polyol binding event of this nature would be intriguing.

3.6 References

1. Francis, K., Nishino, S. F., Spain, J. C., and Gadda, G. (2012) A novel activity for fungal nitronate monooxygenase: detoxification of the metabolic inhibitor propionate-3-nitronate, *Arch. Biochem. Biophys. 521*, 84-89.
2. Gadda, G., and Francis, K. (2010) Nitronate monooxygenase, a model for anionic flavin semiquinone intermediates in oxidative catalysis, *Arch. Biochem. Biophys. 493*, 53-61.
3. Salvi, F., Agniswamy, J., Yuan, H., Vercammen, K., Pelicaen, R., Cornelis, P., Spain, J. C., Weber, I. T., and Gadda, G. (2014) The combined structural and kinetic characterization of a bacterial nitronate monooxygenase from *Pseudomonas aeruginosa* PAO1 establishes NMO class I and II, *J. Biol. Chem. 289*, 23764-23775.
4. Smitherman, C., and Gadda, G. (2013) Evidence for a transient peroxynitro acid in the reaction catalyzed by nitronate monooxygenase with propionate 3-nitronate, *Biochemistry 52*, 2694-2704.

5. Francis, K., Smitherman, C., Nishino, S. F., Spain, J. C., and Gadda, G. (2013) The biochemistry of the metabolic poison propionate 3-nitronate and its conjugate acid, 3-nitropropionate, *IUBMB Life 65*, 759-768.

6. Alston, T. A., Mela, L., and Bright, H. J. (1977) 3-Nitropropionate, the toxic substance of Indigofera, is a suicide inactivator of succinate dehydrogenase, *Proc. Natl. Acad. Sci. USA 74*, 3767-3771.

7. Coles, C. J., Edmondson, D. E., and Singer, T. P. (1979) Inactivation of succinate dehydrogenase by 3-nitropropionate, *J. Biol. Chem. 254*, 5161-5167.

8. Huang, L. S., Sun, G., Cobessi, D., Wang, A. C., Shen, J. T., Tung, E. Y., Anderson, V. E., and Berry, E. A. (2006) 3-nitropropionic acid is a suicide inhibitor of mitochondrial respiration that, upon oxidation by complex II, forms a covalent adduct with a catalytic base arginine in the active site of the enzyme, *J. Biol. Chem. 281*, 5965-5972.

9. Parry, R., Nishino, S., and Spain, J. (2011) Naturally-occurring nitro compounds, *Nat. Prod. Rep. 28*, 152-167.

10. Nishino, S. F., Shin, K. A., Payne, R. B., and Spain, J. C. (2010) Growth of bacteria on 3-nitropropionic acid as a sole source of carbon, nitrogen, and energy, *Appl. Environ. Microbiol. 76*, 3590-3598.

11. Francis, K., and Gadda, G. (2006) Probing the chemical steps of nitroalkane oxidation catalyzed by 2-nitropropane dioxygenase with solvent viscosity, pH, and substrate kinetic isotope effects, *Biochemistry 45*, 13889-13898.

12. Monod, J., Wyman, J., and Changeux, J. P. (1965) On the Nature of Allosteric Transitions: A Plausible Model, *J. Mol. Biol. 12*, 88-118.

13. Kholodar, S. A., Allen, C. L., Gulick, A. M., and Murkin, A. S. (2015) The role of phosphate in a multistep enzymatic reaction: reactions of the substrate and intermediate in pieces, *J. Amer. Chem. Soc. 137*, 2748-2756.

14. Tsang, W. Y., Amyes, T. L., and Richard, J. P. (2008) A substrate in pieces: allosteric activation of glycerol 3-phosphate dehydrogenase (NAD+) by phosphite dianion, *Biochemistry 47*, 4575-4582.

15. Richard, J. P. (2012) A paradigm for enzyme-catalyzed proton transfer at carbon: triosephosphate isomerase, *Biochemistry 51*, 2652-2661.

16. Jencks, W. P. (1975) Binding energy, specificity, and enzymic catalysis: the circe effect, *Adv. Enzymol. Relat. Areas Mol. Biol. 43*, 219-410.

17. Koellner, G., Steiner, T., Millard, C. B., Silman, I., and Sussman, J. L. (2002) A neutral molecule in a cation-binding site: specific binding of a PEG-SH to acetylcholinesterase from *Torpedo californica*, *J. Mol. Biol. 320*, 721-725.

18. Breithaupt, C., Strassner, J., Breitinger, U., Huber, R., Macheroux, P., Schaller, A., and Clausen, T. (2001) X-ray structure of 12-oxophytodienoate reductase 1 provides structural insight into substrate binding and specificity within the family of OYE, *Structure 9*, 419-429.

19. van den Hemel, D., Brige, A., Savvides, S. N., and Van Beeumen, J. (2006) Ligand-induced conformational changes in the capping subdomain of a bacterial old yellow enzyme homologue and conserved sequence fingerprints provide new insights into substrate binding, *J. Biol. Chem. 281*, 28152-28161.

20. Jiang, Y., Trescott, L., Holcomb, J., Zhang, X., Brunzelle, J., Sirinupong, N., Shi, X., and Yang, Z. (2014) Structural insights into estrogen receptor alpha methylation by histone

methyltransferase SMYD2, a cellular event implicated in estrogen signaling regulation, *J. Mol. Biol. 426*, 3413-3425.

21. Kamat, S., Gaikwad, S., Ravi Kumar, A., and Gade, W. N. (2013) Xylitol production by *Cyberlindnera* (*Williopsis*) *saturnus*, a tropical mangrove yeast from xylose and corn cob hydrolysate, *J. Appl. Microbiol. 115*, 1357-1367.
22. Davis, D. J., Burlak, C., and Money, N. P. (2000) Osmotic pressure of fungal compatible osmolytes, *Mycol. Res. 104*, 800-804.
23. Strop, P., and Mayo, S. L. (2000) Contribution of surface salt bridges to protein stability, *Biochemistry 39*, 1251-1255.
24. Yip, K. S., Stillman, T. J., Britton, K. L., Artymiuk, P. J., Baker, P. J., Sedelnikova, S. E., Engel, P. C., Pasquo, A., Chiaraluce, R., Consalvi, V., and et al. (1995) The structure of *Pyrococcus furiosus* glutamate dehydrogenase reveals a key role for ion-pair networks in maintaining enzyme stability at extreme temperatures, *Structure 3*, 1147-1158.
25. Hennig, M., Darimont, B., Sterner, R., Kirschner, K., and Jansonius, J. N. (1995) 2.0 A structure of indole-3-glycerol phosphate synthase from the hyperthermophile *Sulfolobus solfataricus*: possible determinants of protein stability, *Structure 3*, 1295-1306.
26. Spek, E. J., Bui, A. H., Lu, M., and Kallenbach, N. R. (1998) Surface salt bridges stabilize the GCN4 leucine zipper, *Protein Sci. 7*, 2431-2437.
27. Fenton, A. W. (2008) Allostery: an illustrated definition for the 'second secret of life', *Trends Biochem. Sci. 33*, 420-425.
28. Cleland, W. W. (1975) Partition analysis and the concept of net rate constants as tools in enzyme kinetics, *Biochemistry 14*, 3220-3224.

29. Krissinel, E., and Henrick, K. (2004) Secondary-structure matching (SSM), a new tool for fast protein structure alignment in three dimensions, *Acta Crystallogr. D: Biol. Crystallogr. 60*, 2256-2268.

30. Winn, M. D., Ballard, C. C., Cowtan, K. D., Dodson, E. J., Emsley, P., Evans, P. R., Keegan, R. M., Krissinel, E. B., Leslie, A. G., McCoy, A., McNicholas, S. J., Murshudov, G. N., Pannu, N. S., Potterton, E. A., Powell, H. R., Read, R. J., Vagin, A., and Wilson, K. S. (2011) Overview of the CCP4 suite and current developments, *Acta Crystallogr. D: Biol. Crystallogr. 67*, 235-242.

31. Potterton, E., Briggs, P., Turkenburg, M., and Dodson, E. (2003) A graphical user interface to the CCP4 program suite, *Acta Crystallogr. D: Biol. Crystallogr. 59*, 1131-1137.

32. Mijatovic, S., and Gadda, G. (2008) Oxidation of alkyl nitronates catalyzed by 2-nitropropane dioxygenase from *Hansenula mrakii*, *Arch. Biochem. Biophys. 473*, 61-68.

33. Bush, M. T., Touster, O., and Brockman, J. E. (1951) The production of beta-nitropropionic acid by a strain of *Aspergillus flavus*, *J. Biol. Chem. 188*, 685-693.

34. Otwinowski, Z., and Minor, W. (1997) Processing of X-ray diffraction data collected in oscillation mode, *Methods Enzymol. 276*, 307-326.

35. McCoy, A. J., Grosse-Kunstleve, R. W., Storoni, L. C., and Read, R. J. (2005) Likelihood-enhanced fast translation functions, *Acta Crystallogr. D: Biol. Crystallogr. 61*, 458-464.

36. Storoni, L. C., McCoy, A. J., and Read, R. J. (2004) Likelihood-enhanced fast rotation functions, *Acta Crystallogr. D: Biol. Crystallogr. 60*, 432-438.

37. Perrakis, A., Harkiolaki, M., Wilson, K. S., and Lamzin, V. S. (2001) ARP/wARP and molecular replacement, *Acta Crystallogr. D: Biol. Crystallogr. 57*, 1445-1450.

38. Perrakis, A., Morris, R., and Lamzin, V. S. (1999) Automated protein model building combined with iterative structure refinement, *Nat. Struct. Biol. 6*, 458-463.

39. Murshudov, G. N., Vagin, A. A., and Dodson, E. J. (1997) Refinement of macromolecular structures by the maximum-likelihood method, *Acta Crystallogr. D: Biol. Crystallogr. 53*, 240-255.

40. Emsley, P., and Cowtan, K. (2004) Coot: model-building tools for molecular graphics, *Acta Crystallogr. D: Biol. Crystallogr. 60*, 2126-2132.

41. Nielsen, A. T., (Ed.) (1969) *Nitronic acids and esters*, Interscience Publishers, New York.

42. Dewolf, W., Jr., and Segel, I. H. (2000) Simplified velocity equations for characterizing the partial inhibition or nonessential activation of bireactant enzymes, *J. Enzyme Inhib. 15*, 311-333.

4 Conserved Hydration Sites in Pin1 Reveal a Distinctive Water Recognition Motif in Proteins

(This chapter has been submitted verbatim to *Journal of Chemical Information and Modeling* co-authers Arghya Barman, Michael Souffrant, Giovanni Gadda, and Donald Hamelberg. The author's contribution to this chapter involved the collection and interpretation of circular dichroism spectroscopy experiments and editing of the manuscript.)

4.1 Summary

Structural studies of Pin1 revealed two highly conserved water molecules in the catalytic domain. Here, we investigate the significance of these structurally conserved water molecules using computational simulations, analysis of X-ray crystal structures, and CD experiments. Free energy calculations suggest that the tighter binding water molecule is functionally important in stabilizing a critical hydrogen-bonding network in the active site. The weaker-binding water molecule is exchangeable with bulk solvent and is found in a distinctive helix-turn-coil motif. Structural bioinformatics analysis reveals that this motif is present in several other proteins and can trap water, akin to the calcium EF hand. CD studies suggest that this motif by itself is in a P_{II} conformation and needs the protein environment to fully fold into the helix-turn-coil motif. This study provides valuable insights into the role of hydration in the structural integrity of Pin1 that can be exploited in protein engineering and drug design.

4.2 Highlights

- Tightly bound conserved water in Pin1 maintains critical hydrogen-bond network.
- Weaker bound exchangeable water is present in a distinctive helix-turn-coil motif.
- The unique helix-turn-coil motif is found in other proteins with localized water.

- CD spectra confirm the requirement of protein environment to stabilize the motif.

4.3 Introduction

Water molecules play a significant role in chemical biology and have direct involvement with biomolecules, especially when they are localized in well-defined pockets. They are crucial for biomolecular stability, flexibility and function (Nagendra *et al.*, 1998). The presence of water at an internal cavity stabilizes protein structures by hydrating the polar atoms, and the loss of these localized internal water molecules can induce structural unfolding of protein structures (Robinson and Cho, 1999). Conserved water molecules have been suggested to play important roles in stabilization of loop structure for protein-protein interactions, such as the Ω loop in the class A β-lactamase (Bös and Pleiss, 2008). Structurally, conserved water molecules have been found to be an integral part of several classes of proteins, including ribonuclease T1 (Loris *et al.*, 1999), serine proteases (Sreenivasan and Axelsen, 1992), Rossmann fold dinucleotide binding proteins (Bottoms *et al.*, 2002), MHC class 1 proteins (Ogata and Wodak, 2002), aspartic proteinases (Prasad and Suguna, 2002), and protein kinases (Knight *et al.*, 2009). Individual water molecules can be crucial in organic reactions and enzyme function (Kahne and Still, 1988). Water molecules actively participate in hydrolysis and esterification reactions and play a major role in chemical catalysis by taking part in transition state stabilization (Kahne and Still, 1988;Romero and de Meis, 1989). Moreover, studies indicate that water molecules can be crucial for protein-ligand recognition by bridging the interactions (Hamelberg and McCammon, 2004;Sahai and Biggin, 2011). Bridging the interactions of water with ligands can be exploited to enhance the affinity of ligands in drug discovery processes (Michel *et al.*, 2009;Gianti *et al.*, 2015). Another important role of water includes regulating the dynamics of proteins (Hamelberg *et al.*, 2006;Johnson *et al.*, 2010). Conserved water molecules at a site distal from the active site

have been identified in several families of proteins to play significant roles in maintaining the structural integrity of the active site (Barycki *et al.,* 2001). Water molecules can also act as allosteric modulators that can alter the dynamics and function of biomolecules (Prakash *et al.*, 2012). Usually, these structural waters are conserved within a protein family, that is, they occupy nearly identical three-dimensional locations with reference to their associated structures to perform the same function. Recent computational and experimental studies show that mutating the critical water-interacting residue can disrupt the interaction network and alter enzyme activity (Szep *et al.*, 2009;Park and Saven, 2005). These studies therefore indicate that structural water molecules located within the protein core can play an important role, modulating protein structure, flexibility, ligand binding and function.

Peptidyl proline isomerases (PPIases) are a family of enzymes that catalyzes *cis*/*trans* isomerizations of peptide bonds preceding a proline residue (Lang *et al.*, 1987;Yaffe *et al.*, 1997). Pin1 belongs to the Parvulin family of PPIases and catalyzes *cis*/*trans* isomerizations of the prolyl ω bond when the preceding residue is a phosphorylated Ser (pSer) or Thr (pThr) (Bayer *et al.*, 2003;Yaffe *et al.*, 1997;Schutkowski *et al.*, 1998;Ranganathan *et al.*, 1997). Pin1 controls the regulatory action of a pool of *cis*/*trans* pSer/pThr motifs in a multitude of cellular signaling pathways, including DNA repair, cell growth and division, apoptosis and transcription (Lu and Zhou, 2007). The synergy between posttranslational phosphorylation and catalysis of *cis/trans* isomerizations by Pin1 has implications for the proper function of many sub-cellular processes in order to prevent diseases, involving cancers (Theuerkorn *et al.*, 2011;Lu and Zhou, 2007) and Alzheimer's (Bulbarelli *et al.*, 2009;Lu *et al*., 1999;Pastorino *et al.*, 2006). Pin1 is therefore a potential therapeutic target for the treatment of many life-threatening diseases. Structurally, Pin1 contains two conserved water molecules, henceforth referred to as Wat1 and

Wat2, near the active site (Figure 1A). Wat1 forms a hydrogen-bonding network with residues His59, Ser111 and Ser115 (Figure 1B). His59 and Ser115 interact with a critical active site Cys113 residue, which is important for the function and regulation of Pin1 (Ranganathan *et al.*, 1997;Barman and Hamelberg, 2014;Xu *et al.*, 2014;Wang *et al.*, 2015). Wat2 is located near the substrate binding site and is within the crevice of a helix-turn-coil structural motif, which is akin to a well-known EF-hand localization motif for calcium ions (Nakayama and Kretsinger, 1994). Wat2 forms a hydrogen-bonding network with Gln129, Met130 and Glu135 (Figure 1C).

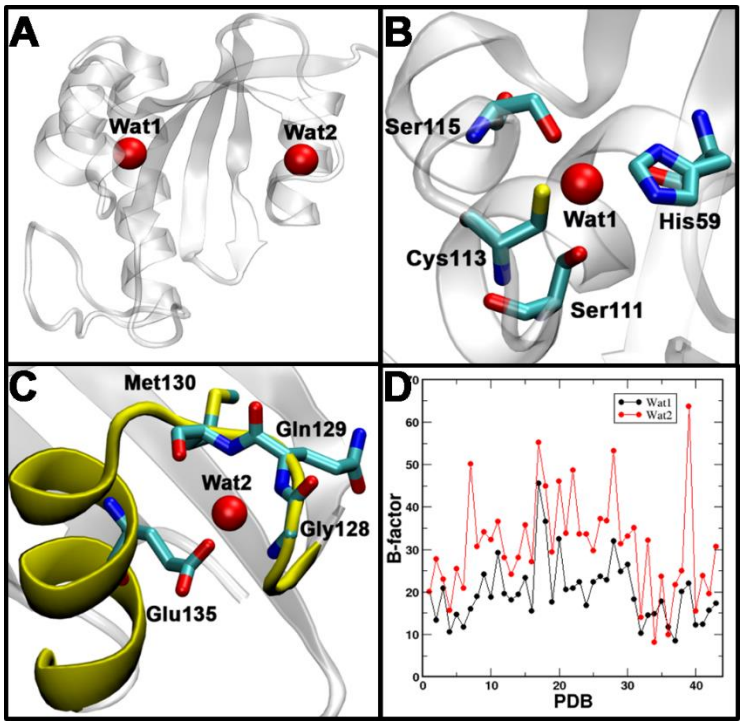

Figure 4.1 Conserved water binding in Pin1.
A) Location of the two conserved water molecules Wat1 and Wat2 in the Pin1 crystal structure (PDB id: 2Q5A). B) Interaction of Wat1 with neighboring active site residues. C) Interaction of Wat2 with the surrounding residues. The helix-turn-coil motif is shown in yellow cartoon. D) The crystallographic B-factors of Wat1 (black) and Wat2 (red) in the corresponding X-ray structure.

Studies are currently being carried out to investigate the atomistic detail of the catalytic mechanism of Pin1 through a number of experimental and theoretical studies (Greenwood *et al.*,

2011;Velazquez and Hamelberg, 2011;Velazquez and Hamelberg, 2013;Vöhringer-Martinez *et al.*, 2012;Schutkowski *et al.*, 1998;Barman and Hamelberg, 2014;Ranganathan *et al.*, 1997;Mercedes-Camacho *et al.*, 2013;Namanja *et al.*, 2011;Di Martino *et al.*, 2014). However, the significance of these conserved water molecules has never been addressed to the best of our knowledge. In this study, detailed free energy calculations and MD simulations have been utilized to address structural and functional roles of these two water molecules. Furthermore, CD spectroscopic studies were performed on the isolated helix-turn-coil motif consisting of 20 amino acid residues to investigate its stability and isolated conformational ensemble. A structural bioinformatics study was also undertaken to investigate the prevalence of similar structural motifs in a non-redundant protein database. Additional atomistic details of Pin1 and its localized hydration may provide necessary information on fully understanding the mechanism of Pin1. A unique structural motif in proteins that can trap water molecules has also been revealed. The motif can serve as an elementary unit in protein engineering and enzyme design.

4.4 Results and Discussion

4.4.1 Crystal Structure Analysis

Forty-seven X-ray crystal structures of the human Pin1 were obtained from the PDB and analyzed. Structural superposition of Pin1 catalytic domain of all structures revealed two sites with conserved waters. Site1 consisted of interactions from the side chains of His59, Ser111 and Ser115, located near the crucial active site residue Cys113. Site2 (Wat2) was located approximately 15 Å away from site1 and was defined by interactions involving the side chains of Gln129, Met130 and Glu135 within a helix-turn-coil motif. Wat1 was absent in the crystal structures with PDB IDs 2XP8 (2.1 Å) and 2ZR6 (3.2 Å), and Wat2 was not resolved in structures with PDB IDs 2XP8 (2.1 Å), 3KAB (2.2 Å) and 3TC5 (1.4 Å). The crystallographic

B-factors for these two water molecules were compiled from their corresponding PDB files and shown in Figure 1D. The plot of B-factors of these two water molecules suggests that Wat1 was, in general, less mobile than Wat2.

4.4.2 Molecular Dynamics Simulations and Free Energy Calculations

MD simulations of Pin1 were carried out in order to further study the dynamics of Wat1 and Wat2. The distances between the backbone carbonyl 'O' of His59, side chain oxygen 'OG' of Ser111 and Ser115, and the oxygen 'O' of Wat1 are shown in Figure 2. The distributions of these distances indicated that these three amino acids strongly interacted with Wat1, with heavy atom-heavy atom distance of ~2.7Å. The distances between the backbone nitrogen 'N' of Gln129, Met130 and side chain oxygen 'OE1' of Glu135, and the oxygen 'O' of Wat2 varied from ~2.7Å to ~3.5Å, suggesting weaker interactions between Wat2 and these residues. Wat1 and Wat2 had a root-mean-square-fluctuation (rmsf) of 0.46Å and 0.62Å respectively, which were consistent with the B-factors of the X-ray crystallographic structural data.

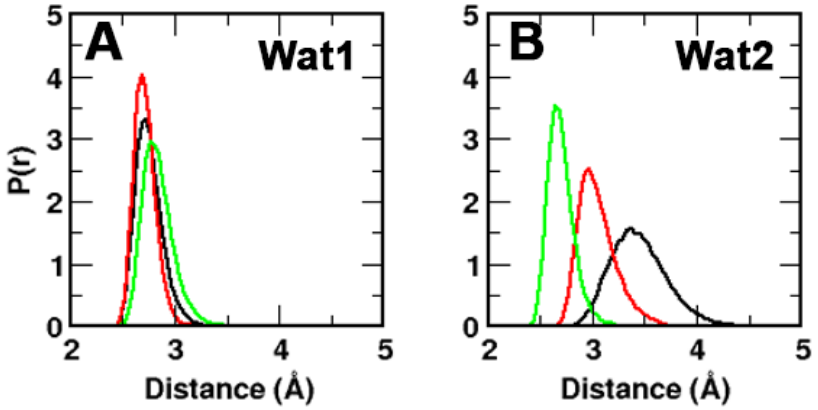

Figure 4.2 Probability distribution of distances of water molecules from interacting neighboring residues. A) The distance between His59(O)-Wat1(O) (black), Ser111(OG)-Wat1(O) (red) and Ser115(OG)-Wat1(O) (green). B) The distance between Gln129(N)-Wat2(O) (black), Met130(N)-Wat2(O) (red), Glu135(N)-Wat2(O) (green).

A more quantitative characterization of these water molecules was explored by calculating their binding free energies. Indeed, a binding free energy of -2.8 ± 0.3 kcal/mol indicated the interaction of Wat1 was highly favorable at site1. Wat1 interacts with the His59, Ser111 and Ser115 residues that are critically important for maintaining a hydrogen-bonding network within the active site of the enzyme. Two MD simulations were performed in presence and absence of Wat1 at site1 to determine the structural role of Wat1 in catalysis. Wat1 was observed to be completely buried and had strong interactions with the polar residues at this site, restricting any exchange with the bulk water during a simulation run for 1 μs. In the presence of Wat1, the distributions of the distances between Cys113 (SG) and Ser115 (OG1) (d1), His59 (N_ε) and Cys113 (SG) (d2), Ser115 (OG1) and His59 (N_ε) (d3), His59 (N_ε) and His157 (N_δ) (d4), and His157 (N_ε) and Thr152 (OG1) (d5) clearly indicated the existence of a strong hydrogen bond network at the active site. However, the absence of Wat1 from its localized site significantly disrupted the hydrogen-bonding network involving the active site residues in d1, d2, and d3, as shown in Figure 3. Furthermore, two additional MD simulations were performed in the presence of the substrate (Ace-FFpSPR-Nme), with and without Wat1 in site1. In the presence of Wat1 and the substrate, the distributions of distances (d1-d5) did not change significantly. However, the hydrogen-bonding network was found to be perturbed in the absence of Wat1 and in the presence of the substrate (Figure S1). The results clearly suggested that Wat1 played a crucial role in the dynamics of the active site of Pin1 in the presence and absence of the substrate, maintaining the integrity of a strong and extended hydrogen-bonding network involving the active site residues.

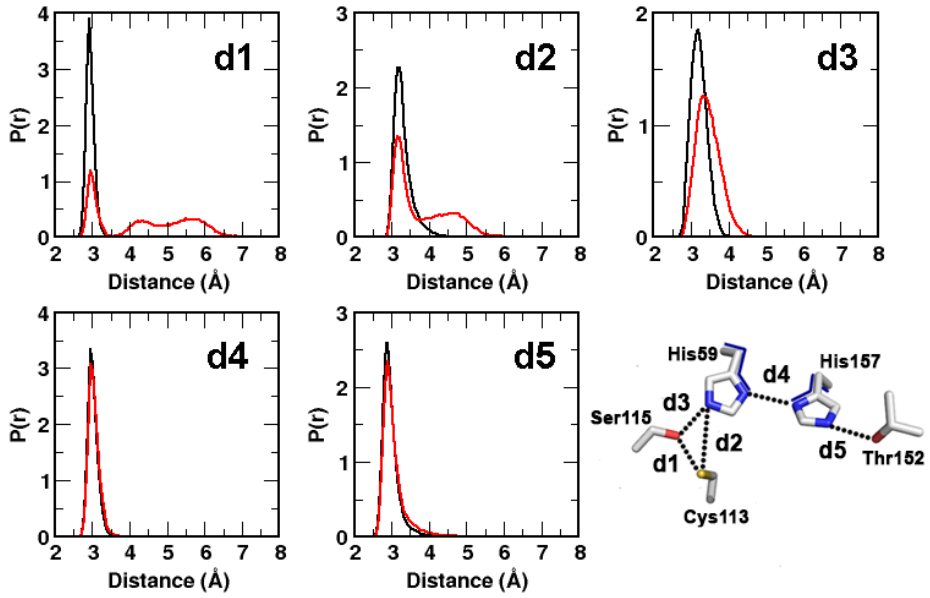

Figure 4.3 Probability distributions of hetero atomic distances among active site residues in the presence and absence of Wat1.
Black and red correspond to the system in the presence and absence of Wat1 respectively; d1 and d2 correspond to the distances between the OG of Ser115 and N_ε of His59 with SG of Cys113, respectively; d3 represents the distance between N_ε of His59 and OG of Ser115; d4 denotes the distance between N_δ of His59 and N_δ of His157; d5 corresponds to the distance between OG1 of Thr152 and N_ε of His59.

Wat2, conversely, exhibited a lower binding free energy (-0.7 ± 0.2 kcal/mol) and was partially exposed to the solvent. The weaker binding free energy of Wat2 was highly correlated with the solvent exchangeability with bulk solvent as observed in a 1μs simulation (Figure S2). A similar Wat2 binding motif was observed in FK506 binding protein (FKBP), another class of PPIases (Park and Saven, 2005;Szep *et al.*, 2009). MD simulations and X-ray crystallographic studies suggested that Wat2 in FKBP played a critical role in structural organization of an active site Trp residue of the enzyme. Structural studies revealed that a single point mutation of a Glu to a Gln residue in the FKBP motif displaced the water molecule, perturbing the Trp residue to adopt an alternative conformation and altering the enzymatic activity (Park and Saven, 2005;Szep *et al.*, 2009). These findings suggested a sequence requirement for the motif to bind a

water molecule. Structural superposition of Pin1 and FKBP shows that the Trp in FKBP is in place of active site Phe136 in Pin1 (Figure S3A). The structural motif and corresponding glutamate residue in Pin1 (Glu135) was highly conserved across different species (Figure S4). The hypothesis of a preferred sequence to trap a water molecule in Pin1 was tested by mutating (*in silico*) Glu135 to Gln and further MD simulations of the variant in the presence of water molecule, Wat2. Wat2 was shown to move to the bulk solvent in less than 50 ns of simulation time of the Pin1-Glu135Gln variant (Figure 4A), with the side chain of Gln partially occupying site2 and leaving no available space for a water molecule to re-enter. The side chain oxygen 'OE1' of Gln of the Pin1-Glu135Gln variant occupied site2 and directly interacted with the backbone 'NH' of residue Gln129 and Met130. The dihedral angle distributions of chi1 and chi2 of the side chain of Phe136 showed no significant impact upon mutating Glu to Gln (Figure S5). The presence of Arg127 and Lys132 in the Wat2 motif seemed to create a highly electropositive environment attracting Glu135 away from the pocket, which resulted in a void that could occupy a water molecule (Figure S3B). However, this particular interaction was lost in the presence of neutral Gln during the Pin1-Glu135Gln simulation.

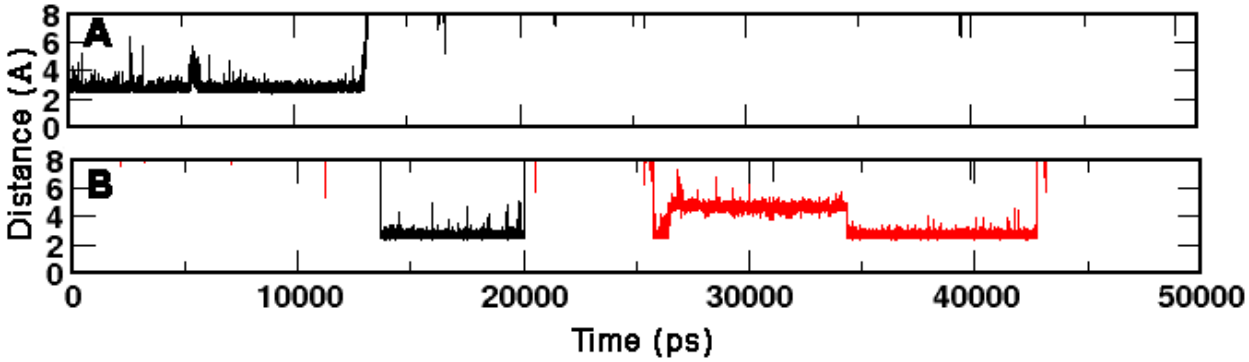

Figure 4.4 MD simulations of Wat2 movements in WT versus hPar14 double mutant.
A) The water molecule (Wat2) of Pin1 moves to the bulk solvent after 13 ns when the Glu135 of Pin1 is mutated to Gln. B) The double mutation (Gly92Lys and Gln95Glu) in hPar14 enable the motif to capture the water molecule. The water is observed to excha nge with the bulk solvent.

4.4.3 Comparison of Pin1 and hPar14

Pin1 is highly homologous to the Parvulin family of *cis/trans* isomerases (Figure S6A). Pin1 has therefore been considered as a special case of the Parvulin family of enzymes with a WW-domain and a phosphate-binding pocket. The catalytic domain of human Pin1 is structurally similar to hPar14, with 36% sequence identity and 44% sequence similarity. Muller et al. have resolved a high resolution X-ray crystal structure of hPar14 that revealed some of the differences to Pin1 (Mueller *et al.*, 2011). Notably, hPar14 only had one distinct water recognition motif, which lacked the conserved water molecule observed in Pin1. Wat2 structural motif of Pin1 is present in hPar14, but Gly92 and Gln95 replace the highly conserved Lys132 and Glu135 residues, respectively, in Pin1 (Figure S6A). The differences from the two residues rendered hPar14 devoid of a localized water molecule. MD simulations of hPar14 were carried out further to study the hydration density as shown in Figure S6B. The structural motif in hPar14 is shown not to localize a water molecule, which agreed with the X-ray crystallographic data. These results are consistent with the structural motif of Wat2 in hPar14 as being necessary but not sufficient to trap a water molecule, in which case, a consensus sequence is also required. This hypothesis was tested by carrying out an MD simulation of hPar14 with a doubly mutated (*in silico*) structural motif (Gly92Lys and Gln95Glu). As hypothesized, the structural motif of the hPar14 variant was shown to accommodate a water molecule that exchanged with bulk solvent, as shown in Figure 4B.

4.4.4 Stability of Isolated Motif

The necessity of both the structural motif and consensus sequence within Pin1 to act as a water-binding site was determined by the use of computations and spectral determinations. The

studies were to determine if the isolated water recognition motif was stable in the absence of the protein construct. The answers to such a question yield importance in structural biology and protein engineering and provide a deeper understanding of protein stability. CD experiments and MD simulations were used to study the 20-amino acid structural motif of the Wat2 binding site in Pin1. Secondary structure analysis of a 100 ns MD simulation trajectory of the isolated structural motif revealed the conformation to be random coil in solution (Figure 5). CD experiments revealed the peptide possessed a polyproline II (P_{II}) conformation at 20 ^{o}C (Figure 6A) (Makowska *et al*., 2006). The P_{II} secondary structure exhibited a CD spectrum depicted by a weak positive band ~217 nm and a negative band around 200 nm (Drake *et al*., 1988). The secondary structure did not change with temperature from 4 to 60 ^{o}C in aqueous buffer (data not shown) and remaining experiments were conducted at 20 ^{o}C. Sodium chloride was titrated into the peptide solution up to 1 mM final concentration in order to induce or stabilize a secondary structure different from P_{II}, but the addition of NaCl did not alter the secondary structure (data not shown). The CD spectral data were consistent with the simulation results, providing additional validation of the predictability of the force field parameters.

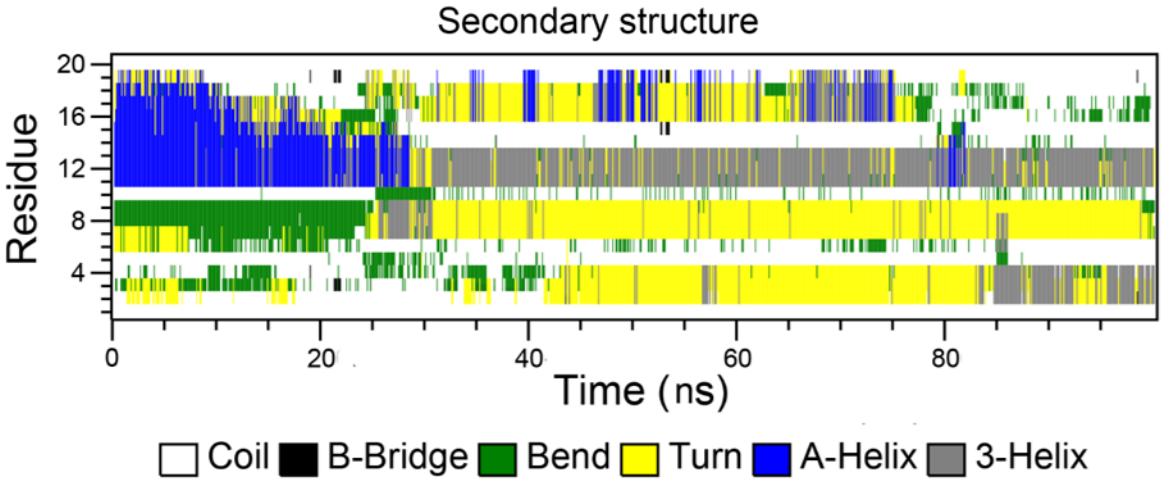

Figure 4.5 Evolution of secondary structure of the isolated Wat2-binding 20mer peptide motif during 100 ns of simulation.

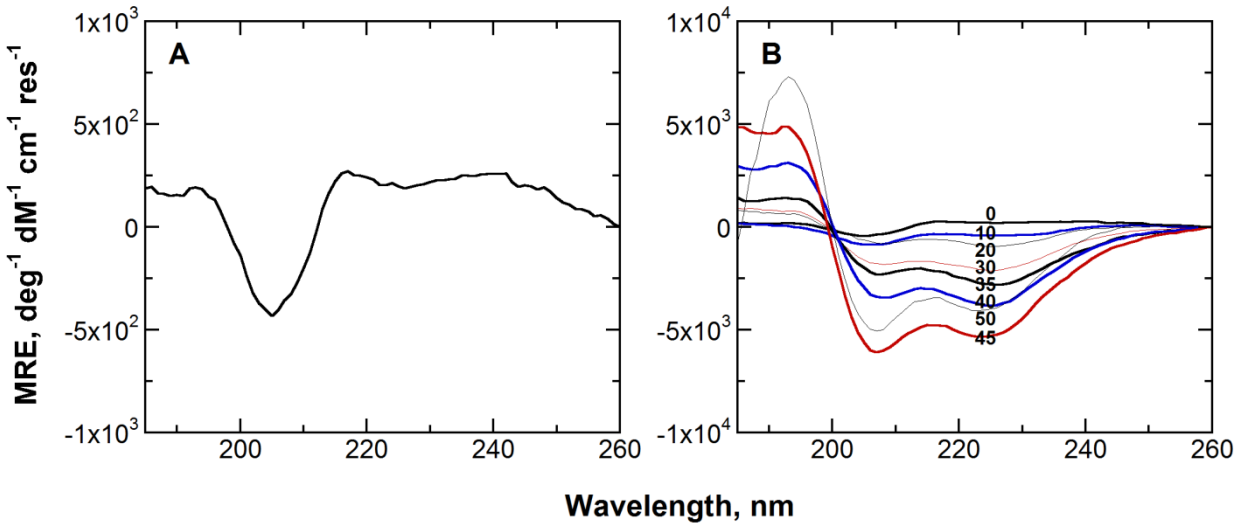

Figure 4.6 CD Spectra of the 20mer peptide in 100 mM KPi, 10 mM NaCl, pH 7.0, at 20 ºC.
A) Peptide in buffered solution prior to titration with TFE. B) Spectral changes due to increasing percentages of TFE (v/v) in the peptide solution. Each spectrum was acquired by the average of 5 scans measured at 50 nm/min and smoothed by the Means-Movement method using Jasco Spectra Analysis Software. See also Figure S7.

TFE was titrated into the peptide solution from 0 to 50 % v/v and the mean residue ellipticity (MRE) is shown in Figure 6B. TFE has been utilized as a cosolvent in solutions containing peptides to alter the hydrophobicity and hydrogen-bonding interactions in the solvent in order to mimic the protein environment (Povey *et al.*, 2007). Upon TFE titration, the pronounced peaks at 204 and 228 nm were altered. Negative peaks at 207 and 224 nm became dominant in the CD spectrum indicating the peptide was developing an α-helical secondary structure (Figure 6B). One isodichroic point was observed at 200 nm indicative of an equilibrium between two dominant secondary structures, likely P_{II} and α-helix. It was not a simple unfolding to folding transition but rather a conversion of P_{II} helix to α-helix upon titrating TFE into the solution. This equilibrium was evident when the negative MRE value was plotted as a function of TFE percent graphically revealing the tendency for Pin1 peptide to adopt an α-helix secondary structure (Figure S7). TFE acted as a mimic of the protein environment that assisted with

inducing the helicity of the peptide, suggesting that the α-helix motif of the peptide was only stable in the protein environment and developed a P_{II} motif without the protein scaffold.

4.4.5 Identification of a Similar Structural Motif in Other Proteins

The functionality of the structural motif binding water in Pin1 prompted further search in other proteins. A search of a non-redundant set of protein structures in the PDB for a similar Wat2 structural motif was carried out using MaDCaT program (Zhang and Grigoryan, 2013) and a 13 amino acid residue probe from Pin1. It was observed that the structural feature of the motif was present in about 1200 non-redundant protein structures in the PDB. Of the approximately 1200 structures, more than 880 structures had resolutions of higher than 2.5 Å. In general, motifs with a water molecule have a Glu at the position equivalent to Glu135 in Pin1 (Figure 7A). Of the 16 structures with Glu, 43% (7 structures) trap a single water molecule in the helix-turn-coil motif (Figure 7B). The remaining 9 structures have a resolved water molecule either close to the helix-turn-coil motif, but not buried, or not at all. (Figure 7A). Alternatively, 95 structures contain a Gln residue in lieu of Glu and only one structure was shown to contain a localized water molecule (Figure 7C). Interestingly, the remaining structures are devoid of a buried water molecule. The presence of Glu in the position of Glu135 in Pin1 from the crystal structure increased the propensity to localize a water molecule at site2 consistent with the MD simulations carried out in this study. In general, the positively charged environment that was observed in the helix–turn-coil motif of Pin1 near the Glu residue stabilized the negative charge likely present on the oxygen atom of the Glu side chain that would create a conducive pocket for the water molecule (Figure S8A-D). When a Gln residue was observed in the motif, the water molecule was only observed in the absence of electropositive residues (Figure S8E). The positively-

charged environment of the motifs containing Gln favored the side chain to occupy the pocket instead of a water molecule (Figure S8D), consistent with the simulation results in this study.

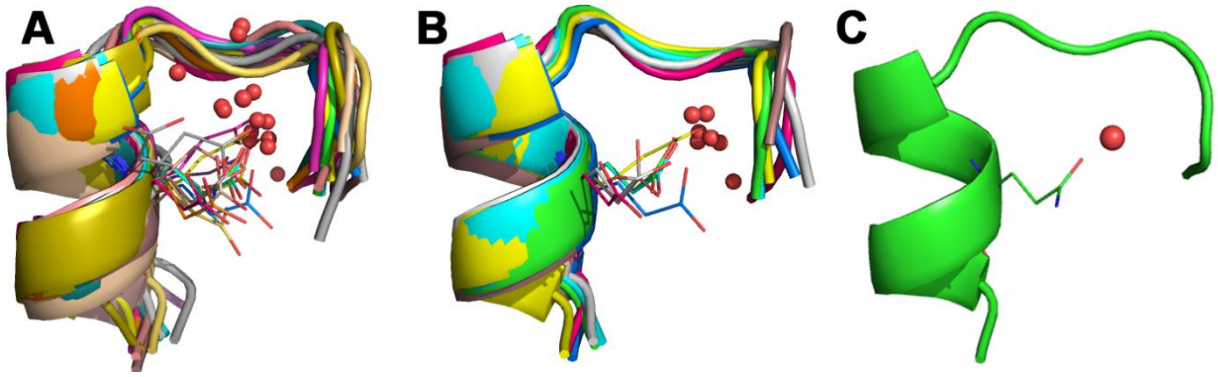

Figure 4.7 Conserved water-binding motifs present in other proteins.
A) The structural motifs having Glu with and without water found in the PDB database using a 13mer peptide probe (RGQMQKPFEDASF) (PDB IDs: 3NXL, 2O70, 2RCH, 3TYI, 1XMI, 1Y89, 2WY7, 3UEN, 4BYZ, 36IC, 1WY5, 2OZT, 3M1I, 1G5B, 3EHM, 2Z67). B) Structural wat er molecules at the crevice formed within the motif having Glu (PDB IDs: 36IC, 1YW5, 2OZT, 3M1I, 1G5B, 3EHM, 2Z67). C) Structure with Gln and water at the cleft (PDB ID: 2W7Y).

4.5 Conclusions

In this study, the roles of two conserved water molecules in the vicinity of the active site of Pin1 were identified and investigated using MD simulations and CD spectroscopic studies. The results are consistent with a water molecule (Wat1) being completely buried and providing stability to the protein. Wat1 is important in maintaining the integrity of the active site involving the side chains of Ser111 and Ser115. Furthermore, it plays a role in an extended hydrogen-bonding network with active site residues such as Cys113, which is involved in modulating the hydrogen-bonding network based on its protonation state. In the absence of this water molecule, the hydrogen-bonding network is disrupted and the active site residues are not properly aligned.

The free energy of binding conserved water, Wat2, suggested a weaker binding. MD simulations revealed this water molecule exchanged with the bulk solvent unlike Wat1. This

study revealed Wat2 is localized in a unique helix-turn-coil structural motif that is present in other protein structures beside Pin1. The structural conformation and amino acid sequence of the motif were both necessary to localize the water molecule. Both MD simulations and CD spectroscopic data were consistent with the isolated water-binding motif as being in a distorted conformation at room temperature, which suggested that the protein environment is necessary for stabilizing the structural motif of the Pin1 sequence. The agreement between the CD experiments and MD simulations further serves as a validation of the molecular mechanics force field parameters. A search of the PDB suggested the Pin1 motif was present in other protein structures and alluded to its function as a conserved water-binding motif. The discovery of this water-binding motif would have implications for protein design and engineering. The sequence of a similar motif could be modified to trap a water molecule in order to enhance the thermodynamic stability of the protein or alter its function.

4.6 Materials and Methods

Structural analysis was performed after downloading all the crystal structures of the human Pin1 from the PDB. PDB files with multiple copies of Pin1 were separated into individual copies to obtain a total of 47 crystal structures (See Table S1 for complete list of PDB structures) and superposed based on the root mean square deviation of the protein backbone atoms. The Debye–Waller factors (B-factors) of the two conserved water molecules in the PDB structures, Wat1 and Wat2, were recorded in order to get a sense of their relative localization. The initial coordinates of Pin1 for all the simulations were taken from a high resolution (1.5 Å) crystal structure with PDB ID 2Q5A (Zhang *et al.,* 2007). Two conserved water molecules, Wat1 and Wat2, correspond to HOH301 and HOH319 in the PDB file, respectively. Only the C-terminal PPIase catalytic domain (residues 50 – 163) was considered in this study. The initial model for

human Parvulin (hPar14) was obtained from the recently resolved high resolution (0.8 Å) crystal structure with PDB ID 3UI4 (Mueller *et al.*, 2011). The isolated 20mer peptide motif, containing consecutive residues from Leu122 to Leu141, was obtained from the Pin1 crystal structure (PDB ID 2Q5A). The 20mer peptide utilized for CD spectral studies consisted of an amino acid sequence of LGAFSRGQMQKPFEDASFAL as synthesized by Sigma Aldrich (St. Louis, MO) with an acetylated N-terminal and an amide on the C-terminal. Sodium chloride and potassium phosphate were purchased from Fisher Scientific (Pittsburgh, PA) and 2,2,2-trifluoroethanol (TFE) was from Sigma Aldrich (St. Louis, MO).

4.7 Experimental Procedure

4.7.1 MD Simulations

All simulations were performed using the AMBER10 (Case *et al.*, 2005) program with the modified version of the Cornell et al. ff99SB (Hornak et al., 2006) force field. The xleap module in AmberTools was used to solvate the system in TIP3P (Jorgensen, 1982) cubic periodic box. All of the bonds involving hydrogen were constrained using SHAKE algorithm (Ryckaert *et al*., 1977). The systems were equilibrated at 300K and a Langevin thermostat with a collision frequency of 1 ps^{-1} to maintain the temperature (Izaguirre *et al.*, 2001). Particle mesh Ewald summation method (Essmann *et al.*, 1995) was used to calculate the electrostatic interactions with a cut off of 9Å for the non-bonded interactions. All simulations were carried out using the NPT ensemble at a constant pressure of 1 bar with a time step of 2 fs to integrate the equation of motion. After a series of minimizations and MD simulations with constraints on each protein, 1 ns of unrestrained MD simulation was performed before the production runs. VMD (Humphrey et al., 1996) and pymol (DeLano, 2002) visualization programs were used for graphical representations.

4.7.2 Free Energy Calculations

The binding free energies of the water molecules were calculated using the double decoupling free energy simulation method, previously described by Hamelberg and McCammon (Hamelberg and McCammon, 2004). This free energy method involves gradually turning off the electrostatic and van der Waals interactions of the bound water molecule from the remainder of the system. In the first of two sets of simulations, the water molecule was transferred from the bulk water to gas phase (ΔG^{o}_{1}). In second set, the water molecule in the binding pocket of the protein complex was transferred to the gas phase (ΔG^{o}_{2}). During the decoupling of the interactions between water molecule and the active site of the protein, the translational degrees of freedom were harmonically constrained to occupy the binding site as defined by the coordinate system of the complex. During the phase change, H_2O_{sol} to H_2O_{gas}, the potential energy term U(sol) was progressively mapped to U(gas) along a chosen path. The map path was chosen by a coupling parameter, λ, which was varied from 0 to 1. Thermodynamic integration (TI) method was used to calculate the free energy difference between the two states. Along the path, 9-point Gaussian quadrature at discrete points of λ_i (0.01592, 0.08198, 0.19331, 0.33787, 0.5, 0.66213, 0.80669, 0.91802, and 0.98408) was used for the integration. The simulation at each λ value was initially equilibrated for 200 ps, following a production run of 200 ps for data collection. All of the free energy calculations were conducted using the same parameters as described earlier for the MD simulations. Each free energy calculation was run in triplicate and the final free energy was estimated by averaging over the calculated free energies from the three independent simulations. The standard error was calculated using the standard deviation of the free energies.

4.7.3 PDB Database Search for Motifs

A non-redundant set of X-ray crystallographic structures from the PDB was searched for the helix-turn-coil structural motif using the MaDCaT program (Zhang and Grigoryan, 2013). MaDCaT uses a distance-map representation of the query structure to search the database against pre-calculated maps of the entire PDB. Here, the central 13-residue (RGQMQKPFEDASF) stretch of sequence from the structural motif (Arg127 to Phe139) from Pin1 was used as a probe to search the PDB. Among the 8 pre-computed databases in MaDCaT, only the minimum redundancy (based on the sequence clusters with 30% redundancy) bc-30.list database was used for the search. The top 2000 results were saved. After removing duplicates (different chains of the same proteins), a set of 1115 structures was saved within the motif dataset. These structures from the motif dataset were further individually analyzed through visual inspection in search of the water containing structural motif.

4.7.4 CD Spectroscopy

CD spectra were acquired in 100 mM KPi, 10 mM NaCl, pH 7.0, at 20 ^{o}C from 185 to 260 nm. Far UV CD spectra were collected on a thermostated Jasco J-710 circular dichroism spectrophotometer (Easton, MD) using a 1 mm path length quartz cuvette. Five scans were taken at a rate of 50 nm/min and corrected with their corresponding blanks to remove background interference from the buffer and TFE, and the resulting average was considered. Spectra were smoothed using the Means-Movement method in the Jasco Spectra Analysis software (Easton, MD).

4.8 Acknowledgments

This study was supported in part by National Science Foundation Grant MCB-1517617 (D.H), CHE-15061518 (G.G.), the Georgia Research Alliance, and a University Fellowship from

the Center for Diagnostics and Therapeutics at Georgia State University (C.S). C.S is a Georgia State University Fellow.

4.9 References

Barman, A. & Hamelberg, D. 2014. Cysteine-Mediated Dynamic Hydrogen-Bonding Network in the Active Site of Pin1. *Biochemistry, 53***,** 3839-3850.

Barycki, J. J., O'brien, L. K., Strauss, A. W. & Banaszak, L. J. 2001. Glutamate 170 of Human l-3-Hydroxyacyl-CoA Dehydrogenase Is Required for Proper Orientation of the Catalytic Histidine and Structural Integrity of the Enzyme. *J. Biol. Chem.,* 276**,** 36718-36726.

Bayer, E., Goettsch, S., Mueller, J. W., Griewel, B., Guiberman, E., Mayr, L. M. & Bayer, P. 2003. Structural Analysis of the Mitotic Regulator hPin1 in Solution: INSIGHTS INTO DOMAIN ARCHITECTURE AND SUBSTRATE BINDING. *J. Biol. Chem.,* 278**,** 26183-26193.

Bös, F. & Pleiss, J. 2008. Conserved Water Molecules Stabilize the Ω-Loop in Class A β-Lactamases. *Antimicrob. Agents Chemother.,* 52**,** 1072-1079.

Bottoms, C. A., Smith, P. E. & Tanner, J. J. 2002. A structurally conserved water molecule in Rossmann dinucleotide-binding domains. *Protein Sci.,* 11**,** 2125-2137.

Bulbarelli, A., Lonati, E., Cazzaniga, E., Gregori, M. & Masserini, M. 2009. Pin1 affects Tau phosphorylation in response to Aβ oligomers. *Mol. Cell. Neurosci.,* 42**,** 75-80.

Case, D. A., Cheatham, T. E., Darden, T., Gohlke, H., Luo, R., Merz, K. M., Onufriev, A., Simmerling, C., Wang, B. & Woods, R. J. 2005. The Amber biomolecular simulation programs. *J. Comput. Chem.,* 26**,** 1668-1688.

Delano, W. L. 2002. 1.1r1 ed.: The PyMOL Molecular Graphics System,DeLano Scientific, Palo Alto, CA.

Di Martino, G. P., Masetti, M., Cavalli, A. & Recanatini, M. 2014. Mechanistic insights into Pin1 peptidyl-prolyl cis-trans isomerization from umbrella sampling simulations. *Proteins: Struct. Funct. Bioinform.,* 82**,** 2943-2956.

Drake, A. F., Siligardi, G. & Gibbons, W. A. 1988. Reassessment of the electronic circular dichroism criteria for random coil conformations of poly(L-lysine) and the implications for protein folding and denaturation studies. *Biophys. Chem.,* 31**,** 143-6.

Essmann, U., Perera, L., Berkowitz, M. L., Darden, T., Lee, H. & Pedersen, L. G. 1995. A smooth particle mesh Ewald method. *J. Chem. Phys.,* 103**,** 8577-8593.

Gianti, E., Carnevale, V., Degrado, W. F., Klein, M. L. & Fiorin, G. 2015. Hydrogen-Bonded Water Molecules in the M2 Channel of the Influenza A Virus Guide the Binding Preferences of Ammonium-Based Inhibitors. *J. Phys. Chem. B,* 119**,** 1173-1183.

Greenwood, A., Rogals, M., De, S., Lu, K., Kovrigin, E. & Nicholson, L. 2011. Complete determination of the Pin1 catalytic domain thermodynamic cycle by NMR lineshape analysis. *J. Biomol. NMR,* 51**,** 21-34.

Hamelberg, D. & Mccammon, J. A. 2004. Standard Free Energy of Releasing a Localized Water Molecule from the Binding Pockets of Proteins: Double-Decoupling Method. *J. Am. Chem. Soc.,* 126**,** 7683-7689.

Hamelberg, D., Shen, T. & Mccammon, J. A. 2006. Insight into the role of hydration on protein dynamics. *J. Chem. Phys.,* 125**,** 094905.

Hornak, V., Abel, R., Okur, A., Strockbine, B., Roitberg, A. & Simmerling, C. 2006. Comparison of multiple Amber force fields and development of improved protein backbone parameters. *Proteins: Struct. Funct. Bioinform.,* 65**,** 712-725.

Humphrey, W., Dalke, A. & Schulten, K. 1996. VMD: Visual molecular dynamics. *J. Mol. Graphics,* 14**,** 33-38.

Izaguirre, J. A., Catarello, D. P., Wozniak, J. M. & Skeel, R. D. 2001. Langevin stabilization of molecular dynamics. *J. Chem. Phys.,* 114**,** 2090-2098.

Johnson, Q., Doshi, U., Shen, T. & Hamelberg, D. 2010. Water's Contribution to the Energetic Roughness from Peptide Dynamics. *J. Chem. Theory Comput.,* 6**,** 2591-2597.

Jorgensen, W. L. 1982. Revised TIPS for simulations of liquid water and aqueous solutions. *J. Chem. Phys.,* 77**,** 4156-4163.

Kahne, D. & Still, W. C. 1988. Hydrolysis of a peptide bond in neutral water. *J. Am. Chem. Soc.,* 110**,** 7529-7534.

Knight, J. D. R., Hamelberg, D., Mccammon, J. A. & Kothary, R. 2009. The role of conserved water molecules in the catalytic domain of protein kinases. *Proteins: Struct. Funct. Bioinform.,* 76**,** 527-535.

Lang, K., Schmid, F. X. & Fischer, G. 1987. Catalysis of protein folding by prolyl isomerase. *Nature,* 329**,** 268-270.

Loris, R., Langhorst, U., De Vos, S., Decanniere, K., Bouckaert, J., Maes, D., Transue, T. R. & Steyaert, J. 1999. Conserved water molecules in a large family of microbial ribonucleases. *Proteins: Struct. Funct. Bioinform.,* 36**,** 117-134.

Lu, K. P. & Zhou, X. Z. 2007. The prolyl isomerase PIN1: a pivotal new twist in phosphorylation signalling and disease. *Nat. Rev. Mol. Cell Biol.,* 8**,** 904-916.

Lu, P.-J., Wulf, G., Zhou, X. Z., Davies, P. & Lu, K. P. 1999. The prolyl isomerase Pin1 restores the function of Alzheimer-associated phosphorylated tau protein. *Nature,* 399**,** 784-788.

Makowska, J., Rodziewicz-Motowidlo, S., Baginska, K., Vila, J. A., Liwo, A., Chmurzynski, L. & Scheraga, H. A. 2006. Polyproline II conformation is one of many local conformational states and is not an overall conformation of unfolded peptides and proteins. *Proc. Natl. Acad. Sci. USA,* 103**,** 1744-9.

Mercedes-Camacho, A. Y., Mullins, A. B., Mason, M. D., Xu, G. G., Mahoney, B. J., Wang, X., Peng, J. W. & Etzkorn, F. A. 2013. Kinetic Isotope Effects Support the Twisted Amide Mechanism of Pin1 Peptidyl-Prolyl Isomerase. *Biochemistry,* 52**,** 7707-7713.

Michel, J., Tirado-Rives, J. & Jorgensen, W. L. 2009. Energetics of Displacing Water Molecules from Protein Binding Sites: Consequences for Ligand Optimization. *J. Am. Chem. Soc.,* 131**,** 15403-15411.

Mueller, J. W., Link, N. M., Matena, A., Hoppstock, L., Rüppel, A., Bayer, P. & Blankenfeldt, W. 2011. Crystallographic Proof for an Extended Hydrogen-Bonding Network in Small Prolyl Isomerases. *J. Am. Chem. Soc.,* 133**,** 20096-20099.

Nagendra, H. G., Sukumar, N. & Vijayan, M. 1998. Role of water in plasticity, stability, and action of proteins: The crystal structures of lysozyme at very low levels of hydration. *Proteins: Struct. Funct. Bioinform.,* 32**,** 229-240.

Nakayama, S. & Kretsinger, R. H. 1994. Evolution of the EF-Hand Family of Proteins. *Annu. Rev. Biophys. Biomol. Struct.,* 23**,** 473-507.

Namanja, A. T., Wang, X. J., Xu, B., Mercedes-Camacho, A. Y., Wilson, K. A., Etzkorn, F. A. & Peng, J. W. 2011. Stereospecific gating of functional motions in Pin1. *Proc. Natl. Acad. Sci. USA,* 108**,** 12289-12294.

Ogata, K. & Wodak, S. J. 2002. Conserved water molecules in MHC class-I molecules and their putative structural and functional roles. *Protein Eng.,* 15**,** 697-705.

Park, S. & Saven, J. G. 2005. Statistical and molecular dynamics studies of buried waters in globular proteins. *Proteins: Struct. Funct. Bioinform.,* 60**,** 450-463.

Pastorino, L., Sun, A., Lu, P.-J., Zhou, X. Z., Balastik, M., Finn, G., Wulf, G., Lim, J., Li, S.-H., Li, X., Xia, W., Nicholson, L. K. & Lu, K. P. 2006. The prolyl isomerase Pin1 regulates amyloid precursor protein processing and amyloid-[beta] production. *Nature,* 440**,** 528-534.

Povey, J. F., Smales, C. M., Hassard, S. J. & Howard, M. J. 2007. Comparison of the effects of 2,2,2-trifluoroethanol on peptide and protein structure and function. *J. Struct. Biol.,* 157**,** 329-38.

Prakash, P., Sayyed-Ahmad, A. & Gorfe, A. A. 2012. The Role of Conserved Waters in Conformational Transitions of Q61H K-ras. *PLoS Comp. Biol.,* 8**,** e1002394.

Prasad, B. V. L. S. & Suguna, K. 2002. Role of water molecules in the structure and function of aspartic proteinases. *Acta Crystallogr. Sect. D. Biol. Crystallogr.,* 58**,** 250-259.

Ranganathan, R., Lu, K. P., Hunter, T. & Noel, J. P. 1997. Structural and Functional Analysis of the Mitotic Rotamase Pin1 Suggests Substrate Recognition Is Phosphorylation Dependent. *Cell,* 89**,** 875-886.

Robinson, G. W. & Cho, C. H. 1999. Role of Hydration Water in Protein Unfolding. *Biophys. J.,* 77**,** 3311-3318.

Romero, P. J. & De Meis, L. 1989. Role of water in the energy of hydrolysis of phosphoanhydride and phosphoester bonds. *J. Biol. Chem.,* 264**,** 7869-7873.

Ryckaert, J.-P., Ciccotti, G. & Berendsen, H. J. C. 1977. Numerical integration of the cartesian equations of motion of a system with constraints: molecular dynamics of n-alkanes. *J. Comput. Chem.,* 23**,** 327-341.

Sahai, M. A. & Biggin, P. C. 2011. Quantifying Water-Mediated Protein–Ligand Interactions in a Glutamate Receptor: A DFT Study. *J. Phys. Chem. B,* 115**,** 7085-7096.

Schutkowski, M., Bernhardt, A., Zhou, X. Z., Shen, M., Reimer, U., Rahfeld, J.-U., Lu, K. P. & Fischer, G. 1998. Role of Phosphorylation in Determining the Backbone Dynamics of the Serine/Threonine-Proline Motif and Pin1 Substrate Recognition†. *Biochemistry,* 37**,** 5566-5575.

Sreenivasan, U. & Axelsen, P. H. 1992. Buried water in homologous serine proteases. *Biochemistry,* 31**,** 12785-12791.

Szep, S., Park, S., Boder, E. T., Van Duyne, G. D. & Saven, J. G. 2009. Structural coupling between FKBP12 and buried water. *Proteins: Struct. Funct. Bioinform.,* 74**,** 603-611.

Theuerkorn, M., Fischer, G. & Schiene-Fischer, C. 2011. Prolyl cis/trans isomerase signalling pathways in cancer. *Curr. Opin. Pharmacol.,* 11**,** 281-287.

Velazquez, H. A. & Hamelberg, D. 2011. Conformational Selection in the Recognition of Phosphorylated Substrates by the Catalytic Domain of Human Pin1. *Biochemistry,* 50**,** 9605-9615.

Velazquez, H. A. & Hamelberg, D. 2013. Conformation-Directed Catalysis and Coupled Enzyme–Substrate Dynamics in Pin1 Phosphorylation-Dependent Cis–Trans Isomerase. *J. Phys. Chem. B,* 117**,** 11509-11517.

Vöhringer-Martinez, E., Duarte, F. & Toro-Labbé, A. 2012. How Does Pin1 Catalyze the Cis–Trans Prolyl Peptide Bond Isomerization? A QM/MM and Mean Reaction Force Study. *J. Phys. Chem. B,* 116**,** 12972-12979.

Wang, J., Tochio, N., Kawasaki, R., Tamari, Y., Xu, N., Uewaki, J.-I., Utsunomiya-Tate, N. & Tate, S.-I. 2015. Allosteric Breakage of the Hydrogen Bond within the Dual-Histidine Motif in the Active Site of Human Pin1 PPIase. *Biochemistry*.

Xu, N., Tochio, N., Wang, J., Tamari, Y., Uewaki, J.-I., Utsunomiya-Tate, N., Igarashi, K., Shiraki, T., Kobayashi, N. & Tate, S.-I. 2014. The C113D Mutation in Human Pin1 Causes Allosteric Structural Changes in the Phosphate Binding Pocket of the PPIase Domain through the Tug of War in the Dual-Histidine Motif. *Biochemistry,* 53**,** 5568-5578.

Yaffe, M. B., Schutkowski, M., Shen, M., Zhou, X. Z., Stukenberg, P. T., Rahfeld, J.-U., Xu, J., Kuang, J., Kirschner, M. W., Fischer, G., Cantley, L. C. & Lu, K. P. 1997. Sequence-Specific and Phosphorylation-Dependent Proline Isomerization: A Potential Mitotic Regulatory Mechanism. *Science,* 278**,** 1957-1960.

Zhang, J. & Grigoryan, G. 2013. Chapter Two - Mining Tertiary Structural Motifs for Assessment of Designability. *In:* AMY, E. K. (ed.) *Methods Enzymol.*: Academic Press.

Zhang, Y., Daum, S., Wildemann, D., Zhou, X. Z., Verdecia, M. A., Bowman, M. E., Lücke, C., Hunter, T., Lu, K.-P., Fischer, G. & Noel, J. P. 2007. Structural Basis for High-Affinity Peptide Inhibition of Human Pin1. *ACS Chem. Biol.,* 2**,** 320-328.

4.10 Supplemental Information

4.10.1 Supplemental Figures

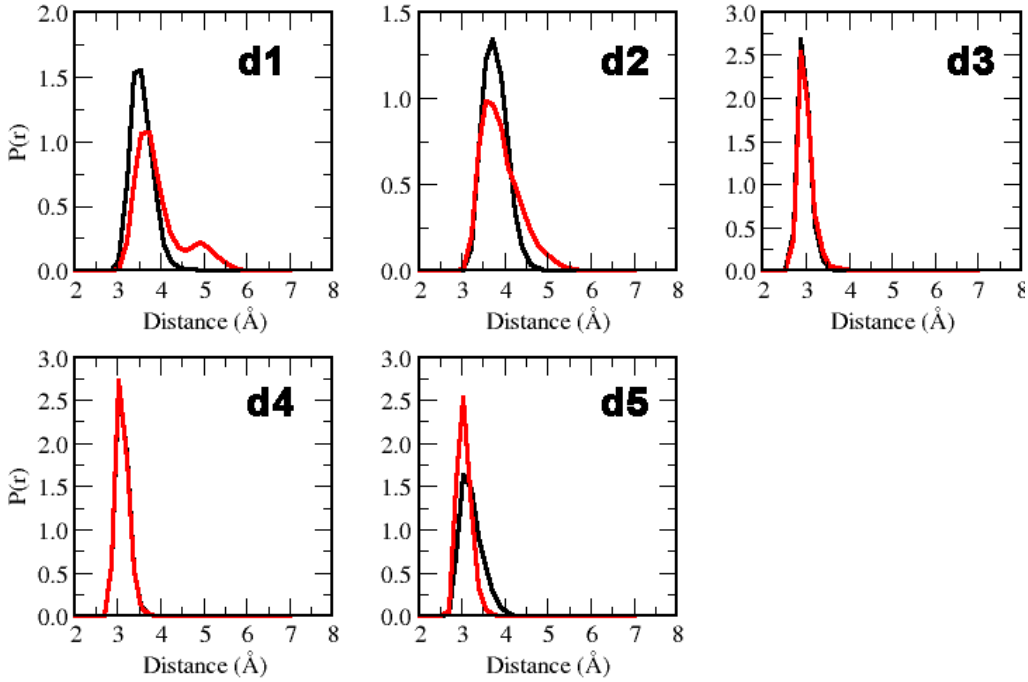

Figure 4.8 S1. related to Figure 3.
Probability distributions of hetero atomic distances (hydrogen bond distance) among the active site residues in the presence of substrate (Ace-FFpSPR-Nme). d1 and d2 correspond to the distances between the OG of Ser115 and Nε of His59 with SG of Cys113, respectively. Distance d3 measures between N_ε of His59 and OG of Ser115. The distance between N_δ of His59 and N_δ of His157 is denoted by d4. Distance d5 measures between OG1 of Thr152 and N_ε of His59. The black line represents the system in presence of Wat1 and the red line is in the absence of Wat1. See Figure 3 for the definitions of d1-d5.

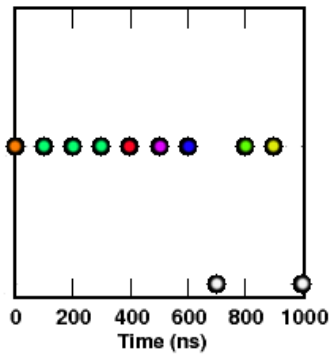

Figure 4.9 S2, related to Figure 4.
The solvent exchangeability of Wat2 during the 1μs simulation of Pin1. Individual snapshot indicates the water is present at the site during most of the simulation and absent at 700ns and 1μs time frame. The

different color code represents different water molecule during the time course of the simulation. White color represents '0' water molecule at that site.

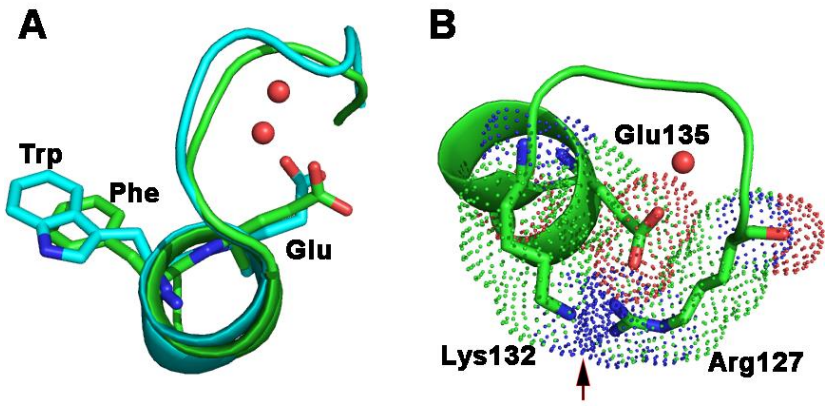

Figure 4.10 S3, related to Figure 4.
A) Structural superposition of the Pin1 (green) and FKBP (cyan) structures. The Trp in FKBP and Phe in Pin1 occupy the same position. B) Highly electropositive environment (marked by the arrow) created by Arg127 and Lys132 in vicinity of Glu135.

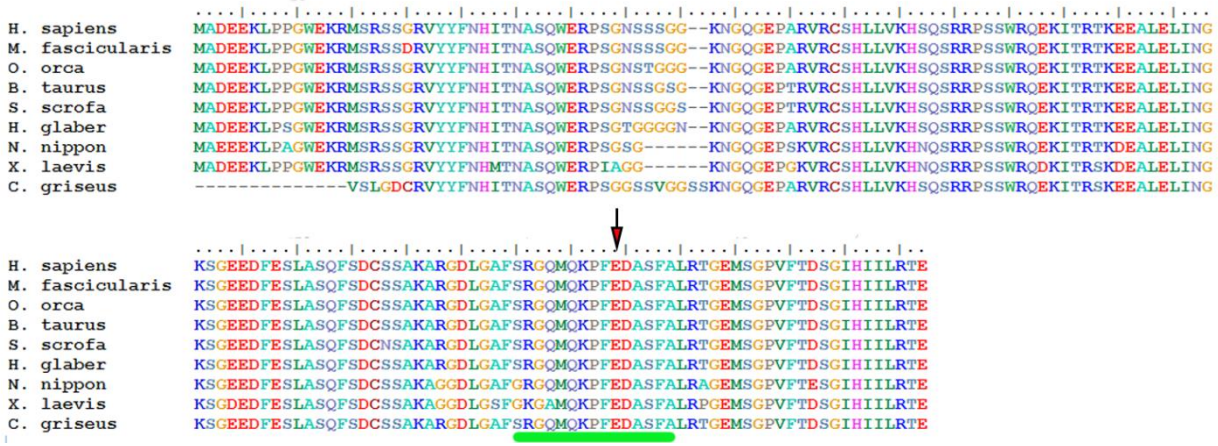

Figure 4.11 S4, related to Figure 4.
Amino acid sequence alignment of Pin1 from different species. The green line represents the structural motif and arrow indicates the conserved Glu residue interacting with water.

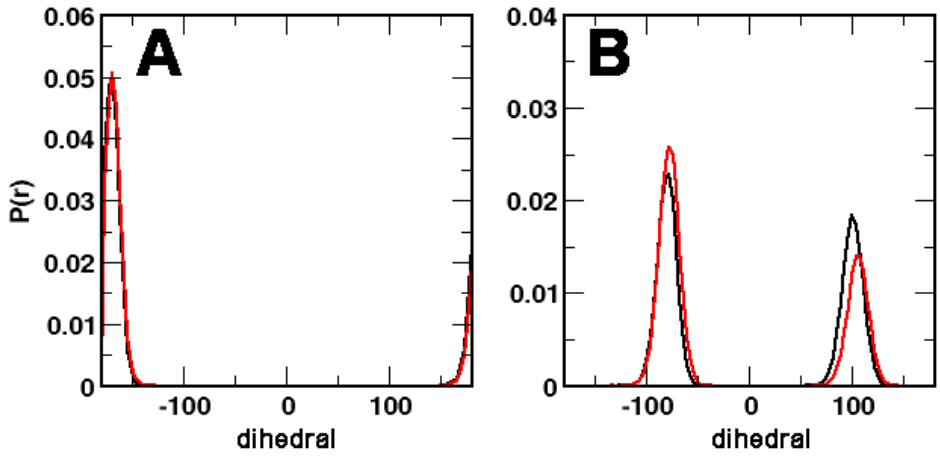

Figure 4.12 S5, related to Figure 4.
The Chi1 (A) and Chi2 (B) dihedral distribution of Phe136 in Pin1 WT (black) and Glu135Gln variant (red).

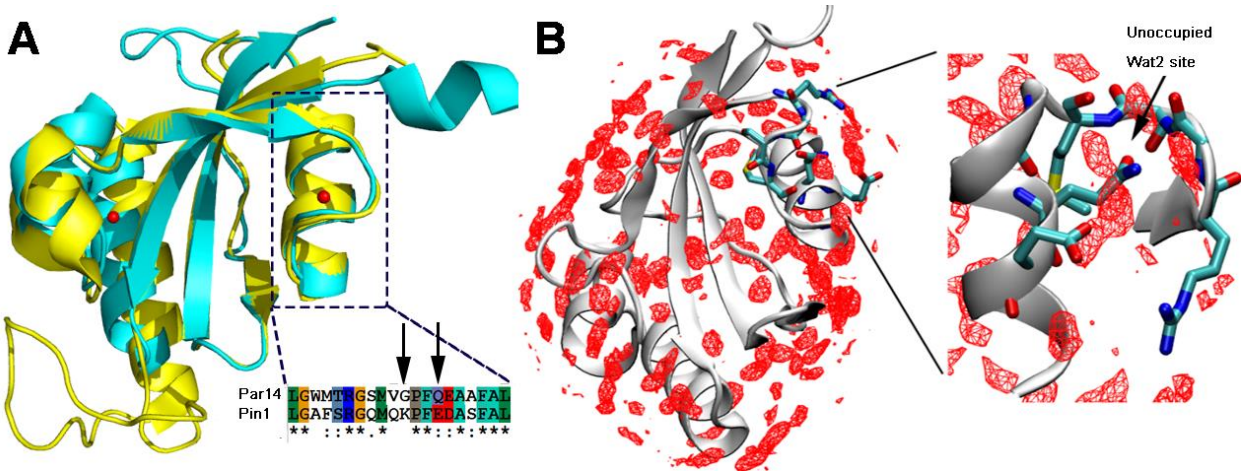

Figure 4.13 S6, related to Figure 4.
A) Superposition of Pin1 (yellow, PDB id 2Q5A) and hPar14 (cyan, PDB id 3UI4) crystal structures. The amino acid sequence alignment of the residues of structural motif in Pin1 and hPar14 is shown in the inset. Two arrows indicate the important residues near the Wat2 binding site. Lys132 in Pin1 is replaced by Gly and Glu135 is replaced by Gln. B) Water occupancy map from the MD simulations of hPar14. The Wat2 binding site is observed to be unoccupied.

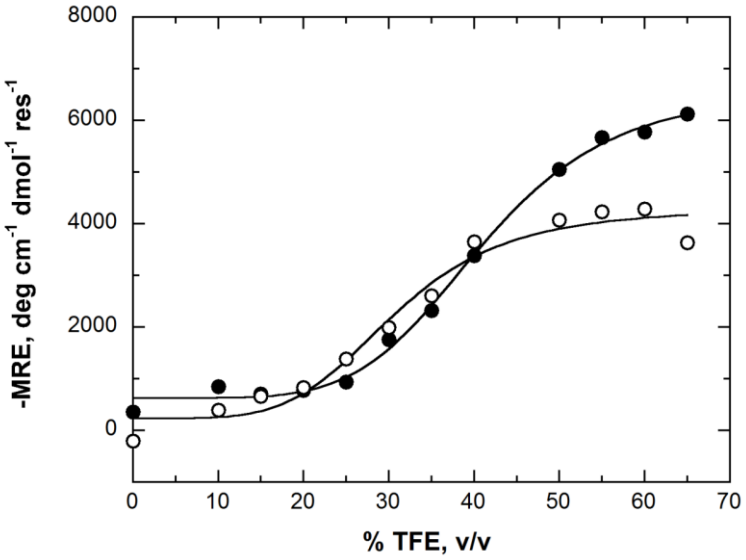

Figure 4.14 S7, related to Figure 6.
Helix induction curve of 20mer Pin1 peptide in 100 mM KPi, 10 mM NaCl, pH 7.0, 20 ºC as a function of increasing percent of TFE (v/v). The magnitudes of the MRE values of Pin1 at 207 nm (●) and 222 nm (○) were plotted. These wavelengths are consistent with the two characteristic peaks observed in CD spectra of peptides and proteins with α-helices as secondary structure. An equilibrium was observed in which two populations exist at low and high percentages of TFE consistent with a shift in secondary structure from P_{II} to α-helix.

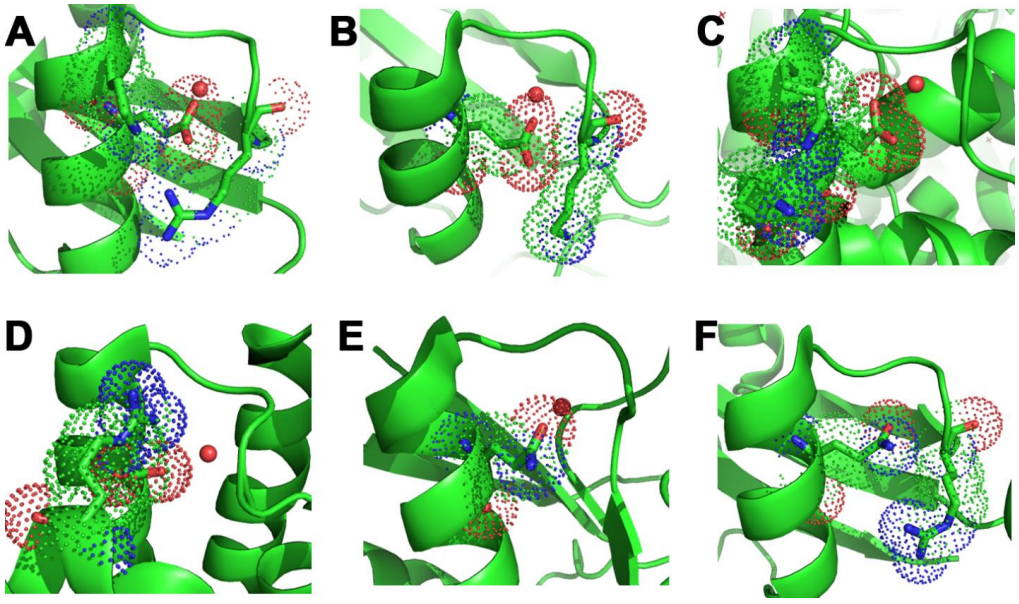

Figure 4.15 S8, related to Figure 7.
A-D) The presence of positive electrostatic potential within the motif or from other portions of the protein can attract the Glu residue and form the water pocket (PDB IDs: A)3I6C, B)1YW5, C)2Z67 and D) 3M1I). E) The pocket can be formed in presence of Gln and absence of the electropositive charged environment (PDB ID: 2W7Y). F) In presence of the electropositive environment the neutral Gln can be moved inwards removing the water from the pocket (PDB ID: 3UI4).

4.10.2 Supplemental Tables

Table 4.1. S1. PDB files of Pin1 used in the study.

1F18, 1PIN, 1ZCN, 2F21, 2ITK, 2Q5A, 2XP3, 2XP4, 2XP5, 2XP6, 2XP7, 2XP8, 2XP9, 2XPA, 2XPB, 2ZQS, 2ZQT, 2ZQU, 2ZQV, 2ZR4, 2ZR5, 2ZR6, 3I6C_A, 3I6C_B, 3IK8_A, 3IK8_B, 3IKD_A, 3IKD_B, 3IKG_A, 3IKG_B, 3JYJ_A, 3JYJ_B, 3KAB, 3KAC_A, 3KAC_B, 3KAD , 3KAF, 3KAG, 3KAH, 3KAI, 3KCE, 3NTP, 3ODK, 3OOB, 3TC5, 3TCZ, 3TDB

Table 4.2. S2. PDB files containing structural water molecules at the crevice having Glu within the motif.

PDB ID (Å)	**Description**
3I6C (1.3)	Structure-based design of novel human Pin1 inhibitors (II).(Dong et al., 2010)
1YW5 (1.6)	The structure of the candida albicans Ess1 prolyl isomerase reveals a well-ordered linked that restrict domain mobility. (Li et al., 2005)
2Z67 (2.5)	Structural insight into RNA dependent eukaryal and archael selenocysteine formation.(Araiso et al., 2008)
3M1I (2.0)	An allosteric mechanism to displace nuclear export cargo from CRM1 and RAnGTP by RanBP1. (Koyama and Matsuura, 2010)
1G5B (2.1)	Bacteriophage labda Ser/Thr Protein phosphatase. (Voegtli et al., 2000)
2OZT (1.4)	Crystal structure of O-succinylbenzoate synthase from Thermosynechococcu elongates BP-1. (Odokonyero et al., 2014)
3EHM (2.0)	Structure of BT1043. (Koropatkin et al., 2009)

4.11 Supplemental References

Araiso, Y., Palioura, S., Ishitani, R., Sherrer, R. L., O'donoghue, P., Yuan, J., Oshikane, H., Domae, N., Defranco, J., Söll, D. & Nureki, O. 2008. Structural insights into RNA-dependent eukaryal and archaeal selenocysteine formation. *Nucleic Acids Res.*, 36**,** 1187-1199.

Dong, L., Marakovits, J., Hou, X., Guo, C., Greasley, S., Dagostino, E., Ferre, R., Johnson, M. C., Kraynov, E., Thomson, J., Pathak, V. & Murray, B. W. 2010. Structure-based design of novel human Pin1 inhibitors (II). *Bioorg. Med. Chem. Lett.*, 20**,** 2210-2214.

Koropatkin, N., Martens, E. C., Gordon, J. I. & Smith, T. J. 2009. Structure of a SusD Homologue, BT1043, Involved in Mucin O-Glycan Utilization in a Prominent Human Gut Symbiont. *Biochemistry,* 48**,** 1532-1542.

Koyama, M. & Matsuura, Y. 2010. An allosteric mechanism to displace nuclear export cargo from CRM1 and RanGTP by RanBP1. *The EMBO Journal,* 29**,** 2002-2013.

Li, Z., Li, H., Devasahayam, G., Gemmill, T., Chaturvedi, V., Hanes, S. D. & Van Roey, P. 2005. The Structure of the Candida albicans Ess1 Prolyl Isomerase Reveals a Well-Ordered Linker that Restricts Domain Mobility. *Biochemistry,* 44**,** 6180-6189.

Odokonyero, D., Sakai, A., Patskovsky, Y., Malashkevich, V. N., Fedorov, A. A., Bonanno, J. B., Fedorov, E. V., Toro, R., Agarwal, R., Wang, C., Ozerova, N. D. S., Yew, W. S., Sauder, J. M., Swaminathan, S., Burley, S. K., Almo, S. C. & Glasner, M. E. 2014. Loss of quaternary structure is associated with rapid sequence divergence in the OSBS family. *Proc. Natl. Acad. Sci. USA,* 111**,** 8535-8540.

Voegtli, W. C., White, D. J., Reiter, N. J., Rusnak, F. & Rosenzweig, A. C. 2000. Structure of the Bacteriophage λ Ser/Thr Protein Phosphatase with Sulfate Ion Bound in Two Coordination Modes. *Biochemistry,* 39**,** 15365-15374.

5 Identification of the Catalytic Base for Alcohol Activation in Choline Oxidase

(This chapter has been published verbatim in Smitherman, C., Rungsrisuriyachai, K., Germann, M.W., and Gadda, G., (2015), *Biochemistry* 54(2), 413-21.)

5.1 Abstract

Choline oxidase catalyzes the oxidation of choline to glycine betaine through a two-step, four-electron reaction with betaine aldehyde as an intermediate. Oxygen is the final electron acceptor. Alcohol oxidation is initiated by the removal of the substrate hydroxyl proton by an unknown active site residue with a pK_a value of ~7.5. In the crystal structure of the enzyme in complex with glycine betaine, H466 is ≤3.1 Å from the carboxylate oxygen of the reaction product, suggesting a possible role in the proton abstraction reaction catalyzed by the enzyme. H466, along with another potential candidate, H351, was previously mutated to alanine, but this failed to establish if either residue was involved in activation of the substrate. In this study, single variants of choline oxidase with H466 and H351 substituted with glutamine were prepared, purified, and characterized. The k_{cat} and k_{cat}/K_m values of the H351Q enzyme in atmospheric oxygen were 45- and 5000-fold lower than those of the wild-type enzyme, respectively, whereas the H466Q enzyme was inactive when assayed polarographically with choline. In the H466Q enzyme, the rate constant for anaerobic flavin reduction (k_{red}) with choline was 1 million-fold lower than in the wild-type enzyme. A comparison of the fluorescence, circular dichroism, and ^{1}H nuclear magnetic resonance spectroscopic properties of the H466Q enzyme and the wild-type enzyme is consistent with the mutation not affecting the topology of the active site or the overall fold of the protein. Thus, the change in the k_{red} value and the lack of oxygen consumption upon mutation of histidine to glutamine are not due to misfolded protein

but rather to the variant enzyme being unable to catalyze substrate oxidation. On the basis of the kinetic and spectroscopic results presented here and the recent structural information, we propose that H466 is the residue that activates choline to the alkoxide for the subsequent hydride transfer reaction to the enzyme-bound flavin.

5.2 Introduction

Choline oxidase (EC 1.1.3.17) is a dimeric, FAD-dependent enzyme that catalyzes the oxidation of choline to glycine betaine through two consecutive, flavin-mediated redox reactions (Scheme 1). Molecular oxygen oxidizes the reduced enzyme, forming hydrogen peroxide.[1-3] The enzyme from *Arthrobacter globiformis* has been characterized through site-directed mutagenesis, steady-state and rapid reaction kinetics, X-ray crystallography, and computational methods,[1, 3-7] allowing for a description of the mechanism of alcohol oxidation at the molecular level. Briefly, choline enters the active site using a gated mechanism controlled by a cluster of hydrophobic residues (M62, L65, V355, F357, and M359) located on the solvent accessible surface of the enzyme.[4] The side chain of E312 establishes an electrostatic interaction with the trimethylammonium group of the substrate, contributing to optimal positioning of the substrate for catalysis.[8] Oxidation of the substrate in the enzyme–substrate complex proceeds through an initial deprotonation of the hydroxyl group that yields an alkoxide from which a rate-limiting hydride transfer to the flavin N(5) atom occurs.[1] The hydride ion tunnels from the alkoxide C^{α} atom to the flavin N(5) atom, within a highly preorganized enzyme–alkoxide complex.[9] Electrostatic interactions between the protein side chains of residues E312 and H466 and the substrate trimethylamine and O atom of the alkoxide, along with the covalent linkage of the flavin to H99, contribute to the preorganization of the substrate and the flavin.[5, 8-11] Several other protein side chains contribute to catalysis or substrate positioning, including

S101,[12] H351,[13] and N510.[14] Although the involvement of a catalytic base with a pK_a of 7.5 has been demonstrated using steady-state and rapid reaction kinetics in wild-type[1, 2] and several variant enzymes,[8, 13, 15] its identity has not yet been established.

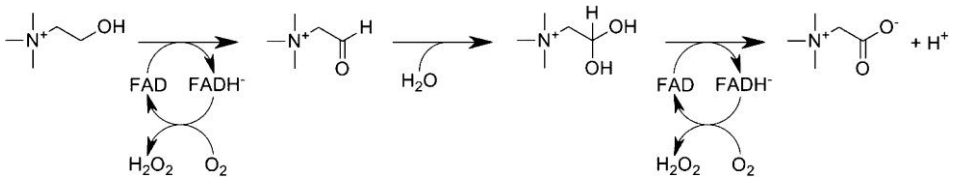

Scheme 5.1 Oxidation of Choline Catalyzed by Choline Oxidase.

Previous studies that aimed to identify the base in choline oxidase initially focused on H466, primarily because it is fully conserved in the glucose–methanol–choline oxidoreductase enzyme superfamily,[16-20] is 4.4 Å from the flavin N(5) atom, and is equivalent to H502 of aryl-alcohol oxidase[16, 21] and H548 of pyranose 2-oxidase,[17, 19] which were recently shown to act as catalytic bases through mechanistic, structural, and computational studies. When H466 of choline oxidase was mutated to alanine, there was a 60-fold decrease in the k_{cat} value, while the pH profile of the k_{cat}/K_m value indicated that a base was still present in the variant enzyme.[15] Similar results were obtained upon replacing H351 with alanine in the active site of the enzyme.[13] The decreased catalytic activity observed in the H466A variant was due to a decrease in the electrophilicity of the enzyme-bound FAD and the inability of the enzyme to stabilize the negatively charged alkoxide species formed in catalysis after substrate activation.[15] The latter conclusion was based on partial rescuing of the k_{cat} value with choline in the H466A enzyme by exogenous imidazolium, rather than imidazole, consistent with the side chain of H466 being protonated in the rate-limiting step for overall enzyme turnover, i.e., during the transfer of the hydride from the alkoxide to the flavin.[15] On the basis of these results, the conclusion that

neither H351 nor H466 is likely to be the base that deprotonates choline for subsequent hydride transfer in the active site of the enzyme was reached.[13, 15, 22] The positive charge on H466 was reversed by engineering an H466D variant of the enzyme, which produced an inactive enzyme unable to stabilize the negative charge on the reduced flavin.[22] The presence of the negatively charged aspartate altered the midpoint redox potential of the flavin from 73 mV in the wild type to −89 mV in the variant and resulted in partial incorporation of the flavin (i.e., ∼0.3 mol of FAD/mol of enzyme) with the majority (i.e., ∼75%) being noncovalently bound.[22]

Our recent determination of the crystal structure of choline oxidase in a complex with glycine betaine to a resolution of 1.95 Å shows that the $N^{\varepsilon 2}$ atom of the H466 side chain is ≤3.1 Å from one of the O atoms of the ligand carboxylate (Figure 1).[6] In contrast, the side chain of H351 is ≤3.2 Å from the C^{α} atom of glycine betaine, which corresponds to the C^{β} atom of choline before its oxidation by the enzyme (Figure 1). The structural data are consistent with mechanistic data showing that H351 is important for substrate binding and positioning, and it contributes to the stabilization of the transition state for the hydride transfer reaction.[6, 13] However, on the basis of the structural information, Salvi *et al.* suggest that H466 may be the base required for alkoxide formation in the catalytic mechanism of choline oxidase. Reexamination of the mechanistic data for the H466A variant would support such a hypothesis. A possible explanation that reconciles the structural and mechanistic data is that hydroxide ion occupying the space vacated by the missing side chain in the H466A enzyme may act as a poor surrogate base in catalysis. On the basis of structural considerations alone, space for hydroxide ion is available in the alanine variant that replaces the histidine at position 466. The positive charge on the trimethylammonium headgroup of the substrate bound in the active site of the enzyme would be a primary effecter for lowering the basicity of water, thereby increasing the

concentration of hydroxide ion in the active site of the mutant enzyme, as previously established in model systems.[23-25]

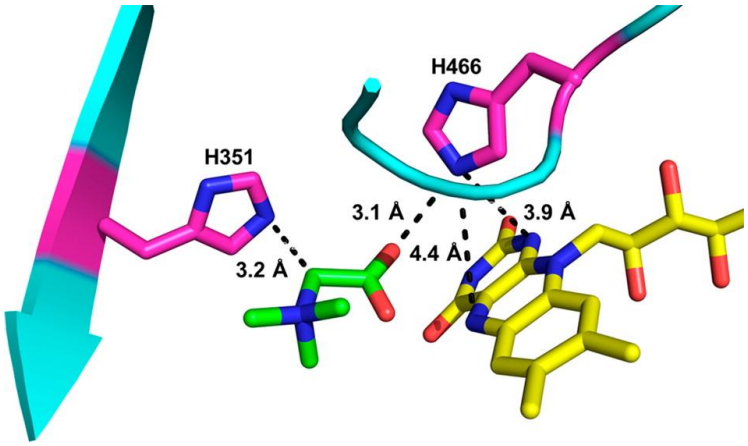

Figure 5.1 Interactions of the histidine residues at positions 466 and 351 of wild-type choline oxidase in complex with the reaction product, glycine betaine (green) (Protein Data Bank entry 4MJW).[6]

In this study, we have replaced H351 and H466 with glutamine to further address the question of which residue acts as a base in the oxidation reaction catalyzed by choline oxidase. We reasoned that in the tight and highly preorganized active site of the enzyme in complex with the substrate a histidine to glutamine replacement would not leave sufficient space for water to intervene in catalysis. While the H351Q enzyme was able to oxidize choline in a standard polarographic assay, although with k_{cat} and k_{cat}/K_m values significantly lower than those of the wild-type enzyme, the H466Q enzyme was completely devoid of enzymatic activity. The results of the mechanistic and spectroscopic studies presented herein allowed us to identify H466 as the residue that acts as the catalytic base in the active site of choline oxidase, thereby providing new insights into the chemical mechanism of the enzyme.

5.3 Experimental Procedures

5.3.1 Materials

Escherichia coli strain Rosetta(DE3)pLysS was from Novagen (Madison, WI). DNase was purchased from Roche (Indianapolis, IN). The QuikChange site-directed mutagenesis kit was from Stratagene (La Jolla, CA). The QIAprep Spin Miniprep kit was from Qiagen (Valencia, CA). Oligonucleotides were synthesized by Sigma Genosys (The Woodlands, TX). Choline, glucose, bovine serum albumin, chloramphenicol, ampicillin, dimethyl sulfoxide, isopropyl β-d-thiogalactopyranoside, phenylmethanesulfonyl fluoride, Luria-Bertani agar and broth, and lysozyme were from Sigma-Aldrich (St. Louis, MO). EDTA and glycerol were from Fisher (Pittsburgh, PA). Deuterium oxide was obtained from Cambridge Isotope Co. (Andover, MA). All other reagents were of the highest purity commercially available.

5.3.2 Methods

5.3.2.1 Site-directed Mutagenesis

A QuikChange kit was used to prepare the H351Q and H466Q enzyme variants. Mutagenesis was performed by following the manufacturer's instructions in the presence of 2% DMSO to overcome the high GC content in the gene by using the pET20b(+) plasmid harboring the wild-type gene (Cod*A*) as a template. The presence of the mutation was confirmed by sequencing at the DNA core facility of Georgia State University using an Applied Biosystems Big Dye Kit on an Applied Biosystems model ABI 377 DNA sequencer. Finally, *E. coli* strain Rosetta(DE3)pLysS competent cells were transformed with the plasmids containing the mutated genes, e.g., pET20b(+)/*codA*-H466Q, and permanent stocks of the cells were prepared and stored at −80 °C.

5.3.2.2 Enzyme Purification

The H466Q and H351Q enzymes were expressed and purified to high levels using methods previously described for the wild-type enzyme with the addition of 10% (v/v) glycerol to all the buffers used for purification to increase enzyme stability and minimize potential loss of flavin.[26-28] The H99N variant enzyme was expressed and purified to high levels as previously described by Quaye *et al*.[5] Fully oxidized variant enzymes were prepared as described by Gadda *et al*.[26]

5.3.2.3 Spectroscopic Studies

To determine if the flavin cofactor was covalently linked to the protein in the H466Q variant, the enzyme at a concentration of 25 μM was denatured with 50% acetonitrile in 20 mM sodium phosphate (pH 7.0). After centrifugation for 15 min at 14000*g* to remove denatured protein, the UV–visible absorption spectrum of the supernatant was determined. The extinction coefficient of the flavin bound to the H466Q enzyme was determined in 20 mM sodium phosphate (pH 7.0) after denaturation of the enzyme with 4 M urea at 40 °C for 1.5 h, based upon the ε_{450} value of 11.3 mM^{-1} cm^{-1} for free FAD and the previously published method by Whitby *et al*.[29] For spectroscopic studies, the enzymes were prepared fresh just prior to being used by gel filtration through PD-10 desalting columns (General Electric, Fairfield, CT). UV–visible absorption spectra were recorded in 20 mM Tris-HCl (pH 8.0) at 25 °C, using an Agilent Technologies diode-array model HP 8453 spectrophotometer. Fluorescence emission spectra were recorded in 20 mM sodium phosphate (pH 7.0) at 15 °C, with a Shimadzu model RF-5301 PC spectrofluorometer using a 1 cm path length quartz cuvette. Protein and flavin excitation wavelengths were initially determined through excitation scanning at 3 nm/min upon setting the emission wavelength to 340 and 520 nm, respectively. All fluorescence spectra were corrected

with the corresponding blanks for any absorption of the buffer and Rayleigh and Raman scatterings. For protein fluorescence, the sample at a concentration of 0.8 μM was excited at 286 nm and the emission scan was determined from 310 to 400 nm; for flavin fluorescence, the sample at an FAD concentration of 3.5 μM was excited at 469 nm (454 nm for the wild-type enzyme) and the emission scan was determined from 475 to 600 nm. Circular dichroic spectra were acquired in 20 mM sodium phosphate (pH 7.0) at 25 °C, at concentrations of protein of 0.1 and 21 μM for the far- and near-UV regions, respectively, and a concentration of flavin of 23 μM for the visible region. Using a 1 cm path length quartz cuvette, five scans were taken at a rate of 50 nm/min and corrected with their corresponding blanks to remove background interference from the buffer, and the resulting average was considered. Nuclear magnetic resonance (NMR) spectra were recorded on a Bruker Avance I 600 NMR spectrometer equipped with a 5 mm QXI probe head. The protein samples were prepared in 20 mM sodium phosphate and 10% D_2O (pH 7.0) at 25 °C, with a final protein concentration of 0.1 mM. A gradient Watergate W5 pulse sequence with a 75 μs delay was used to record 1024 scans for each protein at 25 °C.[30]

5.3.2.4 Enzyme Assays

Enzymatic activities of the H466Q and H351Q enzymes were measured in 50 mM potassium phosphate (pH 7.0) by monitoring the initial rates of oxygen consumption with a computer-interfaced Oxy-32 oxygen-monitoring system (Hansatech Instruments, Inc., Norfolk, England) at 25 °C. The apparent steady-state kinetic parameters of the H351Q enzyme were determined by varying the concentration of choline between 20 and 120 mM and keeping the oxygen concentration constant as atmospheric (i.e., 0.25 mM). Kinetic parameters are expressed for enzyme-bound flavin, using the extinction coefficient of 11400 M^{-1} s^{-1} previously determined for the wild-type enzyme.[26]

[a] The Michaelis–Menten equation for one-substrate kinetics was used.

Anaerobic flavin reduction of the H466Q enzyme was monitored in 20 mM sodium pyrophosphate (pH 8.0–10.0) at 25 °C, using a photodiode array UV–visible spectrophotometer and an anaerobic cuvette equipped with two side arms. The anaerobic cuvette contained the H466Q (20–25 μM in flavin content) and glucose oxidase (final concentration of 0.5 μM) enzymes in the belly of the anaerobic cuvette, whereas 75 (or 60) mM choline was contained in one side arm and 7.5 mM glucose in the other. The cuvette apparatus was made anaerobic by a 20-cycle treatment of flushing with oxygen-free argon and gas removal by applying vacuum. Once the cycles had been completed, the enzymes were mixed with glucose for 30 min to ensure complete scavenging of oxygen traces prior to initiating the reaction by mixing with choline. The initial rates thus determined with 60 and 75 mM choline were similar, consistent with being a good approximation of the rate constants of flavin reduction at a saturating choline concentration.

---

[a]An inaccuracy of up to 25% may have resulted in the determination of the apparent steady-state kinetic parameters of the H351Q enzyme by using the extinction coefficient of the flavin bound to the wild-type enzyme. This does not alter the main conclusion that is drawn in this study that the mutation results in an enzyme that retains the ability to oxidize choline. Because the H351Q enzyme was not investigated further and the kinetic parameters determined at an atmospheric oxygen level cannot be used to draw mechanistic conclusions, we did not attempt a more accurate determination of the concentration of enzyme-bound flavin based on the extinction coefficient of the mutant enzyme.

5.4 Results

5.4.1 Purification of the H351Q and H466Q Enzymes

The H351Q and H466Q enzymes were expressed in recombinant form and purified to high levels as judged by sodium dodecyl sulfate–polyacrylamide gel electrophoresis with the protocol used for the wild-type enzyme.[26, 31] The enzyme-bound flavins in both variants were present throughout the purification procedure as a mixture of oxidized and air-stable anionic flavosemiquinone, requiring dialysis at pH 6.0 to obtain fully oxidized enzymes, as previously reported for wild-type choline oxidase.[31] The absorption maxima in the visible region of the oxidized enzyme variants were centered at 376 and 455 nm for the H351Q enzyme and 361 and 453 nm for the H466Q enzyme.[31] For comparison, wild-type choline oxidase has maxima at 373 and 454 nm. In the H466Q enzyme, the flavin was noncovalently attached to the protein, as it could be extracted upon treatment with acetonitrile and centrifugation to remove denatured protein. The pelleted protein did not contain any flavin, with 100% of the released flavin recovered in the supernatant based on spectral observations (data not shown). This agrees well with previous data showing that replacement of H466 with aspartate or alanine results in ≥75% of the flavin being noncovalently associated with the protein.[15, 22] In contrast, the flavin in wild-type choline oxidase and several other variants characterized thus far is covalently attached to H99.[5, 8, 12-14, 32, 33] Furthermore, the extinction coefficient of the H466Q variant was determined to be 10.4 mM^{-1} cm^{-1} with a λ_{max} of 453 nm. This value was lower than the wild-type value of 11.4 mM^{-1} cm^{-1}, which is consistent with an altered flavin microenvironment.[26]

The apparent steady-state kinetic parameters for the enzyme variants in which H351 or H466 was replaced with glutamine were determined in atmospheric oxygen (i.e., 0.25 mM) with choline as the substrate at pH 7.0 and 25 °C by measuring initial rates of oxygen consumption.

With the H351Q enzyme, the $^{app}k_{cat}$ was 0.33 ± 0.02 s^{-1}, the $^{app}K_m$ was 67 ± 9 mM, and the $^{app}(k_{cat}/K_m)$ was 4.9 ± 0.8 M^{-1} s^{-1}. No oxygen consumption could be detected with the H466Q enzyme with concentrations of choline as high as 100 mM and 10 μM enzyme in the assay reaction mixture. For comparison, wild-type choline oxidase is routinely assayed at an FAD-bound concentration of 0.1 μM, yielding an $^{app}k_{cat}$ of 15 ± 1 s^{-1}, an $^{app}K_m$ of 0.6 ± 0.1 mM, and an $^{app}(k_{cat}/K_m)$ of 25000 ± 6500 M^{-1} s^{-1}.[31] Thus, H466 is clearly an essential residue in the active site of the enzyme, and the H466Q variant was therefore investigated further. Spectroscopic studies were then conducted with the H466Q variant and wild type for comparison to determine if the effect on enzyme activity was due to a lack of structural integrity in the variant enzyme.

5.4.2 Spectroscopic Analysis of the H466Q Enzyme

Our attempts to crystallize the H466Q enzyme and use X-ray crystallography to establish if the mutation affects the overall folding of the enzyme and the topology of the active site were not successful. Consequently, spectroscopic techniques, including circular dichroism of the protein and the flavin, protein and flavin fluorescence, and ^{1}H NMR, were used to compare and contrast the biophysical properties of the H466Q and wild-type enzymes. The use of these techniques allowed for a thorough comparison of the secondary and tertiary structures to establish if the variant enzyme exhibited the same overall fold as the wild-type enzyme.

Figure 2A shows that the far-UV circular dichroic spectra of the H466Q and wild-type enzymes determined at pH 7.0 and 25 °C were practically indistinguishable from one another, indicating that the two enzymes have a similar amount of secondary structure elements. The near-UV circular dichroic spectrum of the H466Q enzyme was also very similar to that of wild-type choline oxidase (Figure 2B), demonstrating that the replacement of H466 with glutamine is not affecting the overall fold or tertiary structure. However, an inversion of polarity in the long

wavelength dichroic band of the flavin around 450 nm was observed in the H466Q enzyme compared to that of the wild-type enzyme (Figure 2C). In principle, the negative dichroic band could be attributed to the change in the microenvironment surrounding the flavin arising from the glutamine replacement of H466 or the absence of a covalent linkage between the flavin C(8) methyl and H99. The visible circular dichroic spectrum of the flavin bound to the H99N variant of choline oxidase, in which the histidyl linkage at the C(8) position is absent,[(5)] was consequently determined, showing a positive dichroic signal in the long wavelength region with same polarity with respect to that of the wild-type enzyme and a weak positive dichroic band that is slightly blue-shifted with respect to that of the wild type (Figure 2C). Thus, inversion of polarity in the visible circular dichroic spectrum of H466Q likely arises from a change in the microenvironment surrounding the flavin ensuing from the replacement of histidine with glutamine.[(34)] The far- and near-UV circular dichroic spectra revealed that both enzymes are folded with the same secondary and tertiary structure. Consistent with these results, the visible circular dichroic spectra also demonstrate that the flavin is contained within the folded enzyme because the induced dichroic signal at long wavelengths in the visible region of the electromagnetic spectrum reports on the protein microenvironment surrounding the isoalloxazine ring of the bound flavin and not free flavin, which lacks chiral centers in the oxidized state and yields a very weak signal.[(35-37)]

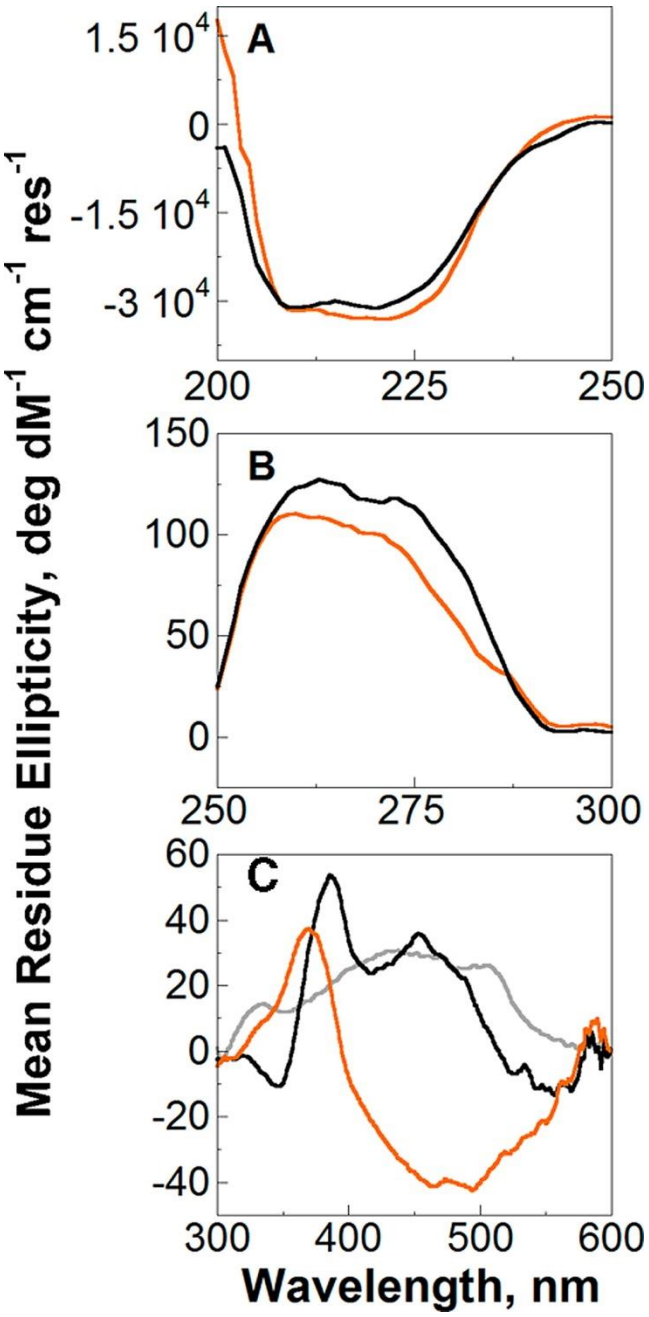

Figure 5.2 Circular dichroic spectra of H466Q (orange), H99N (gray, panel C only), and wild-type (black) enzymes, determined in 20 mM sodium phosphate (pH 7.0) at 25 °C.
(A) Far-UV CD spectra were measured from 200 to 250 nm with protein concentrations of 0.1 µM. (B) Near-UV CD spectra were measured from 250 to 300 nm with protein concentrations of 21 µM. (C) Visible CD spectra were measured from 300 to 600 nm with concentrations of enzyme-bound FAD of 23 µM. Spectra were obtained by averaging five scans at 50 nm/min and were smoothed by the Means-Movement method using Jasco Spectra Analysis software.

The protein fluorescence emission band at 342 nm was 2-fold more intense in the H466Q enzyme than in wild-type choline oxidase (Figure 3A). Similarly, the mutation resulted in a 5-fold increase in flavin fluorescence emission in comparison to that of the wild-type enzyme, with a hypsochromic shift of the band from 528 nm in the wild-type enzyme to 520 nm in the H466Q enzyme (Figure 3B). The flavin fluorescence of the wild-type and H466Q variant enzymes was quenched by >80 and 50%, respectively, in comparison to that of free FAD under the same conditions (data not shown). This agrees well with the visible circular dichroic spectra of both enzymes, in which the flavin was located within the confines of the protein.

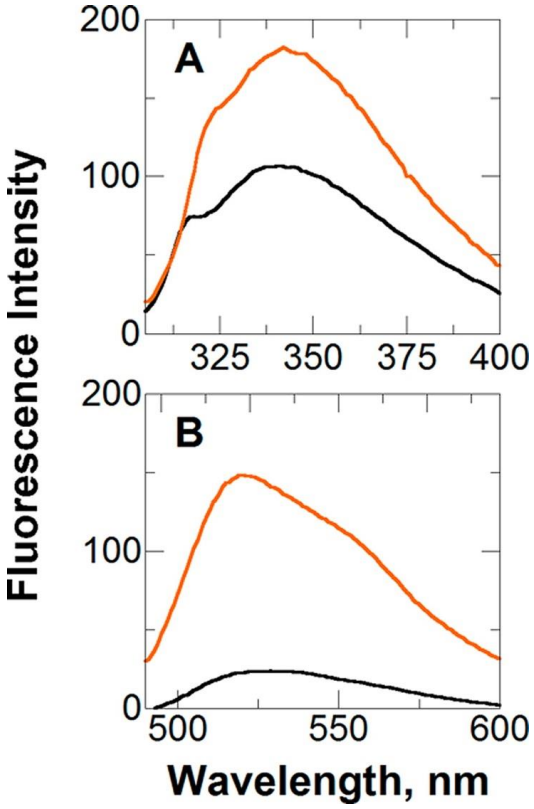

Figure 5.3 Protein and flavin fluorescence emission spectra of H466Q (orange) and wild-type (black) choline oxidase.
Spectra were recorded in 20 mM sodium phosphate (pH 7.0) at 15 °C. (A) Proteins at concentrations of 0.8 µM were excited at 286 nm. (B) Enzyme-boud flavins at concentrations of 3.5 µM were excited at 454 nm (wild type) and 469 nm (H466Q).

The structural integrity of choline oxidase upon replacement of H466 with glutamine was probed also through NMR, by comparing the one-dimensional ^{1}H NMR spectra of the H466Q and wild-type enzymes acquired at pH 7.0 and 25 °C in 90% H_2O. The NMR spectra of the two enzymes are clearly highly similar. Both wild-type and mutated enzymes exhibited good chemical dispersion, consistent with the proteins being folded (Figure 4). A closer comparison of the NMR spectra showed analogous peak patterns, line widths, and intensities in the backbone NH and aromatic regions (10.5–6 ppm) and in the aliphatic region. The resonances near 0 ppm originate from methyl groups that are shifted because of ring current effects.[(38)] Such signals are expected for a folded protein; a comparison shows that both enzymes have an identical fingerprint in this region. The NMR data signify similar overall folds and structure of the wild-type and variant enzymes (Figure 4).

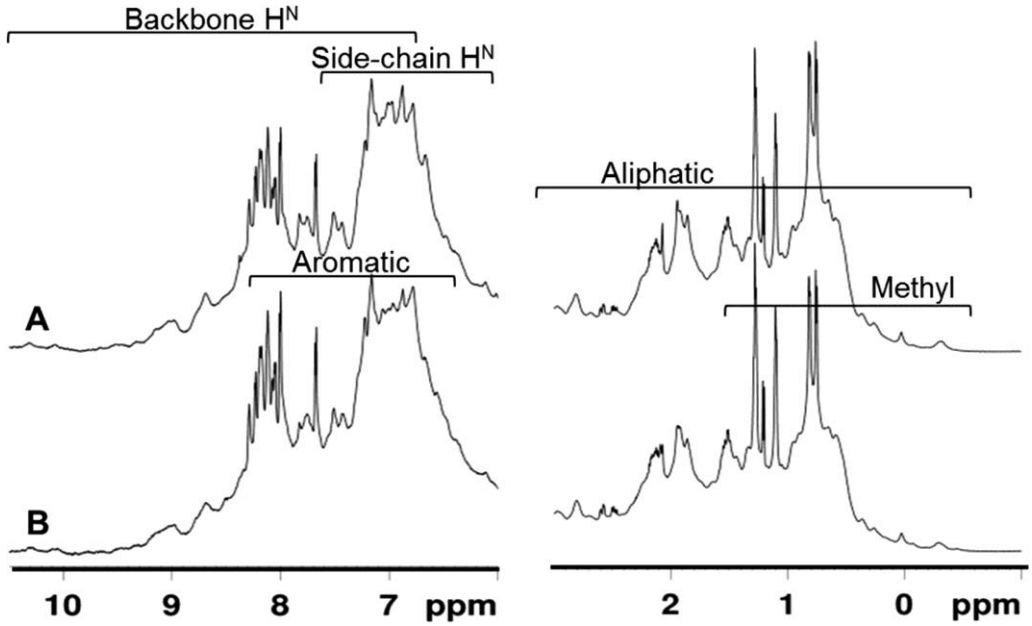

Figure 5.4 1H NMR spectra of (A) H466Q and (B) wild-type choline oxidase in 20 mM sodium phosphate (pH 7.0) and 10% D_2O at 25 °C. Both enzymes had protein concentrations of 0.1 mM.

5.4.3 Anaerobic Flavin Reduction of the H466Q Enzyme

To establish whether the enzyme-bound flavin in the H466Q enzyme could be reduced by the substrate, we incubated anaerobically the enzyme (~25 μM) with 60 mM choline and monitored the changes in absorbance at 453 nm over time. The experiment was initially conducted at pH 10.0 and 25 °C because previous steady-state and rapid reaction kinetics demonstrated that under these conditions the rate of flavin reduction is pH-independent for wild-type choline oxidase and several of its variants.[1, 2, 8, 9, 13, 15, 26, 39] As shown in Figure 5, an ~20% decrease in absorbance at 453 nm was observed over an incubation time of 60 min, indicative of a slow reduction of the enzyme. Full reduction of the flavin could not be observed because of concerns about enzyme stability or photobleaching of the flavin over the extended reaction condition that would be required because of the impaired activity, incubation, and irradiation at 25 °C. This prevented the use of the more common exponential equations employed in rapid kinetic analysis. Instead, the method of the initial rates was used by fitting only the initial portion of the trace at 453 nm. After subtraction of the corresponding value obtained in the absence of choline (Figure 5 inset), the molar concentration of oxidized FAD reduced per unit of time was calculated and used to determine the observed rate constant for flavin reduction (k_{obs}). With 60 mM choline, the observed rate constant for flavin reduction (k_{obs}) thus calculated was (4.6 ± 0.1) × 10^{-5} s^{-1}. When the reduction of the H466Q enzyme was conducted with 75 mM choline, a k_{obs} value of (4.7 ± 0.1) × 10^{-5} s^{-1} was determined. This demonstrates that the enzyme is saturated at these concentrations of choline. Consequently, ~5 × 10^{-5} s^{-1} is a good representation of the limiting rate constant for flavin reduction (k_{red}) at a saturating choline concentration for the H466Q enzyme. For comparison, the k_{red} value at pH 10.0 and 25 °C of wild-type choline oxidase is 93 s^{-1}.[1] When the anaerobic reduction of the H466Q enzyme was conducted at pH

8.0 and 9.0, the k_{red} values at saturating concentrations of choline were 1.3×10^{-7} and 1.9×10^{-6} s^{-1}, respectively. The decrease in the k_{red} values of 2 orders of magnitude at pH 8.0 as compared to those at pH 10.0, i.e., 10^{-7} s^{-1} versus 10^{-5} s^{-1}, is consistent with the hydride transfer reaction catalyzed by the H466Q enzyme being initiated by specific base catalysis through the hydroxide ion present in solution.[23, 40]

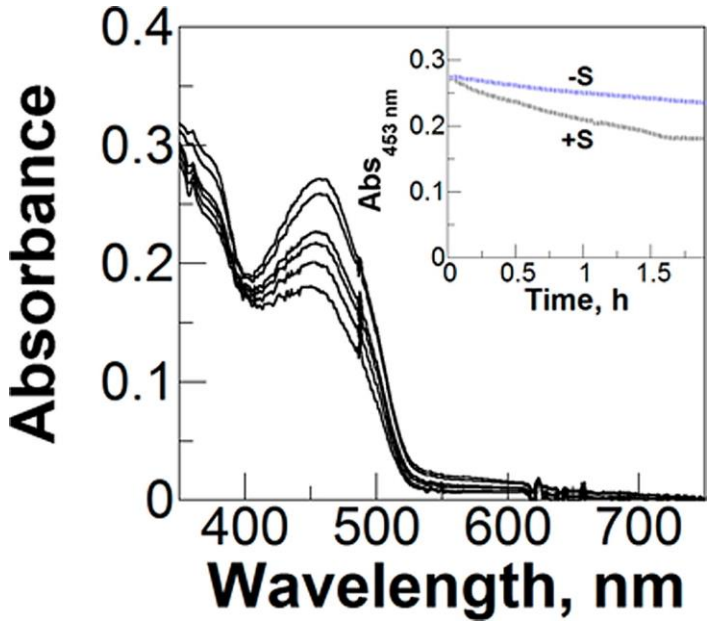

Figure 5.5 Anaerobic flavin reduction of the H466Q enzyme with 60 mM choline in 20 mM sodium pyrophosphate (pH 10.0) at 25 °C. UV–visible absorption spectra were recorded every 60 s from 350 to 750 nm.
The absorbance of the flavin between 400 and 500 nm decreased over the measured time, indicating flavin reduction due to reaction with choline. In the inset, the black trace is the time course of absorbance changes at the λ_{max} of the flavin cofactor, 453 nm, for the H466Q enzyme while the blue trace is that of a control assay in the absence of choline to account for the slow rate of photobleaching of the enzyme-bound flavin caused by intermittent light exposure over the 2 h required to acquire the data.

5.5 Discussion

In the active site of choline oxidase, two histidine residues have the potential to act as a base to deprotonate choline to the alkoxide species, H351 and H466 (Figure 1). This reaction activates the alcohol substrate for the subsequent oxidation through the transfer of a hydride ion to the enzyme-bound flavin.[1, 9] In previous studies, both residues were mutated to alanine,

allowing us to establish mechanistic roles for H351 and H466 in substrate binding and catalysis but failing to demonstrate whether either residue is the essential base required for catalysis.[13, 15] In the investigation presented here, we mutated H351 and H466 to glutamine, purified the enzyme variants, and characterized them for their ability to oxidize choline. The results demonstrated that H466 is essential in the active site of the enzyme, while replacement of H351 with glutamine impaired catalysis without completely abolishing the activity of the enzyme. This is in agreement with previous results obtained upon substitution of H351 with alanine.[13] On the basis of these findings and previous mechanistic and structural information, we conclude that H466 is the base that initiates choline oxidation in the reaction catalyzed by choline oxidase, as discussed below.

In the active site of choline oxidase, H466 is essential for catalysis. Evidence that supports this conclusion comes from both steady-state kinetics and anaerobic reduction of the H466Q enzyme with choline as the substrate. No consumption of oxygen was detected in a Clark-type oxygen electrode when the H466Q enzyme was assayed at enzyme concentrations 100-fold greater than the concentration routinely used with wild-type choline oxidase. These kinetic assays were performed with 100 mM choline, which is 160- and 1.5-fold larger than the $^{app}K_m$ values for choline determined at atmospheric oxygen with the wild-type and H351Q enzymes, respectively. Thus, the H466Q enzyme has an undetectable rate of turnover with choline using the standard kinetic assay routinely employed for choline oxidase. The lack of enzymatic activity of the H466Q enzyme was not due to the misfolded enzyme that may arise from mutating H466 to glutamine, as suggested by anaerobic flavin reduction and spectroscopic data for the H466Q enzyme. The enzyme-bound flavin was indeed reduced upon anaerobic incubation of the H466Q enzyme with choline, although with a rate constant for flavin reduction

(k_{red}) that was 6 orders of magnitude lower than the corresponding k_{red} value of the wild-type enzyme, i.e., $\sim 5 \times 10^{-5}$ s^{-1} compared to 93 s^{-1} at pH 10.0 and 25 °C. Under these conditions, flavin reduction is independent of pH in wild-type choline oxidase and several of its variants.[5, 8, 13, 15] The low k_{red} value determined with the H466Q enzyme agrees well with the lack of oxygen consumption observed when the enzyme is assayed using an oxygen electrode using choline as the substrate. The residual k_{red} determined for the H466Q enzyme using the modified method developed in this study is clearly outside typical ranges seen for enzymatic catalysis, because it would require approximately 1 day for a single catalytic turnover to approach completion[b] at pH 10.0. Hydroxide ion with unusual basicity due to its proximity to the trimethylammonium headgroup of choline is the probable catalyst that activates choline to the alkoxide species in the active site of the H466Q enzyme, as suggested by the effect of pH on the k_{red} value of the H466Q enzyme.

Independent evidence of the H466Q enzyme being folded like the wild-type enzyme comes from the circular dichroism and ^{1}H NMR data, showing that the H466Q and wild-type enzymes had near-UV circular dichroic spectra that lacked significant differences between one another and ^{1}H NMR spectra that did not show significant differences between the two enzymes. Furthermore, the two enzymes had far-UV dichroic spectra that were practically indistinguishable from one another. Taken together, these data are consistent with the

[b]A first-order process of flavin reduction with an apparent rate constant of 10^{-5} s^{-1} has a half-life of 13860 s, equivalent to 3.85 h. Thus, 98.5% completion, which is achieved in six half-lives, would require 23.1 h. In comparison, assuming no loss of activity, the wild-type enzyme would have completed 7.7 million turnovers in the same time span of 23 h as H466Q would only have completed a single turnover.

replacement of H466 with glutamine not inducing significant protein conformational changes in the secondary structure content or overall tertiary structure of the enzyme. In this context, previous studies have shown that the active site of choline oxidase accommodates mutations very well, with enzyme variants showing structures that are identical to that of the wild type, as established by X-ray crystallography for the S101A[12] and V464A[33] enzymes, or with similar spectroscopic, biophysical or kinetic properties as in the case of the H99N,[5] E312D,[8, 10, 41] H351A,[13] V464A/T,[33] H466D/A,[15, 22] and N510A/H/L[14] enzymes.

Mutation of H466 to glutamine affected the spectroscopic properties of the flavin in choline oxidase, as expected because the side chain of H466 is 3.9 Å from the flavin N(1) atom with proper orientation to participate in a H-bond with the N(1) atom of the flavin (Figure 1). Evidence supporting this conclusion comes from the comparison of the fluorescence and circular dichroic spectra of the H466Q enzyme with those of wild-type choline oxidase. The magnitude of the protein fluorescence emission band at 340 nm increased by 2-fold, while that of the flavin at 530 nm increased by 5-fold upon substitution of H466 with glutamine, consistent with a decrease in hydrophobicity around the aromatic residues responsible for protein fluorescence and flavin fluorescence in the active site of the enzyme. Consistent with the observed changes in the absorbance and extinction coefficient of the H466Q enzyme with respect to wild-type choline oxidase, an effect on the hydrophobicity of the surrounding flavin environment is also suggested by the hypsochromic shift of the emission band from 528 to 520 nm in the H466Q enzyme compared to that of the wild type.[42-44] The active site of choline oxidase contains aromatic residues, including W61, F357, Y465, and W331,[6] whose fluorescence emission is likely sensitive to the nature of the side chain at position 466 because of proximity effects. The increase in flavin fluorescence observed in the H466Q enzyme compared to that of the wild type can thus

be ascribed to a diminished quenching of flavin fluorescence exerted by the side chain at position 466 of the protein with glutamine rather than histidine. The positive dichroic peak in the near-UV–visible region (350–400 nm) is comparable to that in the measured CD spectra of other flavoprotein oxidases, such d-amino acid oxidase, l-amino acid oxidase, and glucose oxidase.[45] The hypochromism and blue-shift in the near UV–visible circular dichroic spectra of the H466Q variant are consistent with the fluorescence and absorbance spectral shifts being affected by the altered active site polarity and nearby aromatic residues.[45]

Replacement of H466 with glutamine prevents flavinylation of the protein through the formation of a covalent linkage with H99, which is otherwise observed in wild-type choline oxidase and several of its variants.[5, 8, 12-15, 26, 32, 33] Evidence of this conclusion comes from the analysis of the supernatant obtained through treatment of the H466Q enzyme with acetonitrile followed by centrifugation to remove denatured protein, showing that 100% of the flavin could be extracted from the enzyme. This agrees well with previous results for the H466D variant of choline oxidase, in which ∼75% of FAD was not covalently linked to the protein.[22] Curiously, when H466 was replaced with alanine, there was no effect on enzyme flavinylation,[15] although the reason is unclear and further studies are required. All the other residues previously targeted for mutagenesis in the active site of the enzyme, including S101,[12] E312,[8] H351,[13] V464,[33] and N510A/H/L,[14] retained the cofactor covalently linked to the protein. Thus, the current results obtained with the H466Q enzyme, taken together with the results previously obtained with other variants of choline oxidase, reinforce the importance in the flavinylation process of H466, whose side chain is close to the flavin N(1) and C(2) atoms (Figure 1). In trimethylamine dehydrogenase and monomeric sarcosine oxidase, the presence of a

protein positive charge close to the flavin N(1) and C(2) atoms has been shown to be important in the flavinylation process.[46, 47]

The results of the mutagenesis investigation of H466 presented here and in a previous study in which the residue was mutated to alanine, in conjunction with mechanistic and structural studies using X-ray crystallography of the enzyme in complex with the product of reaction glycine betaine,[6, 15] establish H466 as a key residue playing multiple roles in the catalytic mechanism of choline oxidase. After formation of the enzyme–substrate complex, H466 removes the hydroxyl proton of choline with formation of an alkoxide species (Scheme 2). Previous pH and deuterium kinetic isotope effect studies using steady-state and rapid reaction kinetics are consistent with an intrinsic pK_a value of 7.5 for the catalytic base in the active site of the enzyme, which is now assigned to the side chain of H466.[1, 9, 26, 39, 48] Alcohol deprotonation triggers the subsequent hydride transfer reaction from the C^{α} atom of the alkoxide to the flavin N(5) atom, which is fully rate-limiting for the overall enzyme turnover and the reductive half-reaction in the wild-type enzyme.[1] Hydride transfer occurs in concerted but asynchronous fashion with the proton already residing on the side chain of H466 in the transition state, as established previously by a lack of solvent and large substrate kinetic isotope effects on the k_{red} value for the wild-type enzyme and the partial rescuing of the k_{cat} value in the H466A enzyme by imidazolium.[1, 15] In contrast, previous solvent kinetic isotope effects on the H466A variant revealed a more rate-limiting O–H bond cleavage with a $^{D}(k_{cat}/K_m)$ value of 2.2 compared to the value of 1 observed in the wild-type enzyme.[15] Consequently, mutation of H466 to alanine altered the mechanism from stepwise to concerted,[15] whereas mutation to glutamine completely abolished catalysis (this study). Thus, H466 fills in catalysis a dual role as the base activating the substrate for catalysis and as an electrostatic catalyst stabilizing the partial charge developing on the C^{α} atom of the

alkoxide during substrate oxidation. Mutagenesis, kinetic, and computational studies have recently established that the residue equivalent to H466 in the active site of two other members of the glucose–methanol–choline oxidoreductase enzyme superfamily, namely, H502 in aryl-alcohol oxidase[21] and H548 in pyranose 2-oxidase,[17] also acts as a base in catalysis.

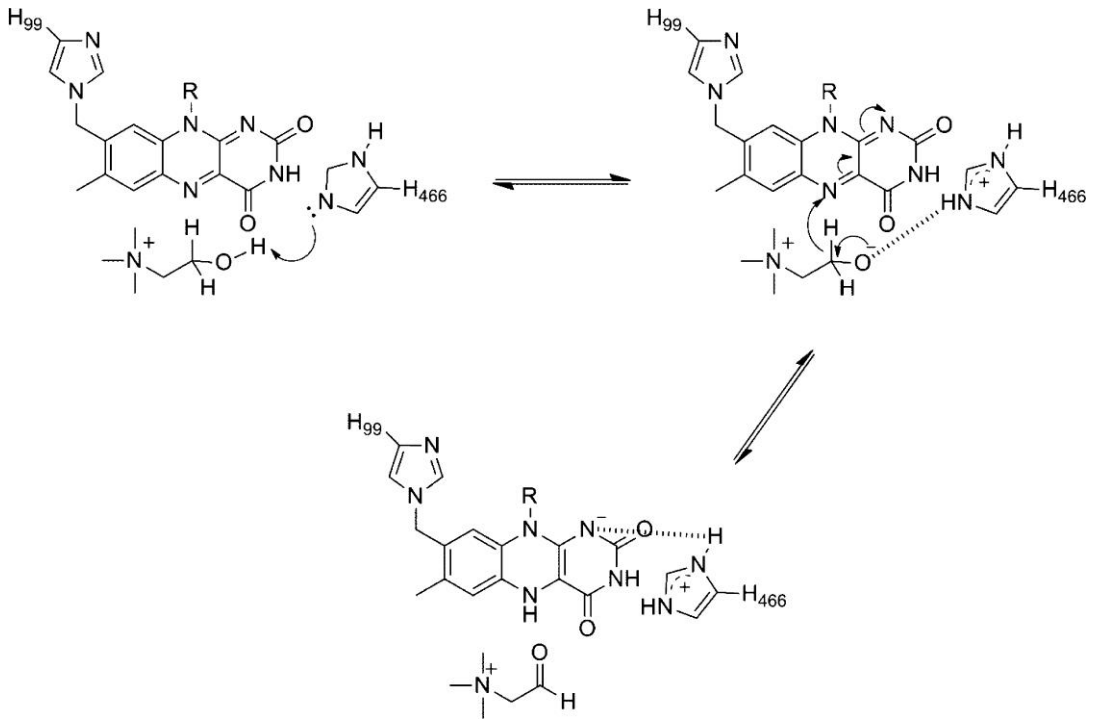

Scheme 5.2 Action of H466 as the Initiator of Alcohol Oxidation and the Stabilizer of the Alkoxide Species and the Anionic Reduced Flavin.

In summary, we have used mutagenesis, along with kinetic and spectroscopic approaches, to establish the identity of the catalytic base in the active site of choline oxidase. The results presented herein on a variant of choline oxidase with H466 substituted with glutamine are consistent with this residue being the base that deprotonates choline to the alkoxide species in the catalytic mechanism of the enzyme. This agrees well with the recent crystallographic structure of the enzyme in complex with glycine betaine, showing that the side chain of H466 is 3.1 Å from one of the carboxylate O atoms of the ligand (Figure 1).[6] The apparent discrepancy in the

results obtained with the H466Q enzyme in this study and the H466A enzyme in a previous study is reconciled with the hydroxide ion likely occupying the space vacated by the imidazole side chain in the latter enzyme and acting as a (poor) catalyst to activate choline to alkoxide for subsequent flavin reduction through hydride transfer. In this respect, previous mechanistic studies have established that a water molecule in the active site of the enzyme is necessary for the hydration of betaine aldehyde prior to the second oxidation reaction yielding glycine betaine.[(1)] Therefore, the histidine residue at position 466 holds multiple functions in the reductive half-reaction of choline oxidase. It exists as an electrostatic catalyst stabilizing the negative charges present on the reduced flavin and alkoxide intermediate and acts as the catalytic base that activates choline. Multiple amino acid substitutions had to be evaluated to elucidate the roles of this important residue in the mechanism of choline oxidase.

5.6 Acknowledgment

We thank Yanyi Chen for providing training on the circular dichroism spectrometer and the reviewers for their insightful suggestions.

5.7 References

1. Fan, F., and Gadda, G. (2005) On the catalytic mechanism of choline oxidase. *J. Am. Chem. Soc.* 127, 2067−2074.

2. Fan, F., Germann, M. W., and Gadda, G. (2006) Mechanistic studies of choline oxidase with betaine aldehyde and its isosteric analogue 3,3-dimethylbutyraldehyde. *Biochemistry* 45, 1979−1986.

3. Gannavaram, S., and Gadda, G. (2013) Relative timing of hydrogen and proton transfers in the reaction of flavin oxidation catalyzed by choline oxidase. *Biochemistry* 52, 1221−1226.

4. Xin, Y., Gadda, G., and Hamelberg, D. (2009) The cluster of hydrophobic residues controls the entrance to the active site of choline oxidase. *Biochemistry* 48, 9599−9605.

5. Quaye, O., Cowins, S., and Gadda, G. (2009) Contribution of flavin covalent linkage with histidine 99 to the reaction catalyzed by choline oxidase. *J. Biol. Chem.* 284, 16990−16997.

6. Salvi, F., Wang, Y. F., Weber, I. T., and Gadda, G. (2014) Structure of choline oxidase in complex with the reaction product glycine betaine. *Acta Crystallogr. D: Biol. Crystallogr.* 70, 405−413.

7. Gadda, G. (2008) Hydride transfer made easy in the reaction of alcohol oxidation catalyzed by flavin-dependent oxidases. *Biochemistry* 47, 13745−13753.

8. Quaye, O., Lountos, G. T., Fan, F., Orville, A. M., and Gadda, G. (2008) Role of Glu312 in binding and positioning of the substrate for the hydride transfer reaction in choline oxidase. *Biochemistry* 47, 243− 256.

9. Fan, F., and Gadda, G. (2005) Oxygen- and temperature dependent kinetic isotope effects in choline oxidase: Correlating reversible hydride transfer with environmentally enhanced tunneling. *J. Am. Chem. Soc.* 127, 17954−17961.

10. Quaye, O., and Gadda, G. (2009) Effect of a conservative mutation of an active site residue involved in substrate binding on the hydride tunneling reaction catalyzed by choline oxidase. *Arch. Biochem. Biophys.* 489, 10−14.

11. Fan, F., and Gadda, G. (2007) An internal equilibrium preorganizes the enzyme-substrate complex for hydride tunneling in choline oxidase. *Biochemistry* 46, 6402−6408.

12. Yuan, H., and Gadda, G. (2011) Importance of a serine proximal to the C(4a) and N(5) flavin atoms for hydride transfer in choline oxidase. *Biochemistry* 50, 770−779.

13. Rungsrisuriyachai, K., and Gadda, G. (2008) On the role of histidine 351 in the reaction of alcohol oxidation catalyzed by choline oxidase. *Biochemistry* 47, 6762−6769.

14. Rungsrisuriyachai, K., and Gadda, G. (2010) Role of asparagine 510 in the relative timing of substrate bond cleavages in the reaction catalyzed by choline oxidase. *Biochemistry* 49, 2483−2490.

15. Ghanem, M., and Gadda, G. (2005) On the catalytic role of the conserved active site residue His466 of choline oxidase. *Biochemistry* 44, 893−904.

16. Hernandez-Ortega, A., Borrelli, K., Ferreira, P., Medina, M., Martinez, A. T., and Guallar, V. (2011) Substrate diffusion and oxidation in GMC oxidoreductases: An experimental and computational study on fungal aryl-alcohol oxidase. *Biochem. J.* 436, 341−350.

17. Wongnate, T., Sucharitakul, J., and Chaiyen, P. (2011) Identification of a catalytic base for sugar oxidation in the pyranose 2- oxidase reaction. *ChemBioChem*. 12, 2577−2586.

18. Rotsaert, F. A., Renganathan, V., and Gold, M. H. (2003) Role of the flavin domain residues, His689 and Asn732, in the catalytic mechanism of cellobiose dehydrogenase from *Phanerochaete chrysosporium*. *Biochemistry* 42, 4049−4056.

19. Wongnate, T., and Chaiyen, P. (2013) The substrate oxidation mechanism of pyranose 2-oxidase and other related enzymes in the glucose-methanol-choline superfamily. *FEBS J.* 280, 3009−3027.

20. Romero, E., and Gadda, G. (2014) Alcohol oxidation of flavoenzymes. *Biomol. Concepts* 5, 299−318.

21. Hernandez-Ortega, A., Lucas, F., Ferreira, P., Medina, M., Guallar, V., and Martinez, A. T. (2012) Role of active site histidines in the two half-reactions of the aryl-alcohol oxidase catalytic cycle. *Biochemistry* 51, 6595−6608.

22. Ghanem, M., and Gadda, G. (2006) Effects of reversing the protein positive charge in the proximity of the flavin N(1) locus of choline oxidase. *Biochemistry* 45, 3437−3447.

23. Jencks, W. P. (1969) *Catalysis in Chemistry and Enzymology*, Dover Publications, Inc., New York.

24. Jencks, W. P. (1958) The reaction of hydroxylamine with activated acyl groups. II. Mechanism of the reaction. *J. Am. Chem. Soc.* 80, 4585−4588.

25. Epstein, J., Plapinger, R. E., Michel, H. O., Cable, J. R., Stephani, R. A., Hester, R. J., Billington, C., Jr., and List, G. R. (1964) Reactions of isopropyl methylphosphonofluoridate with substituted phenols. I. *J. Am. Chem. Soc.* 86, 3075−3084.

26. Ghanem, M., Fan, F., Francis, K., and Gadda, G. (2003) Spectroscopic and kinetic properties of recombinant choline oxidase from *Arthrobacter globiformis*. *Biochemistry* 42, 15179−15188.

27. Raibekas, A. A., and Massey, V. (1997) Glycerol-assisted restorative adjustment of flavoenzyme conformation perturbed by site-directed mutagenesis. *J. Biol. Chem.* 272, 22248−22252.

28. Raibekas, A. A., and Massey, V. (1996) Glycerol-induced development of catalytically active conformation of *Crotalus adamanteus* L-amino acid oxidase in vitro. *Proc. Natl. Acad. Sci. USA* 93, 7546−7551.

29. Whitby, L. G. (1953) A new method for preparing flavin-adenine dinucleotide. *Biochem. J.* 54, 437−442.

30. Liu, M. L., Mao, X. A., Ye, C. H., Huang, H., Nicholson, J. K., and Lindon, J. C. (1998) Improved WATERGATE pulse sequences for solvent suppression in NMR spectroscopy. *J. Magn. Reson.* 132, 125− 129.

31. Fan, F., Ghanem, M., and Gadda, G. (2004) Cloning, sequence analysis, and purification of choline oxidase from *Arthrobacter globiformis*: A bacterial enzyme involved in osmotic stress tolerance. *Arch. Biochem. Biophys.* 421, 149−158.

32. Finnegan, S., Yuan, H., Wang, Y. F., Orville, A. M., Weber, I. T., and Gadda, G. (2010) Structural and kinetic studies on the Ser101Ala variant of choline oxidase: Catalysis by compromise. *Arch. Biochem. Biophys.* 501, 207−213.

33. Finnegan, S., Agniswamy, J., Weber, I. T., and Gadda, G. (2010) Role of valine 464 in the flavin oxidation reaction catalyzed by choline oxidase. *Biochemistry* 49, 2952−2961.

34. van Berkel, W. J. H., and Muller, F. (1989) The temperature and pH dependence of some properties of p-hydroxybenzoate hydroxylase from *Pseudomonas fluorescens. Eur. J. Biochem.* 179, 307−314.

35. Kelly, S. M., and Price, N. C. (2000) The use of circular dichroism in the investigation of protein structure and function. *Curr. Protein Pept. Sci.* 1, 349−384.

36. Shiga, K., Horuke, K., Nishina, Y., Otani, S., Watari, H., and Yamano, T. (1978) A study of flavin-protein and flavoprotein-ligand interactions. *J. Biochem.* 85, 931−941.

37. Visser, A. J. W. G., van Berkel, W. J. H., and de Kok, A. (1995) Changes in secondary structure and flavin microenvironment between *Azotobacter vinelandii* lipoamide dehydrogenase and several deletion mutants from circular dischroism. *Biochim. Biophys. Acta* 1229, 381− 385.

38. Wuthrich, K. (1985) NMR of proteins and nucleic acids, John Wiley & Sons, Inc., New York.

39. Gadda, G. (2003) pH and deuterium kinetic isotope effects studies on the oxidation of choline to betaine-aldehyde catalyzed by choline oxidase. *Biochim. Biophys. Acta* 1650, 4−9.

40. Richard, J. P. (1998) The enhancement of enzymatic rate accelerations by Bronsted acid-base catalysis. *Biochemistry* 37, 4305− 4309.

41. Quaye, O., Nguyen, T., Gannavaram, S., Pennati, A., and Gadda, G. (2010) Rescuing of the hydride transfer reaction in the Glu312Asp variant of choline oxidase by a substrate analogue. *Arch. Biochem. Biophys.* 499, 1−5.

42. Yagi, K., Ohishi, N., Nishimoto, K., Choi, J. D., and Song, P. S. (1980) Effect of hydrogen bonding on electronic spectra and reactivity of flavins. *Biochemistry* 19, 1553−1557.

43. Weber, G., and Farris, F. J. (1979) Synthesis and spectral properties of a hydrophobic fluorescent probe: 6-Propionyl-2-(dimethylamino)naphthalene. *Biochemistry* 18, 3075−3078.

44. Kotaki, A., and Yagi, K. (1970) Fluorescence properties of flavins in various solvents. *J. Biochem*. 68, 509−516.

45. Edmondson, D. E., and Tollin, G. (1971) Circular dichroism studies of the flavin chromophore and of the relation between redox properties and flavin environment in oxidases and dehydrogenases. *Biochemistry* 10, 113−124.

46. Mewies, M., Packman, L. C., Mathews, F. S., and Scrutton, N. S. (1996) Flavinylation in wild-type trimethylamine dehydrogenase and differentially charged mutant enzymes: A

study of the protein environment around the N1 of the flavin isoalloxazine. *Biochem. J.* 317 (Part 1), 267−272.

47. Trickey, P., Wagner, M. A., Jorns, M. S., and Mathews, F. S. (1999) Monomeric sarcosine oxidase: Structure of a covalently flavinylated amine oxidizing enzyme. *Structure* 7, 331−345.

48. Gadda, G. (2003) Kinetic mechanism of choline oxidase from *Arthrobacter globiformis*. *Biochim. Biophys. Acta* 1646, 112−118.

6 Excited State Proton Transfers in Choline Oxidase

6.1 Abstract

Excited state proton transfers (ESPT) occur during the excitation of a fluorophore acting as an acid donating a proton to a nearby molecule. Alternatively, an acid molecule can donate a proton to a nearby fluorophore acting as a base. This phenomenon can be revealed through the observation of a pH-dependence on the fluorescence emission. A redistribution of a fluorophore electrons occurs once the species is excited, altering the ionization state, leading to an ESPT. This biophysical process has been observed in model systems and small proteins, such as malonaldehyde and green fluorescent protein by using NMR, isotopic replacement, or fluorescence. In this study, choline oxidase (CHO) was used to investigate ESPT in the absence of active site ligands or substrates. To this aim, the ground state, fluorescence excited state and emission spectra were measured and the emission spectra were shown to be pH-dependent. Isotopic and mutagenic studies were utilized to further investigate ESPT occurring between the flavin cofactor bound to CHO and protein proton acceptors present in the active site and the formation of a C4a flavin adduct in the excited state. Notably, no ESPT were observed with free FAD in the presence or absence of imidazole or in the H466Q variant of CHO, likely reflecting lack of suitable protein construct and proper positioning of a proton acceptor. The results presented reveal, for the first time, ESPT processes can occur in a flavoprotein oxidase and can be easily detected using fluorescence spectroscopy.

6.2 Introduction

Flavin mononucleotide (FMN) or flavin adenine dinucleotide (FAD) are utilized by a wide array of enzymes to catalyze many biological processes including but not limited to

detoxification, oxidation, biosynthesis, and DNA damage repair.[1] FAD and FMN are produced enzymatically from vitamin B2, or riboflavin, and exhibit strong absorbance in the UV and visible regions of the electromagnetic spectrum.[2-6] The hydrophobic contribution of the xylene moiety and the hydrophilic pyridine moiety provide riboflavin, FAD, FMN, and flavin analogs with the adaptability to catalyze various redox reactions. The redox state of the flavin during catalysis can be followed by monitoring the spectral changes of the UV-Visible absorption and fluorescence spectra of the conjugated isoalloxazine ring as the oxidation and reduced states of the flavin exhibit different UV-Visible absorbance and fluorescence spectral signatures. The three different redox states include oxidized, neutral and anionic semiquinones, and neutral and anionic hydroquinones and are characterized by different number of electrons and protons. The absorption and fluorescence spectra of the isoalloxazine moiety are sensitive to environmental changes (i.e. changes in pH, temperature, solvent, etc) not solely due to catalytic processes.[7-10] An example of environmental perturbations has been observed with blue shifts in UV-Visible absorption spectra of flavins in hydrophobic environments as observed by Smitherman *et al.* and others.[7, 8, 11, 12]

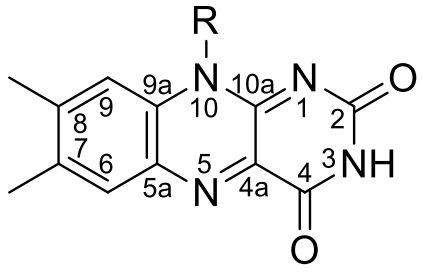

R = Phosphorylated riboflavin (FMN)
or
Adenosine diphosphate (FAD)

Figure 6.1 Chemical structure of the isoalloxazine moiety drawn as using IUPAC numbering. The R group denotes either the ribityl group of flavin mononucleotide or the additional adenosine monophosphate moiety of flavin adenine dinucleotide.

Flavin-dependent enzymes are capable of carrying out a wide array of chemical reactions due to the versatility of the isoalloxazine ring (Figure 6.1) by catalyzing single and double electron transfers and nucleophilic and electrophilic reactions.[13-15] Flavin-dependent enzymes utilize the protein construct to maximize the desired chemical reaction and minimize unproductive side reactions.[16] The protein environment surrounding the flavin is fine-tuned to specific catalytic functionality with specific substrates by active site amino acid residues altering the polarity and redox potential of the cofactor. Choline oxidase from *Arthrobactor globiformis* (CHO) exhibited a decrease in ~160 mV in the redox potential when a neutral histidine residue located near the N(1)-C(2) locus of the isoalloxazine ring was mutated to a negatively charged aspartate residue.[17] Covalent bonds that anchor the flavin to the protein modulate the chemistry of hydride transfers or nucleophilic attacks in the enzymatic reactions.[14, 18-21] The flavin cofactor in CHO is covalently-linked to the protein by an 8α-N(3)-histidyl linkage to H99.[20] H99 is mutated to an asparagine and subsequently the linkage is broken resulting in a change in flavin reduction by more than 45 times.[20] These enzymatic reactions are mostly monitored in the ground state by following flavin absorbance changes. Light processes, such as DNA repair, have been shown to be catalyzed by the flavin cofactor in the excited state as evidence of changes in fluorescence spectra during catalysis.[22] Light-triggered flavin-dependent enzymes have progressed to carry out all biological processes as excited state reactions once the flavin cofactors have been excited by photons.[22-24]

Enzymes have evolved to catalyze reactions through different mechanisms by triggering a transition of the enzyme complex to a different electronic energy state from what is reached during transition states in the ground state.[25] Flavin-containing proteins that catalyze reactions in the excited state can be classified into four families of photoreceptors: phototropins[26],

cryptochromes[27], light-oxygen-voltage (LOV) domains[28], and BLUF proteins.[29] These photoreceptors assist in catalyzing essential biological processes by first activating a flavin fluorophore to the singlet or triplet state prior to catalysis.[27, 30, 31] Transfers of electrons, protons, hydrogen atoms, and nucleophilic reactions have been shown to occur in the excited state as observed through fluorescence spectral changes which trigger conformational changes in the protein.[22, 23] Both FAD and FMN are chromophores in blue-light photo-sensors and can be widely-used as diagnostic tools within the cell to monitor hydrogen peroxide detection using their intrinsic fluorescence properties.[32, 33] In LOV domains, the FMN cofactor is reduced in the ground state and then excited to the singlet state which triggers a conformational change in the protein.[22] Increase in the cofactor's energy state triggers the formation of a covalent bond between the C4a atom of the flavin and a thiol group of a cysteine side chain.[24] Several groups have postulated mechanisms of adduct formation in these proteins which can be further read at [22, 34-36]. Lanzl *et al.* proposed radical mechanism in which the thiol group acquired an electron in the triplet state followed by a proton abstraction from the cysteine group to the N(5) atom of the flavin.[37] A second mechanism of action proposed by Conrad *et al.* begins with the deprotonation of the cysteine thiolate group and simultaneous protonation at the N(5) atom of the flavin producing a carbocation on the C4a and a reactive thiol.[38]

Excited state reactions, specifically proton transfers, have been observed in numerous biological processes due to a culmination of effects that include a photolabile fluorophore contained within a protein active site with a nearby proton donor or acceptor. Ground state proton transfer reactions involve a substrate being converted to product through a transition state while the enzyme system remains in the electronic ground state. Conversely, excited state proton transfer reactions occur at a higher energy state due to electronic transitions in the chemical

bonds involved in the chemical reaction being at a higher energy state due to absorption of photons. The electronic distribution of the flavin moiety is altered as the fluorophore absorbs photons.[39] This causes a redistribution of charges on the isoalloxazine ring, in turn, altering the polarity and ionization states in the singlet and triplet states of the flavin.[39] The ionization constants of the N(3) and N(5) atoms of the flavin change in that the N(3) becomes more acidic due to a decrease in pK_a and N(5) atom becomes more basic due to an increase in pK_a values.[40-43] A classic example of this phenomenon was observed as a tautomerization occurring from alloxazine to isoalloxazine in the lumichrome excited state via an excited state proton transfer (ESPT).[44] Once lumichrome was excited by light, the proton located on the N(1) atom of alloxazine was transferred to the N(10) atom forming the isoalloxazine phototautomer as facilitated by acetic acid or pyridine.[44] The ESPT was monitored by following fluorescence spectral changes of the photolabile flavin fluorophore in the presence of a proton acceptor.[44] ESPT have been observed in other flavin analogs in solution and in light-triggered flavin-dependent photoreceptors when excited by light.[22, 29, 41, 42, 44, 45] Therefore it is likely that, if excited, other flavin-dependent enzymes catalyze ESPT with a nearby proton acceptor available in the active site.

Choline oxidase from *Arthrobacter globiformis* (CHO) is an FAD-dependent enzyme that utilizes general base catalysis to oxidize its substrate.[11, 14] CHO has been thoroughly characterized both structurally and biochemically in which most of the active site residues have been mutated and characterized.[11, 14, 20, 46-51] A member of the Glucose-Methanol-Choline (GMC) oxidoreductase superfamily, CHO catalyzes the oxidation of choline to glycine betaine through two reduction-oxidation reactions using an FAD cofactor and oxygen as the final electron acceptor.[14] With CHO serving as a model enzyme, fluorescence studies comparing the ground

and excited states and emission of the enzyme were carried out as a function of pH. The hypothesis of ESPT occurring in the active site of enzymes containing flavins as cofactors with an active site base will be tested using CHO as a model.

Experimental Procedures

6.2.1 Materials

Recombinant choline oxidase and choline oxidase variant enzymes, H466Q and S101A, were obtained through expression and purification methods previously described.[11, 19, 21, 52] Flavin adenine dinucleotide, glucose oxidase, and glucose were purchased from Sigma Aldrich (St. Louis, MO). Glycerol was purchased from Fisher (Pittsburgh, PA). Deuterium oxide was obtained from Cambridge Isotope Co. (Andover, MA). All other reagents were of the highest purity commercially available.

6.2.2 UV-Visible Absorption and Fluorescence Studies

All enzymes were prepared fresh just prior to UV-Visible absorption and fluorescence spectroscopic measurements by gel-filtration through PD-10 desalting columns (General Electric, Fairfield, CT) into 20 mM sodium pyrophosphate, pH 6.0, 9.0-10.0 or 20 mM sodium phosphate, pH 7.0-8.0. UV-visible absorption spectra were recorded at 15 ^{o}C, using an Agilent Technologies diode-array model HP 8453 spectrophotometer (Agilent Technologies, Santa Clara, CA). Fluorescence excitation and emission spectra were recorded at 15 ^{o}C with a thermostatted Shimadzu Spectrofluorometer Model RF-5301 PC. Wavelength accuracy of the spectrofluorometer was ± 1.5 nm with a response time of 20 ms and a sampling interval of 1 nm. Flavin excitation and emission scans were measured at a scanning speed of 3 nm/s. Gel-filtered enzymes, CHO-wt and CHO variants, were diluted to a final FAD concentration of 3.5 μM using

the extinction coefficients experimentally determined previously.[11, 18, 19, 53] Each enzyme was excited at 450 nm and the emission scan was measured from 475 to 650 nm. The λ_{max} value of the initial emission scan was then used to measure the excitation scan from 300 to 500 nm. The λ_{max} value of the excitation scan (the single peak with the largest measured intensity) was used to acquire the emission scan from 475 to 650 nm to determine the λ_{em} value. The λ_{em} value was used to acquire the excitation scan to measure the λ_{ex} value (the single peak with the largest measured intensity). Enzyme samples that were prepared in deuterated buffers underwent the same gel-filtration procedure used for protiated buffers with an adjusted pD value for the isotope effect observed from the pH electrode.[54] The pD values were determined by addition of 0.4 to the pH electrode readings.[55] The contribution of solvent viscosity in fluorescence spectra due to the presence of heavy isotopes was measured in the presence of 10% glycerol (v/v) as the viscosigen with relative viscosity equivalent to that of D_2O.[56]

Anaerobic fluorescence spectra were measured in 20 mM sodium pyrophosphate, pH 6.0 and 10.0, at 15 ^{o}C using an anaerobic fluorescence cell with glass pouch cuvette (FireflySci, Brooklyn, NY). The anaerobic cuvette contained 7 mM glucose in buffer whereas CHO variant S101A (5 μM in flavin content) and glucose oxidase (1μM final concentration) enzymes were housed in the side arm. The fluorescence cuvette cell was made anaerobic by a 15 min treatment of flushing with oxygen-free argon. Once the oxygen was removed, the enzymes were mixed with glucose to ensure complete scavenging of oxygen traces prior to measuring the fluorescence excitation and emission spectra for an additional 15 min.

6.2.3 Data Analysis

The λ_{em} values determined as a function of pL were fit to Eq. 1. Here λ_{lim1} and λ_{lim2} are the limiting values at low and high pL of the fluorescence emission, and K_a is the dissociation constant for relevant ionizable group(s).

$$(\lambda_{em}) = \frac{\Delta\lambda_{lim1} + \Delta\lambda_{lim2}\left(\frac{10^{-pK_a}}{10^{-pH}}\right)}{1 + \frac{10^{-pK_a}}{10^{-pH}}} \quad (1)$$

6.3 Results

6.3.1 pH-Dependence on the Fluorometry of CHO-wt

The ground and excited states and the emission spectra of CHO-wt were measured as a function of pH from pH 6.0 to 10.1. At pH 6.0, the enzyme exhibited similar λ_{max} values in ground (absorbance) and excited states spectra with λ_{ex} value of 465 nm and λ_{GS} value of 458 nm, a 7 nm red shift from the ground state to the excited state (Figure 6.2, Panel A). The enzyme was excited at the experimentally determined λ_{max} value of 465 nm and the emission scan was acquired from 495 to 650 nm (Figure 6.2, Panel A). The emisison maximum (λ_{em}) was 523 nm.

Fluorescence excitation and emission spectra were also measured from pH 7.0 to pH 10.1 (Table 6.1) with only pH 6.0 and 10.1 shown in Figure 6.2. All data are shown in Table 6.1. At pH 10.1, the UV-visible absorption spectrum of CHO exhibited two peaks with λ_{max} values at 351 and 449 nm (Figure 6.2, Panel B). The excitation spectrum revealed a single peak with a λ_{max} at 401 nm and a shoulder at 324 nm. The flavin-bound cofactor was excited at 401 nm and the emission spectrum was scanned from 450 to 650 nm revealing a maximum at 528 nm (Figure 6.2, Panel B). Thus, at pH 10.1, the λ_{ex} value of the flavin bound to wild-type CHO exhibited a blue shift of 48 nm from the ground state maximum value, i.e., from 449 nm to 401 nm. Such a

large shift in the excitation spectrum and the presence of a single peak at ~400 nm was consistent with the formation of a flavin C4a adduct formed in the excited state. The measured λ_{em} values were plotted as a function of pH and fit with Eq. 1 (Figure 6.3, Panel A). The wavelength of the emission peaks increased with increasing pH from a limiting value of 521 ± 2 nm at low pH (λ_{lim1}) to 534 ± 4 nm at high pH (λ_{lim2}) with a pK_a of 7.9 ± 0.5 (Figure 6.3).

Table 6.1. UV-Visible absorption and fluorescence spectra maxima of CHO wild-type enzyme obtained at 15 °C.[a]

pH	λ_{GS}, nm	λ_{ex}, nm	λ_{em}, nm	Stokes Shift, nm
6.0	458	465	523	58
7.0	456	441	521	60
7.5	457	443	522	79
8.0	452	401	530	129
9.0	449	401	532	131
10.1	449	401	528	127

[a]Reaction conditions are 20 mM NaPPi, pH 6.0, 9.0-10.1 and 20 mM NaPi, pH 7.0-8.0 and all spectral measured in a 10 mm quartz cuvette.

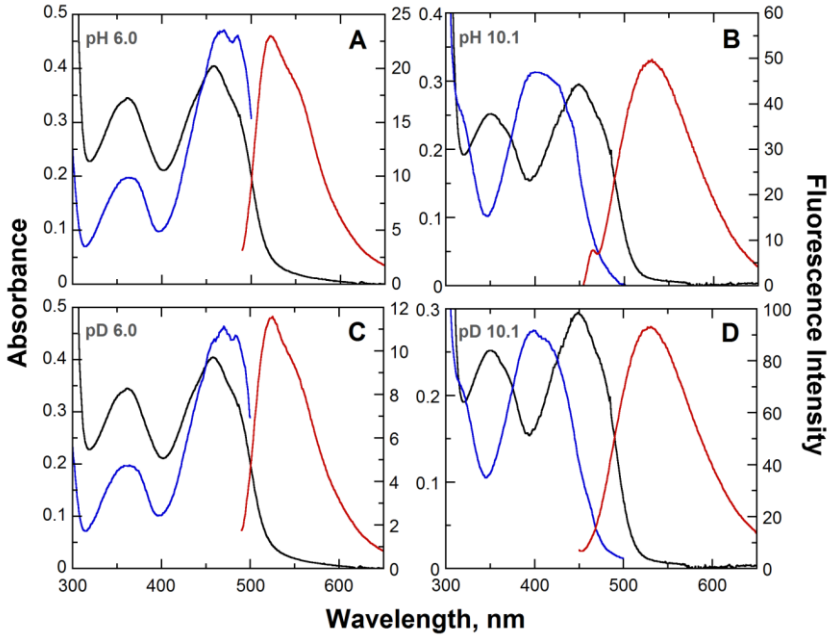

Figure 6.2 Fluorescence and absorption spectroscopy of choline oxidase.
Spectra are for absorbance (black), fluorescence excitation (blue), and fluorescence emission (red) at 15 ºC, in 20 mM sodium pyrophosphate and the pH or pD indicated. Wild-type enzyme at pH 6.0 (*A*); wild-type enzyme at pH 10.1 (*B*); wild-type enzyme at pD 6.0 (*C*); wild-type enzyme at pD 10.1 (*D*)

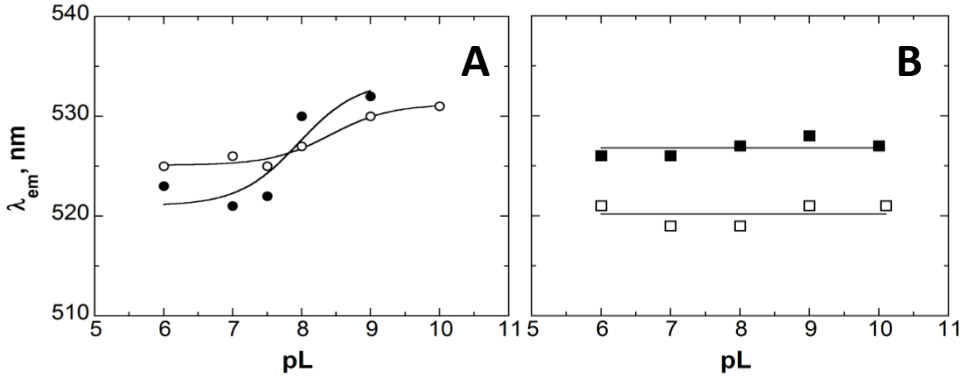

Figure 6.3 pL-Dependence on the maximal emissive peak.
Panel A: wild-type enzyme at 15 ºC in 20 mM sodium pyrophosphate (pL 6.0, 8.0-10.0) or 20 mM sodium phosphate (pL 7.0, 7.5) buffers prepared in H_2O (●) or D_2O (○); Panel B: H466Q variant enzyme in the same buffers prepared in H_2O (□); FAD dissolved in the same buffers p repared in H_2O (■). pL represents the negative logarithm of the concentration of protium or deuterium ions. Data for wild-type enzyme were fit with Eq 1.

6.3.2 pD-Dependence on the Fluorometry of CHO-wt in Deuterium Oxide (D_2O)

Fluorescence spectra of CHO-wt were recorded in deuterated buffers from pD 6.0 to 10.1 (Table 6.2). Isotopic substitution of all solvent exchangeable protons was used to probe whether the pH-dependence on fluorescence emission was due to a proton transfer in the excited state. The most likely candidate for the proton donor would be the N(3) atom of the flavin because the pK_a of the hydrogen bond has been measured to drop from ~10 in the ground state to ~7 in the excited state.[45, 57-59] Data reported in Table 6.2 of the wild-type in D_2O reveal a similar trend as observed of wild-type enzyme in H_2O. The λ_{ex} and λ_{GS} decreased with increasing pD concomitantly as λ_{em} was increasing. As shown in Figure 6.3, Panel A, the λ_{em} values were plotted as a function of pD and were observed to increase with increasing pD measuring a pK_a of 8.4 ± 0.2 with two offsets at low and high pD with limiting values of λ_{lim1} = 525 ± 1 nm and λ_{lim2} = 531 ± 1 nm, respectively. The limiting values calculated in the pD profile of CHO-wt emission in D_2O were similar to the enzyme observed in H_2O experiments with the pK_a shifted upward by ~0.4 units. A pD-dependence on the fluorescence emission was attributed to a proton being transferred during the excited state consistent with an ESPT (Figure 6.2, Panels C-D). A change in the shape of both excitation and emission spectra in the presence of a heavy isotope, D_2O, was also consistent with an ESPT (Figure 6.2, Panel B, Panel D).[60-62]

Table 6.2. UV-Visible absorption and fluorescence spectra maxima of CHO wild-type enzyme obtained at 15 ºC in deuterated buffer.[a]

pD	λ_{GS}, nm	λ_{ex}, nm	λ_{em}, nm	Stokes Shift, nm
6.0	455	465	525	60
7.0	455	442	526	84
7.5	454	422	525	103
8.0	454	400	527	127
9.0	451	401	530	129
10.0	450	399	531	132

[a]Reaction conditions are 20 mM NaPPi, pD 6.0, 9.0-10.1 and 20 mM NaPi, pD 7.0-8.0 in deuterated water with spectra measured in a 10 mm quartz cuvette.

Fluorescence spectra of CHO-wt were recorded in buffers containing 10 % (v/v) glycerol as a control for the D_2O experiments. Data are shown in Table 6.3. The λ_{max} values of ground and excited state and emission in glycerol-added buffers did not differ more than 5% from λ_{max} values observed in protiated buffers without glycerol. Therefore, the changes in the fluorescence spectra of the wild-type enzyme in deuterated buffer were consistent with an effect due to isotopically-labeled solvent and not a change in the viscosity of the solvent.

Table 6.3. UV-Visible absorption and fluorescence spectra maxima of CHO wild-type enzyme obtained at 15 ºC in buffers containing 10 % glycerol (v/v).[a]

pH	λ_{GS}, nm	λ_{ex}, nm	λ_{em}, nm	Stokes Shift, nm
6.0	458	469	522	53
7.0	456	469	522	53
7.5	454	443	523	80
8.0	455	419	523	104
9.0	451	400	529	129
10.0	448	400	530	130

[a]Reaction conditions are 20 mM NaPPi, pH 6.0, 9.0-10.1, 10% glycerol (v/v) and 20 mM NaPi, pH 7.0-8.0, 10% glycerol (v/v) with spectra measured in a 10 mm quartz cuvette.

6.3.3 pL-Dependence on the Fluorometry of CHO variant, H466Q

UV-Visible absorbance and fluorescence spectral studies were carried out with the H466Q variant enzyme to probe the role of histidine as a catalyst in the ESPT in the active site of CHO. The histidine residue at the 466 position is located on the *si* face of the flavin cofactor near the N(1)-C(2) locus of the isoalloxazine ring approximately 4.6 Å from the N(3) atom (Figure 6.4). UV-visible absorption, excitation and emission spectra were measured from pH 6.0 to 10.1 at 15 ^{o}C with only the spectra at pH 10.1 shown in Figure 6.5. Excited state spectra exhibited red shifts in the ground state from 450 nm to 469 nm from pH 6.0 to 10.1. All spectral peaks (i.e. λ_{GS}, λ_{ex}, λ_{em}) at each pH value tested are reported in Table 6.4. The average values for λ_{GS}, λ_{ex}, λ_{em} are 453, 468.6, and 520 nm, respectively. Fluorescence spectra of H466Q were also measured in deuterated buffers as prepared for the wild-type enzyme. In deuterated buffer, λ_{max} values of the ground and excited states and emission were 453, 464, and 521 nm, respectively (Table 6.5). The λ_{ex} and λ_{em} values were, thus, independent of pH and pD. Lack of pL effects on λ_{ex} and λ_{em} values were consistent with the absence of ESPT in the H466Q variant. If an ESPT was occurring in the variant enzyme, any amount of C4a flavin intermediate have formed in the excited state and decayed on a time scale faster than that observed in the wild-type enzyme.[41] The time scale for the decay of the C4a flavin intermediate would have to be slower for any flavin adduct intermediate to accumulate and therefore be detected.

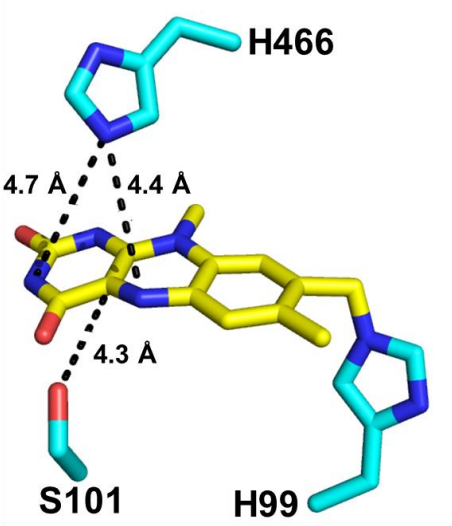

Figure 6.3 Active site of CHO (4MJW) highlighting H466 and S101 residues.

Table 6.4. UV-Visible absorption and fluorescence spectra maxima of CHO variant enzyme, H466Q, obtained at 15 ºC.[a]

pH	λ_{GS}, nm	λ_{ex}, nm	λ_{em}, nm	Stokes Shift, nm
6.0	455	469	521	52
7.0	451	471	519	48
8.0	453	469	519	50
9.0	455	466	521	55
10.1	451	468	521	53

[a]Reaction conditions are 20 mM NaPPi, pH 6.0, 9.0-10.1 and 20 mM NaPi, pH 7.0-8.0 with spectra measured in a 10 mm quartz cuvette.

Table 6.5. UV-Visible absorption and fluorescence spectra maxima of CHO variant enzyme, H466Q, obtained in deuterated buffer at 15 ºC.[a]

pD	λ_{GS}, nm	λ_{ex}, nm	λ_{em}, nm	Stokes Shift, nm
6.0	453	464	522	58
7.0	453	463	520	57
8.0	454	464	521	57
9.0	453	464	521	57
10.1	453	465	521	56

[a]Reaction conditions are 20 mM NaPPi, pD 6.0, 9.0-10.1 and 20 mM NaPi, pD 7.0-8.0 with spectra measured in a 10 mm quartz cuvette.

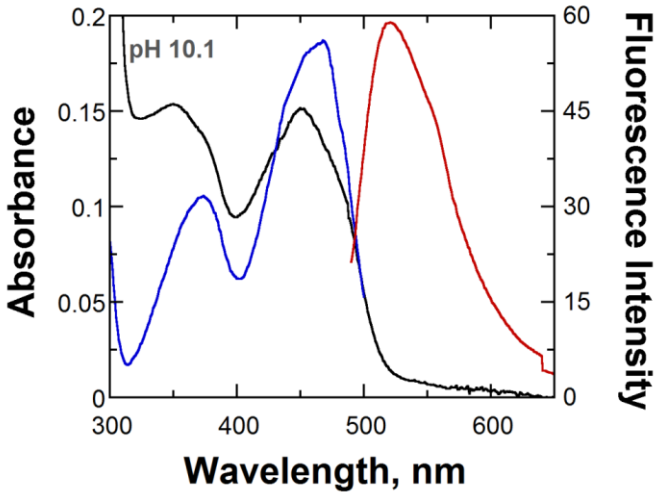

Figure 6.4 Fluorescence and absorption spectroscopy of H466Q variant enzyme in 20 mM sodium pyrophosphate, pH 10.1.
Spectra are for absorbance (black), fluorescence excitation (blue), and fluorescence emission (red) at 15 ºC, in 20 mM sodium pyrophosphate, pH 10.1.

6.3.4 Fluorometry of CHO variant, S101A, in H_2O

The formation of the excited state intermediate detected spectrophotometrically in CHO-wt enzyme at basic pH was consistent with the spectrum of a flavin C4a adduct due to the single peak observed at ~400 nm.[22] The most likely candidates available to form a covalent bond with the C4a atom of the flavin is a serine residue at the 101 position (Figure 6.4), oxygen, or hydroxide ions. The pK_a of the S101 residue is likely lowered in the active site of CHO allowing for the deprotonation of the hydroxyl group at high pH which, in turn, attacks the C4a of the flavin. The role of S101 residue in the formation of the C4a flavin adduct was probed using S101A variant of CHO. The S101A variant was gel-filtered into 20 mM NaPPi, pH 10.0, using a PD-10 column and diluted to a final FAD concentration of 6 µM using the experimentally determined extinction coefficient.[21] The excitation and emission spectra are shown in Figure 6.6. The excited state spectrum was similar to the observed spectrum of CHO-wt at pH 10.1 in that a single peak was observed with maximal fluorescence at 396 nm with the variant also producing a

shoulder at 417 nm. The flavin was excited at 396 nm and fluorescence emission was measured from 475 to 650 nm. Maximum fluorescence emission was observed at 526 nm and, again, excited at 417 nm with emission maximum at 528 nm.

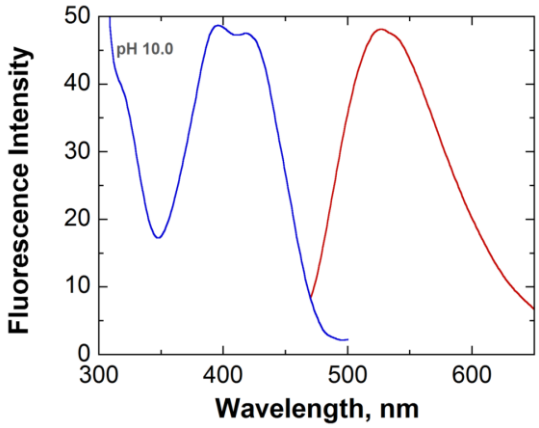

Figure 6.5 Fluorescence and absorption spectroscopy of S101A variant enzyme in 20 mM sodium pyrophosphate, pH 10.0.
Spectra are for fluorescence excitation (blue) and fluorescence emission (red) at 15 ºC, in 20 mM sodium pyrophosphate, pH 10.0.

Fluorescence spectra of the S101A variant were measured in 20 mM NaPPi, pH 6.0, 15 ºC and observed to have similar shape to the wild-type enzyme at pH 6.0 with two peaks detected. The excitation scan revealed two peaks present at acidic pH, unlike a single peak at ~400 nm like observed in the excitation spectrum at pH 10.0 (Figure 6.2). The excitation scan of H466Q variant at pH 6.0 was very similar in shape to CHO-wt at acidic pH in which two peaks and a pronounced shoulder were observed spectrally with the minor peak at 365 nm, major at 461 nm, and a shoulder at 486 nm (Figure 6.7). The flavin was excited at 461 nm and the emission was measured from 480 to 650 nm producing two unresolved peaks. The major

emission peak was observed at 522 nm with a pronounced shoulder at 546 nm. These results are consistent with the absence of ESPT in S101A variant of CHO at pH 6.0.

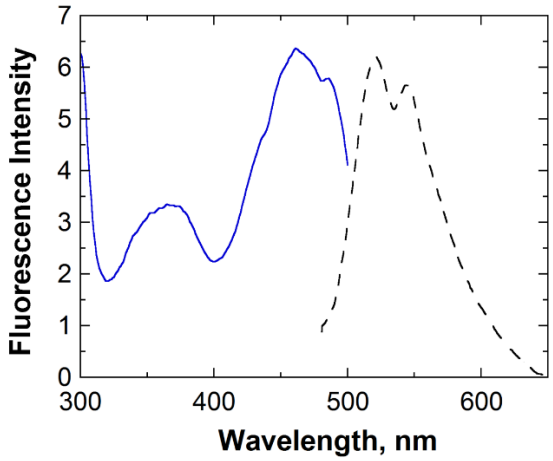

Figure 6.6 Fluorescence and absorption spectroscopy of S101A variant enzyme in 20 mM sodium pyrophosphate, pH 6.0.
Spectra are for fluorescence excitation (blue) and fluorescence emission (black dash) at 15 ºC, in 20 mM sodium pyrophosphate, pH 6.0.

6.3.5 Anaerobic Fluorescence Spectroscopy of S101A Variant

The light-induced flavin species, if not formed with S101, would likely be formed either by a covalent bond with oxygen or hydroxide ions present in the active site. Fluorescence spectra of S101A variant of CHO were measured with oxygen removed from the enzyme-buffer solution using oxygen-free argon flushing and glucose/glucose oxidase oxygen scavenging system. The excitation scan of the S101A variant of CHO shown in Figure 6.8 at pH 10.0 showed a single broad spectrum with a major and minor peak at 395 and 420 nm, respectively. The fluorescence emission yielded a λ_{max} of 529 nm with excitation wavelength set to 395 nm. The maxima spectral peaks in an anaerobic environment were not different from the peaks measured in the presence of oxygen. These results are consistent with the origin of the flavin C4a adduct not originating from either oxygen or the S101 residue in the active site of CHO.

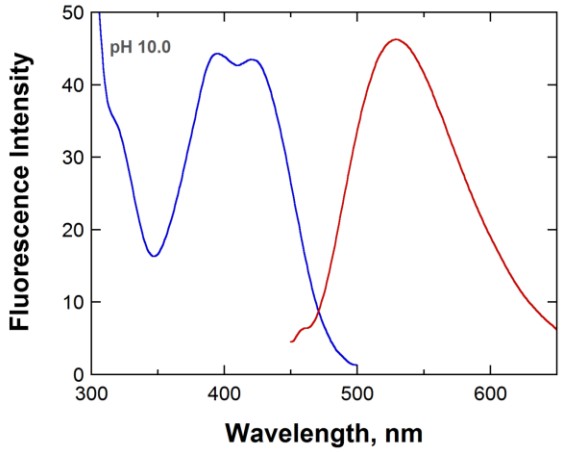

Figure 6.7 Anaerobic fluorescence and absorption spectroscopy of S101A variant enzyme in 20 mM sodium pyrophosphate, pH 10.0.
Spectra are for absorbance (black), fluorescence excitation (blue), and fluorescence emission (red) at 15 ºC, in 20 mM sodium pyrophosphate, pH 10.0.

6.3.6 pH-Dependence on the Fluorometry of Flavin Adenine Dinucleotide (FAD) in H_2O or 1,4-dioxane

The role of the surrounding protein environment provided within the active site of the enzyme that contains the FAD cofactor in ESPT of CHO was probed by measuring fluorescence spectra of FAD in the same conditions as CHO-wt in the presence and absence of imidazole or 1,4-dioxane ± imidazole. The maxima values of the absorbance, excitation, and emission spectra did not differ by more than 2 nm in the pH range from 6.0 to 10.0 (Table 6.5, λ_{em} shown in Figure 6.3, Panel B) with the average maxima of λ_{GS}, λ_{ex}, and λ_{em} as measured in buffer were 450, 454, and 527 nm respectively (Table 6.8). Fluorescence spectra were measured upon the addition of 100 mM and 300 mM imidazole in the buffered flavin solution. Exogenous imidazole was added to the FAD solution to probe the role of H466 in recovering ESPT by adding a proton acceptor to the solution. The maximal absorbance and fluorescence peak values from pH 6.0 to

10.0 are reported in Tables 6.6-6.7 with average values reported in Table 6.8. λ_{max} in buffers containing imidazole did not vary from those observed in the absence of imidazole.

Table 6.5. UV-Visible absorption and fluorescence spectra maxima of FAD obtained at 15 ºC.[a]

pH	λ_{GS}, nm	λ_{ex}, nm	λ_{em}, nm	Stokes Shift, nm
6.0	450	455	526	71
7.0	449	454	526	72
8.0	451	455	527	72
9.0	450	454	528	74
10.0	451	453	527	74

[a]Reaction conditions are 20 mM NaPPi, pH 6.0, 9.0-10.1 and 20 mM NaPi, pH 7.0-8.0 with spectra measured in a 10 mm quartz cuvette.

Table 6.6. UV-Visible absorption and fluorescence spectra maxima of FAD obtained in the presence of 100 mM imidazole at 15 ºC.[a]

pH	λ_{GS}, nm	λ_{ex}, nm	λ_{em}, nm	Stokes Shift, nm
6.0	450	454	527	73
7.0	450	454	526	72
8.0	449	454	528	74
9.0	449	453	527	74
10.0	449	453	526	73

[a]Reaction conditions are 20 mM NaPPi, pH 6.0, 9.0-10.1 and 20 mM NaPi, pH 7.0-8.0 with spectra measured in a 10 mm quartz cuvette.

Table 6.7. UV-Visible absorption and fluorescence spectra maxima of FAD obtained in the presence of 300 mM imidazole at 15 ºC.[a]

pH	λ_{GS}, nm	λ_{ex}, nm	λ_{em}, nm	Stokes Shift, nm
6.0	450	454	527	73
7.0	450	454	526	72
8.0	449	454	528	74
9.0	449	453	527	74
10.0	449	453	526	73

[a]Reaction conditions are 20 mM NaPPi, pH 6.0, 9.0-10.1 and 20 mM NaPi, pH 7.0-8.0 with spectra measured in a 10 mm quartz cuvette.

Table 6.8 λ_{max} values of free FAD in varying solvents ± varying amounts of imidazole; concentrations listed in the table represent imidazole in the buffered solution or 1,4-dioxane solvent. Spectra maxima did not differ by more than 2 nm and therefore only the average values were presented. Buffers used were 20 mM NaPPi, pH 6.0, 8.0-10.0, or 20 mM NaPi, 7.0 plus imidazole at the concentration listed. Buffer was replaced as the solvent with 1,4-dioxane ± imidazole.

	0 mM	100 mM	300 mM	1,4-dioxane	1,4-dioxane + 10 mM imidazole
λ_{GS}, nm	450	449	449	471	-
λ_{ex}, nm	454	454	452	472	470
λ_{em}, nm	527	527	525	548	546
Stokes shift, nm	73	73	73	76	76

Fluorescence measurements were repeated with 1,4-dioxane as solvent to observe changes, if any, due to an increase in the hydrophobicity of the surrounding flavin environment in comparison to the active site of the protein. The absorbance spectrum of the cofactor was quenched in the 1,4-dioxane solution as evidence by the presence of two peaks at 274 and 471 nm in the UV-visible spectrum, not different from the observed maximal peak of the λ_{ex}; values reported in Table 6.5. No changes in the λ_{GS}, λ_{ex}, λ_{em}, and Stokes shift values were observed with or without the addition of exogenous imidazole. These data were consistent with free FAD not catalyzing ESPT in buffers ranging in pH from 6.0 to 10.0 and in 1,4-dioxane establishing the importance of a protein construct for modulating flavin reactivity in catalyzing ESPT from the N(3) to the N(5) atoms of the flavin.

6.4 Discussion

In this study evidence has been presented in support of the observation of an ESPT in CHO from the N(3) atom of the oxidized flavin cofactor onto the N(5) atom of the flavin via an active site base. The hydrogen bond at the N(3) atom of the isoalloxazine is delocalized due to a decrease in pK_a in the excited state and transferred onto the N(5) atom of the flavin (Scheme 1, Step B).[45, 57, 59] Based on previously published computational studies on the excitation of π orbitals in lumiflavin, protonation is favored at the N(5) atom of the isoalloxazine ring due to electron density accumulating at N(5) atom in both the singlet and triplet states.[57] The pK_a of

N(3) atom in the excited state was calculated to be lowered from ~10 to ~7 in flavin analogs studied[29, 63-65] as attributed to a lack of conjugation between the π-electron system and its p orbitals in the alloxazine structure.[58, 59, 66] The pL-dependence observed on the fluorescence emission of CHO wild-type enzyme revealed a change in ionization consistent with a proton transfer in the excited state of the enzyme. The pL profile of fluorescence emission plateaus at low and high pL values with a single inflection point. Although not defined, the two limbs observed in the pL profile for emission at basic and acid pH values are indicative of two different flavin species stabilized prior to the flavin fluorescing. As pL increased, the equilibrium shifted towards ESPT event as evidence of a large red shift in emission λ_{max}.[67, 68] Thus an increase in pL likely shifted the equilibrium between the ionized (species formed after Step B in Scheme 6.1) and un-ionized (species formed after Step A in Scheme 6.1) species formed prior to fluorescence emission.[67, 68]

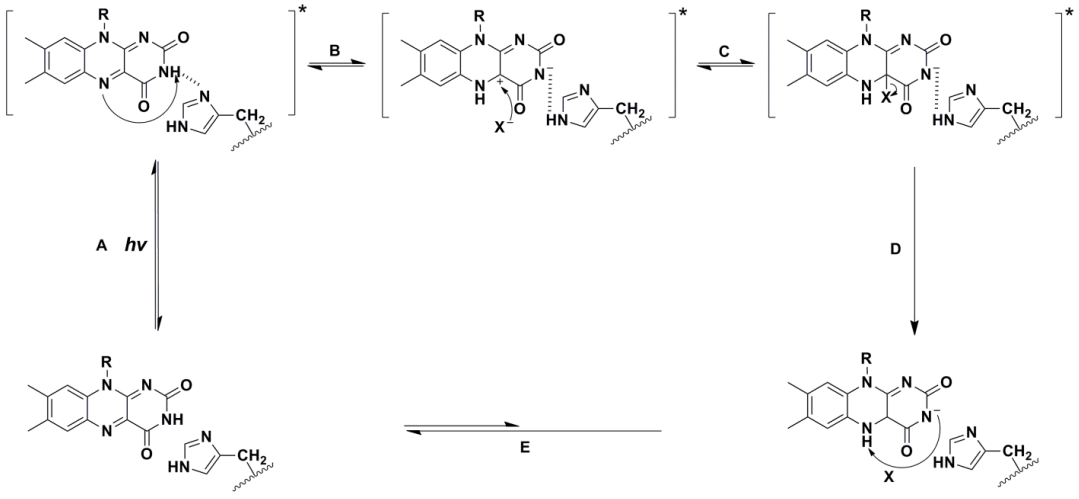

Scheme 6.1 Schematic representation of excited state reaction in CHO-wt.
The oxidized flavin cofactor of CHO was excited to the singlet state by photons using light (A). At basic pH, the active site histidine facilitated a proton abstraction of the proton from the N(3) atom of the flavin to the N(5) atom yielding a charged, oxidized flavin *(B)*. The positive charge likely developed at the C4a position becomes a highly reactive electrophile forming a covalent bond with a nearby nucleophile, X *(C)*. Fluorescence emission returned the charged, oxidized flavin to the ground state. The charged flavin is not a stable species because the pK_a values of the N(5) and N(3) atoms returned to ground state values [61] *(D)* and the proton on the N(5) atom was transferred back to the N(3) via H466 *(E)*. At acidic pH, the active site histidine was protonated and unable to accept a proton from the N(3) atom leading to the reversible *(A)* step.

H466 is essential for ESPT in CHO for transferring a proton from the N(3) atom to the N(5) atom of the flavin in the excited state as evidence from the fluorescence data with H466Q variant enzyme. Previous studies carried out on a glutamine variant have shown that H466 is the catalytic base that activates the alcohol substrate for catalysis through the abstraction of a hydroxyl proton.[11] The H466 residue was the likely candidate that abstracts the proton on the N(3) atom of the flavin and then transfer the proton to the N(5) atom. Fluorescence experiments with H466Q variant yielded pH-independent emission spectra consistent with an absence of proton transfers in the excited state. Previous fluorescence studies of lumichrome revealed a secondary molecule important in facilitating ESPT from the N(1) to the N(10) atoms (lumichrome nomenclature) via pyridine or acetic acid molecules.[44] As the concentration of pyridine increased, the equilibrium of the dominant flavin species shifted from lumichrome to 7,8-dimethylisoalloxazine as monitored by a red-shift in the λ_{max} of fluorescence emission.[44] In the case of CHO-wt, a pK_a of ~8.0 was observed in the λ_{em} pH profile (Figure 6.3, Panel A). If the pK_a is assigned to the active site base, approximately 99.9 % of the base would be deprotonated at pH 10.1, consistent with an active site base in a deprotonated ionization state capable of accepting and transferring a proton. At pH 6.0, the base is approximately 99.9 % protonated and incapable of accepting and transferring a proton. Hence the active site base, H466, is needed to facilitate a proton transfer in the excited state of CHO-wt.

A C4a flavin adduct was formed in the active site of CHO in its excited state and spectroscopically-detected as evidence by the formation of a single excitation peak at ~400 nm. The electrons on the N(5) atom of the flavin acquire the proton from the N(3) atom via H466 during ESPT thus creating a positive charge on the C4a atom (Scheme 6.1). This yields an

ionized but neutral flavin (Scheme 6.1). The carbocation produced on the C4a atom of the flavin after ESPT is a highly reactive electrophile readily forming a covalent adduct with hydroxide ions in the active site of CHO. The current study revealed the formation of a C4a flavin adduct did not originate with oxygen or an active site serine residue but likely hydroxide ions consistent with the presence of the a single excitation peak at ~400 nm in the absence of oxygen and in the S101A variant of CHO (Figures 6.6-6.8). The likely candidate for a negatively charged group reacting with the C4a atom of the flavin was hydroxide ions present in the active site. As pH increased, the effective concentration of hydroxide ions increased prompting the formation of covalent bonds with the C4a atom of the flavin in the excited state yielding a C4a-hydroxy adduct.[69, 70] Flavin-dependent photoreceptors that catalyze biological reactions in the excited state have shown to form a covalent bond with the C4a atom of the flavin with an active site cysteine residue.[22, 24] Evidence for the flavin C4a-cysteinyl adduct formed between the two charged species, flavin C4a adduct and cysteine thiol group, were shown by spectral changes of the flavin and the formation of a single spectral peak at ~400 nm. In the absence of light, LOV domains have two characteristic flavin peaks at 375 and 447 nm which become shifted to form a single peak with λ_{max} of approximately 400 nm once activated by light.[24, 38]

The imidazole moiety and protein scaffold are essential in providing an environment conducive to ESPT in CHO. The pH-dependence on the fluorescence emission observed in the wild-type enzyme is no longer present in the H466Q variant and free FAD in solution consistent with a disruption in ESPT in the two latter cases. Addition of imidazole was proposed to mimic H466 as a catalytic base and restoring ESPT with the free FAD alone. However, fluorescence emission of FAD in the presence of a histidine analog did not restore ESPT as indicative by a pH-independent emission spectra in the presence and absence of imidazole. Fluorescence

experiments conducted on FAD in 1,4-dioxane revealed an influence of solvent polarity on the fluorescence spectra. Thus, the lack of ESPT with free FAD in the pH range tested was consistent with the flavin cofactor being in close proximity to the proton acceptor, H466, and constrained within the protein active site.[68] In the lumichrome fluorescence studies and the current study, hydrogen-bonding interactions must be established in the ground state between the proton donor and acceptor, or flavin and H466/imidazole, prior to a proton transfer occurring in the excited state.[66] Evidence for the hydrogen-bonding interaction comes from previously published spectral data conducted by Smitherman *et al.*[11] and this study (Figure 6.2, Figure 6.5). Hydrogen-bonding interactions in the ground state were clearly disrupted when the histidine residue was mutated to a glutamine as observed in the near UV to visible absorbance region between 300-400 nm (Figure 6.5). Evidence for disruption in hydrogen-bonding interactions comes from the red shift in the excited state of H466Q from 450 nm to 469 nm. Hydrogen-bonding interactions were also disrupted between the flavin and imidazole in 1,4-dioxane and the hydrophobicity of the flavin environment was altered. The red shift of the major peak observed in the excited state of FAD in 1,4-dioxane was indicative to an increase in hydrophobicity but not an ESPT.[71]

In conclusion, ESPT were observed in CHO, a flavoprotein oxidase not classified as a photoreceptor, along with the formation of a C4a flavin adduct detected in the excited state. The flavin cofactor bound to CHO and H466 residue are both essential in excited state reactions occurring in CHO. The flavin cofactor and nearby histidine were optimally positioned for both species to participate in acid-base catalysis in the excited state of the enzyme as evidence of the experiments conducted with free FAD in the presence of exogenous imidazole. The results presented in this study were consistent with three conditions required for ESPT to occur in a

flavin-dependent enzyme. This event was driven by the ability of a photolabile, flavin species to acquire the energy from photons (1) while being buried within the constructs of a protein active site (2). Finally, the proton acceptor must be a histidine residue positioned near the N(3) and N(5) atoms of the flavin (3). Further investigations using fluorescence spectroscopy will be carried out in order to identify this phenomenon in other flavin-dependent enzymes.

6.5 Acknowledgement

This study was supported in part by Grants MCB-1121695 (G.G.) and CHE 1506518 (G.G.) from the NSF and a University Fellowship from the Center for Diagnostics and Therapeutics at Georgia State University (C.S.). The authors wish to thank Dan Su for and preparation of the anaerobic samples and thoughtful discussions.

6.6 References

1. Miura, R. (2001) Versatility and specificity in flavoenzymes: control mechanisms of flavin reactivity, *Chem. Rec. 1*, 183-194.
2. Jung, M. Y., Kim, S. K., and Kim, S. Y. (1995) Riboflavin-sensitized photooxidation of ascorbic acid: kinetics and amino acid effects., *Food Chem. 53*, 397-403.
3. Halliwell, B. (1996) Antioxidants in human health and disease, *Annu. Rev. Nutr. 16*, 33-50.
4. Chen, L., Hu, J. Y., and Wang, S. Q. (2012) The role of antioxidants in photoprotection: a critical review, *J. Am. Acad. Dermatol. 67*, 1013-1024.
5. Rivlan, R. S., and Pinto, J. T. (2001) In *Handbook of Vitamins* (Rucker, R. B., Suttie, J. W., and McCormick, D. B., Eds.) Third ed., CRC Press.
6. Tayler, M. B., and Radda, G. K. (1971) Flavins as photosensitizers, *Methods Enzymol. 18*, 496-506.

7. Yagi, K., Ohishi, N., Nishimoto, K., Choi, J. D., and Song, P. S. (1980) Effect of hydrogen bonding on electronic spectra and reactivity of flavins, *Biochemistry 19*, 1553-1557.

8. Kotaki, A., and Yagi, K. (1970) Fluorescence properties of flavins in various solvents, *J. Biochem. 68*, 509-516.

9. Edmondson, D. E., and Tollin, G. (1971) Circular dichroism studies of the flavin chromophore and of the relation between redox properties and flavin environment in oxidases and dehydrogenases, *Biochemistry 10*, 113-124.

10. Mewies, M., Packman, L. C., Mathews, F. S., and Scrutton, N. S. (1996) Flavinylation in wild-type trimethylamine dehydrogenase and differentially charged mutant enzymes: a study of the protein environment around the N1 of the flavin isoalloxazine, *Biochem. J. 317 (Pt 1)*, 267-272.

11. Smitherman, C., Rungsrisuriyachai, K., Germann, M. W., and Gadda, G. (2015) Identification of the catalytic base for alcohol activation in choline oxidase, *Biochemistry 54*, 413-421.

12. Weber, G., and Farris, F. J. (1979) Synthesis and spectral properties of a hydrophobic fluorescent probe: 6-propionyl-2-(dimethylamino)naphthalene, *Biochemistry 18*, 3075-3078.

13. Smitherman, C., and Gadda, G. (2013) Evidence for a transient peroxynitro acid in the reaction catalyzed by nitronate monooxygenase with propionate 3-nitronate, *Biochemistry 52*, 2694-2704.

14. Fan, F., and Gadda, G. (2005) On the catalytic mechanism of choline oxidase, *J. Amer. Chem. Soc. 127*, 2067-2074.

15. Gadda, G., and Fitzpatrick, P. F. (1998) Biochemical and physical characterization of the active FAD-containing form of nitroalkane oxidase from Fusarium oxysporum, *Biochemistry 37*, 6154-6164.

16. Romero, E., and Gadda, G. (2014) Alcohol oxidation by flavoenzymes, *Biomol. Concepts 5*, 299-318.

17. Ghanem, M., and Gadda, G. (2006) Effects of reversing the protein positive charge in the proximity of the flavin N(1) locus of choline oxidase, *Biochemistry 45*, 3437-3447.

18. Finnegan, S., Yuan, H., Wang, Y. F., Orville, A. M., Weber, I. T., and Gadda, G. (2010) Structural and kinetic studies on the Ser101Ala variant of choline oxidase: catalysis by compromise, *Arch. Biochem Biophys. 501*, 207-213.

19. Ghanem, M., and Gadda, G. (2005) On the catalytic role of the conserved active site residue His466 of choline oxidase, *Biochemistry 44*, 893-904.

20. Quaye, O., Cowins, S., and Gadda, G. (2009) Contribution of flavin covalent linkage with histidine 99 to the reaction catalyzed by choline oxidase, *J. Biol. Chem. 284*, 16990-16997.

21. Yuan, H., and Gadda, G. (2011) Importance of a serine proximal to the C(4a) and N(5) flavin atoms for hydride transfer in choline oxidase, *Biochemistry 50*, 770-779.

22. Losi, A., and Gartner, W. (2012) The evolution of flavin-binding photoreceptors: an ancient chromophore serving trendy blue-light sensors, *Annu. Rev. Plant Biol. 63*, 49-72.

23. Zoltowski, B. D., and Gardner, K. H. (2011) Tripping the light fantastic: blue-light photoreceptors as examples of environmentally modulated protein-protein interactions, *Biochemistry 50*, 4-16.

24. Zoltowski, B. D., Nash, A. I., and Gardner, K. H. (2011) Variations in protein-flavin hydrogen bonding in a light, oxygen, voltage domain produce non-Arrhenius kinetics of adduct decay, *Biochemistry 50*, 8771-8779.

25. Petersen, F. N. R., and Bohr, H. G. (2010) The mechanisms of excited states in enzymes, *Theor. Chem. Acc. 125*, 345-352.

26. Fankhauser, C., and Christie, J. M. (2015) Plant phototropic growth, *Curr. Biology 25*, R384-R389.

27. Wang, J., Du, X. L., Pan, W. S., Wang, X. J., and Wu, W. J. (2015) Photoactivation of the cryptochrome/photolyase superfamily, *J. Photoch. Photobio. C 22*, 84-102.

28. Kutta, R. J., Magerl, K., Kensy, U., and Dick, B. (2015) A search for radical intermediates in the photocycle of LOV domains, *Photochem. Photobiol. Sci. 14*, 288-299.

29. Li, G., and Glusac, K. D. (2008) Light-triggered proton and electron transfer in flavin cofactors, *J Phys. Chem. A 112*, 4573-4583.

30. Krauss, U., Lee, J., Benkovic, S. J., and Jaeger, K. E. (2010) LOVely enzymes - towards engineering light-controllable biocatalysts, *Microb. Biotechnol. 3*, 15-23.

31. Zeugner, A., Byrdin, M., Bouly, J. P., Bakrim, N., Giovani, B., Brettel, K., and Ahmad, M. (2005) Light-induced electron transfer in *Arabidopsis* cryptochrome-1 correlates with *in vivo* function, *J. Biol. Chem. 280*, 19437-19440.

32. Liang, B., Guo, X., Fang, L., Hu, Y., Yang, G., Zhu, Q., Wei, J., and Ye, X. (2015) Study of direct electron transfer and enzyme activity of glucose oxidase on graphene surface, *Electrochem. Comm. 50*, 1-5.

33. Hockberger, P. E., Skimina, T. A., Centonze, V. E., Lavin, C., Chu, S., Dadras, S., Reddy, J. K., and White, J. G. (1999) Activation of flavin-containing oxidases underlies light-induced production of H_2O_2 in mammalian cells, *Proc. Natl. Acad. Sci. USA 96*, 6255-6260.

34. Kennis, J. T., and Groot, M. L. (2007) Ultrafast spectroscopy of biological photoreceptors, *Curr. Opin. Struct. Biol. 17*, 623-630.

35. Alexandre, M. T., Domratcheva, T., Bonetti, C., van Wilderen, L. J., van Grondelle, R., Groot, M. L., Hellingwerf, K. J., and Kennis, J. T. (2009) Primary reactions of the LOV2 domain of phototropin studied with ultrafast mid-infrared spectroscopy and quantum chemistry, *Biophys. J. 97*, 227-237.

36. Pfeifer, A., Majerus, T., Zikihara, K., Matsuoka, D., Tokutomi, S., Heberle, J., and Kottke, T. (2009) Time-resolved Fourier transform infrared study on photoadduct formation and secondary structural changes within the phototropin LOV domain, *Biophys. J. 96*, 1462-1470.

37. Lanzl, K., Sanden-Flohe, M. V., Kutta, R. J., and Dick, B. (2010) Photoreaction of mutated LOV photoreceptor domains from *Chlamydomonas reinhardtii* with aliphatic mercaptans: implications for the mechanism of wild type LOV, *Phys. Chem. Chem. Phys. 12*, 6594-6604.

38. Conrad, K. S., Manahan, C. C., and Crane, B. R. (2014) Photochemistry of flavoprotein light sensors, *Nat. Chem. Biol. 10*, 801-809.

39. Lewis, A. (1978) The molecular mechanism of excitation in visual transduction and bacteriorhodopsin, *Proc. Natl. Acad. Sci. USA 75*, 549-553.

40. Quick, M., Weigel, A., and Ernsting, N. P. (2013) Fluorescence following excited-state protonation of riboflavin at N(5), *J. Phys. Chem. B 117*, 5441-5447.

41. Lasser, N., and Feitelson, J. (1975) Excited-state reactions of oxidized flavin derivatives, *Photochem. Photobiol. 21*, 249-254.

42. Lasser, N., and Feitelson, J. (1977) Protonation and deprotonation equilibria of lumichrome., *Photochem. Photobiol. 25*, 451-456.

43. Sichula, V., Kucheryavy, P., Khatmullin, R., Hu, Y., Mirzakulova, E., Vyas, S., Manzer, S. F., Hadad, C. M., and Glusac, K. D. (2010) Electronic properties of N(5)-ethyl flavinium ion, *J. Phys. Chem. A 114*, 12138-12147.

44. Song, P. S., Sun, M., Koziolow, A., and Koziol, J. (1974) Phototautomerism of lumichromes and alloxazines, *J. Am. Chem. Soc. 96*, 4319-4323.

45. Koziol, J., and Koziolowa, A. (1977) Studies on physicochemical properties of alloxazines, In *International Meeting on Flavins and Flavoproteins* (Ostrowski, W., Ed.), pp 81-107.

46. Salvi, F., Wang, Y. F., Weber, I. T., and Gadda, G. (2014) Structure of choline oxidase in complex with the reaction product glycine betaine, *Acta Crystallogr. Sect. D: Biol. Crystallogr. 70*, 405-413.

47. Gannavaram, S., and Gadda, G. (2013) Relative timing of hydrogen and proton transfers in the reaction of flavin oxidation catalyzed by choline oxidase, *Biochemistry 52*, 1221-1226.

48. Finnegan, S., Agniswamy, J., Weber, I. T., and Gadda, G. (2010) Role of valine 464 in the flavin oxidation reaction catalyzed by choline oxidase, *Biochemistry 49*, 2952-2961.

49. Rungsrisuriyachai, K., and Gadda, G. (2010) Role of asparagine 510 in the relative timing of substrate bond cleavages in the reaction catalyzed by choline oxidase, *Biochemistry 49*, 2483-2490.

50. Rungsrisuriyachai, K., and Gadda, G. (2008) On the role of histidine 351 in the reaction of alcohol oxidation catalyzed by choline oxidase, *Biochemistry 47*, 6762-6769.

51. Quaye, O., Lountos, G. T., Fan, F., Orville, A. M., and Gadda, G. (2008) Role of Glu312 in binding and positioning of the substrate for the hydride transfer reaction in choline oxidase, *Biochemistry 47*, 243-256.

52. Pennati, A., and Gadda, G. (2009) Involvement of ionizable groups in catalysis of human liver glycolate oxidase, *J. Biol. Chem. 284*, 31214-31222.

53. Ghanem, M., Fan, F., Francis, K., and Gadda, G. (2003) Spectroscopic and kinetic properties of recombinant choline oxidase from *Arthrobacter globiformis*, *Biochemistry 42*, 15179-15188.

54. Salomaa, P., Schaleger, L. L., and Long, F. A. (1964) Solvent deuterium isotope effects on acid-base equilibria, *J. Am. Chem. Soc. 86*.

55. Schowen, K. B., and Schowen, R. L. (1982) Solvent isotope effects of enzyme systems, *Methods Enzymol. 87*, 551-606.

56. Kirincic, S., and Klofutar, C. (1999) Viscosity of acueous solutions of poly(ethylene glycol)s at 298.15K., *Fluid Phase Equilib. 115*, 311-325.

57. Salzmann, S., and Marian, C. M. (2008) Effects of protonation and deprotonation on the excitation energies of lumiflavin, *Chem. Phys. Lett. 463*, 400-404.

58. Koziolowa, A. (1978) Tautomerism and ionization of excited alloxazines in aqueous solutions of inorganic acids and their salts, *Zeszyty Naukowe - Akademia Ekonomiczna w Poznaniu, Seria 1: Prace z Zakresu Towaroznawstwa i Chemii 80*, 104-109.

59. Koziolowa, A. (1979) Solvent and methyl substituent effect on phototautomerism and ionization of alloxazines, *Photochem. Photobiol. 29*, 459-471.

60. Bunton, C. A. (1961) Isotope effects in deuterium oxide solution. I. Acid-base equilibria, *J. Amer. Chem. Soc. 83*, 42-47.

61. Song, P. S., Sun, M., Koziolow, A., and Koziol, J. (1973) Phototautomerism of lumichromes and alloxazines, *J. Amer. Chem. Soc. 96*, 4319-4323.

62. Stryer, L. (1966) Excited-state proton-transfer reactions. A deuterium isotope effect on fluorescence, *J. Amer. Chem. Soc. 88*, 5708-5712.

63. Tyagi, A., and Penzkofer, A. (2010) pH-dependence of the absorption and emission behaviour of lumiflavin in aqueous solution, *J. Photochem. Photobio. A: Chemistry 215*, 108-117.

64. Drossler, P., Holzer, W., Penzkofer, A., and Hegemann, P. (2002) pH-dependence of the absorption and emission behaviour of riboflavin in aqueous solution, *Chem. Phys.282*, 429-439.

65. Schulman, S. G. (1971) pH-dependence of fluorescence of riboflavin and related isoalloxazine derivatives, *J. Pharm. Sci. 60*, 628-631.

66. Sikorska, E., Szymusiak, H., Khemelinskii, I. V., Koziolow, A., Spanget-Larsen, J., and Sikorska, M. (2003) Spectroscopy and photophysics of alloxazines studied in their ground and first excited singlet states, *J. Photochem. Photobio. A: Chemistry 158*, 45-53.

67. Tolbert, L. M., and Solntsev, K. M. (2002) Excited-state proton transfer: From constrained systems to "super" photoacids to superfast proton transfer., *Acc. Chem. Res. 35*, 19-27.

68. Kurtin, W. E., Latino, M. A., and Song, P. S. (1967) A study of photochemistry of flavins in pyridine and with a donor, *Photochem. Photobiol. 6*, 247-259.

69. Jencks, W. P. (1969) *Catalysis in Chemistry and Enzymology*, Dover Publications, Inc., New York.

70. Richard, J. P. (1998) The enhancement of enzymatic rate accelerations by Bronsted acid-base catalysis, *Biochemistry 37*, 4305-4309.

71. Koziol, J. (1969) Studies on flavins in organic solvents. 3. Spectral behaviour of lumiflavin, *Photochem. Photobiol. 9*, 45-53.

6.7 Appendix

Fluorescence spectroscopy experiments on additional flavin-dependent enzymes were carried out as a function of pL using the same protocol found in the text. The enzymes in the study include an additional CHO variant, H99N, glucose oxidase, glycolate oxidase, D-arginine dehydrogenase (DADH), H48F variant of DADH, and nitronate monooxygenase from *Cyberlindnera saturnus*.

Table 6.6 UV-Visible absorption and fluorescence spectra maxima values of CHO variant enzyme, H99N, obtained at 15 °C.

pH	λ_{GS}, nm	λ_{ex}, nm	λ_{em}, nm	Stokes Shift, nm
5.5	449	454	525	71
6.0	451	452	522	70
7.0	451	453	524	71
8.0	451	453	524	71
9.0	449	453	524	71
10.0	447	454	528	74
10.5	450	454	527	73

[a]Reaction conditions are 20 mM NaPPi, pH 5.5-6.0, 9.0-10.5 and 20 mM NaPi, pH 7.0-8.0 with spectra measured in a 10 mm quartz cuvette.

Table 6.7 UV-Visible absorption and fluorescence spectra maxima values of GO obtained at 15 °C.

pH	λ_{GS}, nm	λ_{ex}, nm	λ_{em}, nm	Stokes Shift, nm
4.0	452	465	529	64
5.5	452	466	527	61
6.0	452	465	528	63
6.5	452	464	533	69
7.0	451	465	533	68
8.0	455	456	536	80
9.0	453	456	536	80

[a]Reaction conditions are 20 mM NaPPi, pH 4.0-6.5, 9.0 and 20 mM NaPi, pH 7.0-8.0 with spectra measured in a 10 mm quartz cuvette.

Table 6.8 UV-Visible absorption and fluorescence spectra maxima values of glucose oxidase, GO, obtained at 15 ºC in deuterated buffer.

pD	λ_{GS}, nm	λ_{ex}, nm	λ_{em}, nm	Stokes Shift, nm
5.0	451	455	517	62
6.0	454	452	521	69
7.0	454	451	527	76
7.5	453	445	524	79
8.0	455	451	527	76
9.0	453	445	529	84

[a]**Reaction conditions are 20 mM NaPPi, pH 5.0-6.0, 9.0 and 20 mM NaPi, pH 7.0-8.0 with spectra measured in a 10 mm quartz cuvette.**

Table 6.9 UV-Visible absorption and fluorescence spectra maxima values of glycolate oxidase, GOX, obtained at 15 ºC.

pH	λ_{GS}, nm	λ_{ex}, nm	λ_{em}, nm	Stokes Shift, nm
5.0	451	454	526	72
9.5	451	455	539	84

[a]**Reaction conditions are 20 mM NaPPi, pH 5.0 and 9.5-10.1 with spectra measured in a 10 mm quartz cuvette.**

Table 6.10 UV-Visible absorption and fluorescence spectra maxima values of D-arginine dehydrogenase, DADH, obtained at 15 ºC.

pH	λ_{GS}, nm	λ_{ex}, nm	λ_{em}, nm	Stokes Shift, nm
6.0	447	452	513	61
7.0	448	453	510	57
8.0	446	451	508	57
8.5	446	452	508	56
9.0	447	452	511	59
10.1	447	452	511	59

[a]**Reaction conditions are 20 mM NaPPi, pH 6.0, 8.5-10.1 and 20 mM NaPi, pH 7.0-8.0 with spectra measured in a 10 mm quartz cuvette.**

Table 6.11 UV-Visible absorption and fluorescence spectra maxima values of D-arginine dehydrogenase, DADH, obtained at 15 ºC in deuterated buffers.

pD	λ_{GS}, nm	λ_{ex}, nm	λ_{em}, nm	Stokes Shift, nm
6.0	447	454	513	59
7.0	446	454	511	57
8.0	446	454	511	59
9.0	446	454	510	58
10.0	447	452	511	59

[a]Reaction conditions are 20 mM NaPPi, pH 6.0, 9.0-10.0 and 20 mM NaPi, pH 7.0-8.0 with spectra measured in a 10 mm quartz cuvette.

Table 6.12 UV-Visible absorption and fluorescence spectra maxima values of D-arginine dehydrogenase, DADH, variant, H48F, obtained at 15 ºC.

pH	λ_{GS}, nm	λ_{ex}, nm	λ_{em}, nm	Stokes Shift, nm
6.0	445	453	512	59
7.0	445	452	511	59
8.0	446	453	511	58
9.0	447	452	512	60
10.0	447	454	515	61

[a]Reaction conditions are 20 mM NaPPi, pH 6.0, 9.0-10.0 and 20 mM NaPi, pH 7.0-8.0 with spectra measured in a 10 mm quartz cuvette.

Table 6.13 UV-Visible absorption and fluorescence spectra maxima values of nitronate monooxygenase from *Cyberlindnera saturnus*, CsNMO, obtained at 15 ºC.

pH	λ_{GS}, nm	λ_{ex}, nm	λ_{em}, nm	Stokes Shift, nm
6.0	446	454	517	63
7.0	446	458	517	59
8.0	446	457	518	61
9.0	445	457	518	61
10.0	446	458	517	60

[a]Reaction conditions are 20 mM NaPPi, pH 6.0, 9.0-10.0 and 20 mM NaPi, pH 7.0-8.0 with spectra measured in a 10 mm quartz cuvette.

7 General Discussion and Conclusions

This dissertation is focused on the biochemical and structural investigations of nitronate monooxygenases (NMO) and the roles of histidine residues in select flavoprotein oxidases. Mechanistic investigations of NMO have been carried out using pH, X-ray crystallography, rapid and steady-state kinetics, and UV-visible and time-resolved absorbance spectroscopy.[1-3] These studies have allowed the mechanism for the oxidation of propionate 3-nitronate (P3N) by NMO to be proposed and further studied. Through choline oxidase (CHO) and its variants, histidine residues have been observed to hold multiple roles in enzyme turnover. The various roles of this amino acid have been investigated using site-directed mutagenesis, steady-state kinetics, pH and kinetic isotope effects, UV-visible absorbance, fluorescence, and circular dichroic spectroscopy, X-ray crystallography, and NMR.[4-9] In addition, fluorescence spectroscopic studies were carried out on other select flavin-dependent enzymes, choline oxidase (CHO) and variants of CHO, in order to observe the influence of an active site histidine in the excited state. The findings from this dissertation provide insight on advances in the flavin field mechanistically and spectroscopically.

NMO catalyzes the oxidation of P3N to products through a single electron transfer mechanism.[(2)] Formation of the Michaelis complex triggers a single electron transfer from the P3N substrate to the flavin cofactor forming the anionic flavosemiquinone.[2] Once oxygen enters the system, two paths of reoxidation of the anionic flavosemiquinone have been proposed depending upon what species oxygen reacts with first.[10] Oxygen in the triplet state can reoxidize the flavin first forming superoxide.[2, 11, 12] Radical coupling between the superoxide and P3N radicals can produce the peroxy-nitro acid intermediate. Alternatively, oxygen could react with the P3N radical forming a superoxy-nitro acid. The anionic flavosemiquinone would be

reoxidized by donating the electron to the radical superoxy-nitro acid species forming the peroxy-nitro acid intermediate. Heavy isotope labeling and rapid quench analyses to trap these radical and peroxy intermediates would shed light on the oxygen reactivity path utilized by NMO to reoxidize the anionic flavosemiquinone.

The crystal structure of the first eukaryotic NMO from *Cyberlindnera saturnus* (CsNMO) has been resolved to 1.65 Å. Solving the three-dimensional structure of CsNMO will allow for future site-directed mutagenesis of amino acid residues to elucidate their structural and kinetic roles during enzymatic turnover.[(3)] Resolving the structure revealed an allosteric binding site for a mixed activator, PEG. A random coil/loop was on the surface of CsNMO was identified in the newly resolved crystal structure occupied by a bound PEG molecule, a first for NMO enzymes. The study in Chapter III identified a pocket on the surface of the enzyme created by a surface loop held in position by lysine residue-derived salt bridge creating a binding site for a PEG molecule. Steady-state kinetics revealed PEG 3350 was a mixed activator of CsNMO with respect to P3N. Steady-state kinetics were measured with a second NMO enzyme, NMO from *Pseudomonas aeruginosa* (PaNMO), with P3N as substrate and yielded no effects on the kinetics in the presence of PEG 3350 in the reaction mixture. The discovery of a mixed activator of CsNMO may have implications on enzyme regulation in the cell. The source of the enzyme, *Cyberlindnera saturnus*, has been shown to produce polyols similar to ethylene glycol monomers of PEG to alter osmotic pressure within the cell.[13] The presence of PEG bound to the surface loop on the CsNMO enzyme, albeit unknown to be a natural compound, may shed light on the physiological mechanism of the enzyme and future drug design or regulatory models.

With a newly resolved crystal structure, residues in the active site of CsNMO have been proposed: A24, N77, F79, H147, Y321, Y325, and L348. Residues surrounding the isoalloxazine

ring of the flavin specifically include M23 A24, N77, H147, H276, and L348. Amino acid residues located near the xylene moiety of flavin isoalloxazine rings are typically hydrophobic in flavin-dependent enzymes.[10, 14, 15] The hydrophobic C7 and C8 atoms are prone to being stabilized when surrounded by a hydrophobic environment (i.e. leucine, tryptophan, valine, phenylalanine amino acids).[10] In structurally-resolved NMOs, a histidine-leucine pair (CsNMO) or tyrosine-tryptophan pair (PaNMO) were found in proximity to the C7 and C8 methyl groups of the flavin (Figure 7.1). The presence of leucine and histidine residues in CsNMO in lieu of a tryptophan and tyrosine in PaNMO may lead to larger differences in the mechanisms between these enzymes. Both members of the same class of enzymes, Y254 and W325 in PaNMO were fully conserved in all of the Class I NMO enzymes except CsNMO. Tyrosine residues located near the xylene moiety of the flavin cofactor have been shown to modulate flavin reactivity in numerous enzymes.[16-19] Blue light receptors using FAD (BLUF) and photosystem II are two examples of proteins that contain tyrosine residues near the C7-C8 atoms of the flavin cofactors.[17, 20, 21] These proteins catalyze single electron transfers in the excited state.[17, 20-22] Mutations of the tyrosine residue to phenylalanine, tryptophan and fluorinated tyrosine uncovered the importance of the amino acid in photoactivation of the flavin and the lifetime of the flavin excited state.[17, 23, 24] The replacement of a tyrosine residue in the fungal CsNMO enzyme with a histidine residue may shed light on how the flavin redox is modulated in CsNMO and how the histidine residue might vary biological output, function, or product formation in comparison to the other NMO enzymes found in this class of enzymes.[17]

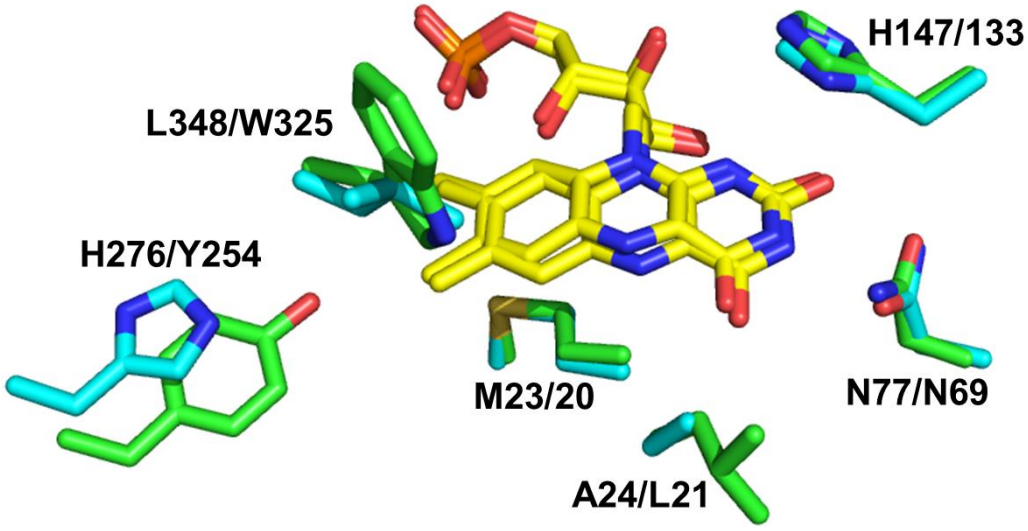

Figure 7.1. Active site residues of CsNMO (cyan, listed first) and PaNMO (green, listed second). FMN cofactors both shown in yellow. Taken from Chapter 3 of this dissertation.

Another histidine residue that has been shown to modulate flavin redox potential is H466 in choline oxidase from *Arthrobacter globiformis* (CHO). CHO is a model enzyme that demonstrates the multiple roles histidine residues can hold throughout catalysis such as electrostatic and general base catalysts and hydrogen-bonding interactions. Evidence for these three roles of histidine residues in CHO are derived from the pH effects, primary and solvent kinetic isotope effects, site-directed mutagenesis, UV-visible absorbance and fluorescence spectroscopy, NMR, and rapid and steady-state kinetics studies.[4, 6-9] CHO catalyzes the oxidation of choline to glycine betaine through a two-step hydride transfer by activating the alcohol substrate to initiate catalysis.[8] The findings in this dissertation are consistent with H466 activating the choline substrate by abstracting the hydroxyl proton via general base catalysis.[4] Upon proton abstraction, H466 acquires a positive charged which, in turn, is used to stabilize the negative charge accumulated on the N(1)-C(2) locus of the flavin hydroquinone formed via hydride transfer from the alpha carbon of choline onto the N(5) atom of the flavin.[9] Both solvent and substrate kinetic isotope effects, site-directed mutagenesis and steady-state kinetics from this

and previous studies are consistent with H466 being essential for both proton abstraction and stabilization of the transition state.[8, 9] H466 may have a role in the oxidative half-reaction of CHO. The histidine residue would need to return to a neutral ionization state to participate in the next reductive half-reaction. Thus, H466 likely acts as a general acid donating the proton either to the solvent or oxygen to form hydrogen peroxide completing the enzymatic redox cycle.

Histidine residues participate in catalysis in ground state reactions such as the case with CHO and choline as well as in the excited state. Studies from this dissertation have demonstrated, for the first time, the observation of excited state reactions (ESR) in CHO which a proton is transferred from the N(3) atom to the N(5) atom of the flavin via H466. Fluorescence spectroscopy monitored using a thermostatted spectrofluorometer has provided a simpler approach to study ESR in flavin-dependent enzymes by following the changes in flavin fluorescence emission as a function of pH. Photons from the Xenon lamp of the spectrofluorometer provided the energy to excite the flavin to a higher energy state. The pK_a of the N(3) atom has been shown to decrease concomitantly with the pK_a of the N(5) atom increasing. The ionization constants and dipole moments of the isoalloxazine ring have shown to be altered in the singlet and triplet states leading to ESR.[25-30] This allows for a proton to be removed from the N(3) atom of the flavin and placed on the N(5) atom producing a positive charge on the C4a atom of the flavin.[31-33] At basic pH (pH > 7), a single spectroscopic peak was observed in the excited state with λ_{max} value of ~400 nm consistent with a C4a flavin adduct.[34-37] The increased concentration of hydroxide ions was due to increasing pH likely led to the formation of a C4a-hydroxy flavin adduct in which the negatively charged OH reacted with the positive-charged C4a atom on the flavin. The transfer of a proton in the excited state and stabilization of the charges accumulated on the ionized flavin formed after Step B in Scheme 7.1

are both facilitated by H466 in CHO as evident from fluorescent experiments with CHO variant, H466Q, as shown in Chapter VI. Consequently, the increase in effective concentration of OH^- and the catalytic base, H466, due to basic pH shifted the equilibrium of the excited state flavin species to its ionized form that was susceptible to nucleophilic attack (Species formed after Step B in Scheme 7.1).[38] Other flavin-dependent oxidase, such as glucose oxidase (GO), have an active site histidine residue similar in function and position to H466 in CHO.[39] H516 in GO behaves as a catalytic base likely capable of facilitating ESPT in the active site of the enzyme. Future investigations on the pH-dependence of the fluorescence signals including computational studies on the ionization constants and dipole moments of the protein-bound flavin in the excited states of these flavin-dependent oxidases would shed light on ground state and excited state reactions within the same enzyme active site.

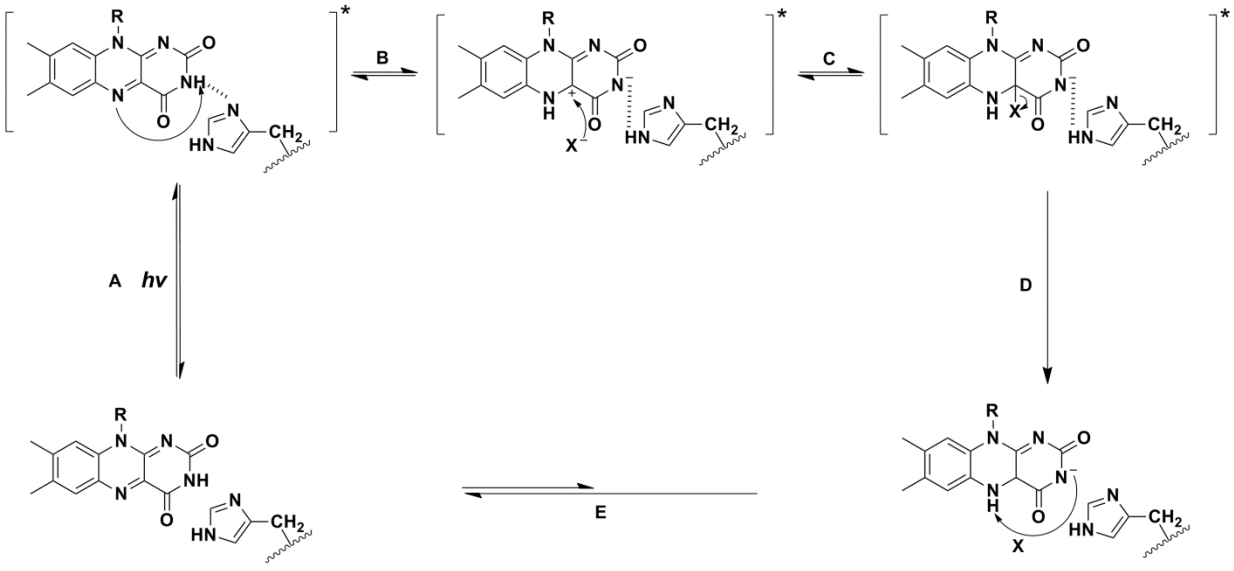

Scheme 7.1 Schematic representation of excited state reaction in CHO-wt as taken from Chapter 6.

Chapter IV elaborates on a study that uses collaborative efforts of both computational and spectroscopy experimentations to provide evidence for a single water molecule being responsible for the integrity of the protein configuration. The identification of conserved water recognition binding motifs in Pin1-type proteins have shed light on the importance of water molecules in retaining structural components of proteins. The water molecule was not observed in the catalytic pocket of the Pin1 enzyme but located near the surface of the protein away from the active site. The amino acid sequence of Pin1 protein that was observed to be in close contacts with the water molecule was identified as having a secondary structure of a helix-turn-coil motif. In this study, the helix-turn-coil motif has been identified in more than 800 X-ray crystal structures. The prevalence of the motif in so many structures indicated the significance of a motif likely analogous to the calcium EF hand. The motif observed in the Pin1 protein was then isolated from the protein and synthesized *in vitro* and the secondary structure was studied. The secondary structure of the peptide was investigated without the remaining protein construct using circular dichroism spectroscopy. However, the helix-turn-motif secondary structure identified in the Pin1 protein was not observed when the peptide was measured in solution without the remaining protein construct. It was not until the use of an additional stabilizer, trifluoroethanol, was the Pin1 peptide stabilized in the helix-turn-coil motif.

In conclusion, this dissertation has provided insights into the mechanisms of Class I NMOs and CHO from *A. globiformis* and revealed for the first time excited state reactions in the active site of CHO. The importance of a histidine residue in having multiple roles to assist in enzyme catalysis has been established using the mechanistic investigations of CHO by means of steady-state and rapid kinetics and fluorescence studies. The recently resolved crystal structure of CsNMO provided mechanistic insights on a newly identified mixed activation mechanism

with P3N as substrate in the presence of PEG 3350. Fluorescence spectroscopic investigations of CHO and its variants (H466Q and S101A) offered new understandings in flavin reactivity in the excited state. The mechanistic and spectroscopic studies in this dissertation have laid the groundwork for future investigations on excited state reactions in flavin-dependent oxidases and allosteric studies on Class I NMO enzymes.

7.1 References

1. Mijatovic, S., and Gadda, G. (2008) Oxidation of alkyl nitronates catalyzed by 2-nitropropane dioxygenase from *Hansenula mrakii*, *Arch. Biochem. Biophys. 473*, 61-68.

2. Smitherman, C., and Gadda, G. (2013) Evidence for a transient peroxynitro acid in the reaction catalyzed by nitronate monooxygenase with propionate 3-nitronate, *Biochemistry 52*, 2694-2704.

3. Salvi, F., Agniswamy, J., Yuan, H., Vercammen, K., Pelicaen, R., Cornelis, P., Spain, J. C., Weber, I. T., and Gadda, G. (2014) The combined structural and kinetic characterization of a bacterial nitronate monooxygenase from *Pseudomonas aeruginosa* PAO1 establishes NMO class I and II, *J. Biol. Chem. 289*, 23764-23775.

4. Smitherman, C., Rungsrisuriyachai, K., Germann, M. W., and Gadda, G. (2015) Identification of the catalytic base for alcohol activation in choline oxidase, *Biochemistry 54*, 413-421.

5. Rungsrisuriyachai, K., and Gadda, G. (2008) On the role of histidine 351 in the reaction of alcohol oxidation catalyzed by choline oxidase, *Biochemistry 47*, 6762-6769.

6. Ghanem, M., and Gadda, G. (2006) Effects of reversing the protein positive charge in the proximity of the flavin N(1) locus of choline oxidase, *Biochemistry 45*, 3437-3447.

7. Fan, F., Germann, M. W., and Gadda, G. (2006) Mechanistic studies of choline oxidase with betaine aldehyde and its isosteric analogue 3,3-dimethylbutyraldehyde, *Biochemistry 45*, 1979-1986.

8. Fan, F., and Gadda, G. (2005) On the catalytic mechanism of choline oxidase, *J. Amer. Chem. Soc. 127*, 2067-2074.

9. Ghanem, M., and Gadda, G. (2005) On the catalytic role of the conserved active site residue His466 of choline oxidase, *Biochemistry 44*, 893-904.

10. Ghisla, S., and Massey, V. (1986) New flavins for old: artificial flavins as active site probes of flavoproteins, *Biochem. J. 239*, 1-12.

11. Gannavaram, S., and Gadda, G. (2013) Relative timing of hydrogen and proton transfers in the reaction of flavin oxidation catalyzed by choline oxidase, *Biochemistry 52*, 1221-1226.

12. Chaiyen, P., Fraaije, M. W., and Mattevi, A. (2012) The enigmatic reaction of flavins with oxygen, *Trends Biochem. Sci. 37*, 373-380.

13. Kamat, S., Gaikwad, S., Ravi Kumar, A., and Gade, W. N. (2013) Xylitol production by *Cyberlindnera* (*Williopsis*) *saturnus*, a tropical mangrove yeast from xylose and corn cob hydrolysate, *J. Appl. Microbiol. 115*, 1357-1367.

14. Crozier-Reabe, K., and Moran, G. R. (2012) Form follows function: structural and catalytic variation in the class a flavoprotein monooxygenases, *Int. J. Mol. Sci. 13*, 15601-15639.

15. Ji, Y., Mao, G., Wang, Y., and Bartlam, M. (2013) Structural insights into diversity and n-alkane biodegradation mechanisms of alkane hydroxylases, *Front. Microbiol. 4*, 58.

16. Ishikita, H. (2007) Influence of the protein environment on the redox potentials of flavodoxins from *Clostridium beijerinckii*, *J. Biol. Chem. 282*, 25240-25246.

17. Mathes, T., van Stokkum, I. H., Stierl, M., and Kennis, J. T. (2012) Redox modulation of flavin and tyrosine determines photoinduced proton-coupled electron transfer and photoactivation of BLUF photoreceptors, *J. Biol. Chem. 287*, 31725-31738.

18. Fraaije, M. W., and Mattevi, A. (2000) Flavoenzymes: diverse catalysts with recurrent features, *Trends Biochem. Sci. 25*, 126-132.

19. Ghisla, S., and Massey, V. (1989) Mechanisms of flavoprotein-catalyzed reactions, *FEBS J. 181*, 1-17.

20. Keough, J. M., Jenson, D. L., Zuniga, A. N., and Barry, B. A. (2011) Proton coupled electron transfer and redox-active tyrosine Z in the photosynthetic oxygen-evolving complex, *J. Amer. Chem. Soc. 133*, 11084-11087.

21. Moore, G. F., Hambourger, M., Kodis, G., Michl, W., Gust, D., Moore, T. A., and Moore, A. L. (2010) Effects of protonation state on a tyrosine-histidine bioinspired redox mediator, *J. Phys. Chem. B 114*, 14450-14457.

22. Huynh, M. H., and Meyer, T. J. (2007) Proton-coupled electron transfer, *Chem. Rev. 107*, 5004-5064.

23. Bonetti, C., Stierl, M., Mathes, T., van Stokkum, I. H., Mullen, K. M., Cohen-Stuart, T. A., van Grondelle, R., Hegemann, P., and Kennis, J. T. (2009) The role of key amino

acids in the photoactivation pathway of the Synechocystis Slr1694 BLUF domain, *Biochemistry 48*, 11458-11469.

24. Shibata, Y., Murai, Y., Satoh, Y., Fukushima, Y., Okajima, K., Ikeuchi, M., and Itoh, S. (2009) Acceleration of electron-transfer-induced fluorescence quenching upon conversion to the signaling state in the blue-light receptor, TePixD, from Thermosynechococcus elongatus, *J. Phys. Chem. B 113*, 8192-8198.

25. Koziol, J. (1969) Studies on flavins in organic solvents. 3. Spectral behaviour of lumiflavin, *Photochem. Photobiol. 9*, 45-53.

26. Koziol, J., and Koziolowa, A. (1977) Studies on physicochemical properties of alloxazines, In *International Meeting on Flavins and Flavoproteins* (Ostrowski, W., Ed.), pp 81-107.

27. Koziolowa, A. (1978) Tautomerism and ionization of excited alloxazines in aqueous solutions of inorganic acids and their salts, *Zeszyty Naukowe - Akademia Ekonomiczna w Poznaniu, Seria 1: Prace z Zakresu Towaroznawstwa i Chemii 80*, 104-109.

28. Koziolowa, A. (1979) Solvent and methyl substituent effect on phototautomerism and ionization of alloxazines, *Photochem. Photobiol. 29*, 459-471.

29. Song, P. S., Sun, M., Koziolow, A., and Koziol, J. (1974) Phototautomerism of lumichromes and alloxazines, *J. Am. Chem. Soc. 96*, 4319-4323.

30. Salzmann, S., and Marian, C. M. (2008) Effects of protonation and deprotonation on the excitation energies of lumiflavin, *Chem. Phys. Lett. 463*, 400-404.

31. Tyagi, A., and Penzkofer, A. (2011) Absorption and emission spectroscopic characterization of lumichrome in aqueous solutions, *Photochem. Photobiol. 87,* 524-533.

32. Salzmann, S., and Marian, C. M. (2008) Effects of protonation and deprotonation on the excitation energies of lumiflavin, *Chem. Physics Lett. 463,* 400-404.

33. Schulman, S. G. (1971) pH dependence of fluorescence of riboflavin and related isoalloxazine derivatives, *J. Pharm. Sci. 60,* 628-631.

34. Losi, A., and Gartner, W. (2012) The evolution of flavin-binding photoreceptors: an ancient chromophore serving trendy blue-light sensors, *Annu. Rev. Plant Biol. 63,* 49-72.

35. Alexandre, M. T., Domratcheva, T., Bonetti, C., van Wilderen, L. J., van Grondelle, R., Groot, M. L., Hellingwerf, K. J., and Kennis, J. T. (2009) Primary reactions of the LOV2 domain of phototropin studied with ultrafast mid-infrared spectroscopy and quantum chemistry, *Biophys. J. 97,* 227-237.

36. Conrad, K. S., Manahan, C. C., and Crane, B. R. (2014) Photochemistry of flavoprotein light sensors, *Nat. Chem. Biol. 10,* 801-809.

37. Lanzl, K., Sanden-Flohe, M. V., Kutta, R. J., and Dick, B. (2010) Photoreaction of mutated LOV photoreceptor domains from *Chlamydomonas reinhardtii* with aliphatic mercaptans: implications for the mechanism of wild type LOV, *Phys. Chem. Chem. Phys. 12*, 6594-6604.

38. Jencks, W. P. (1969) *Catalysis in Chemistry and Enzymology,* Dover Publications, Inc., New York.

39. Leskovac, V., Trivic, S., Wohlfahrt, G., Kandrac, J., and Pericin, D. (2005) Glucose oxidase from *Aspergillus niger*: the mechanism of action with molecular oxygen, quinones, and one-electron acceptors, *Int. J. Biochem. Cell Biol. 37*, 731-750.